Introduction

The aim of experimental work

Hydrogen is considered as the next generation energy carrier that can offer a non-polluting, inexhaustible, efficient, and potentially cost-effective energy source. As a fuel it allows to reduce greenhouse gas effect, a problem that is now more pronounced with the recent concern about global warming. For these reasons, a hydrogen-*based* economy should involve necessarily a production by alternative energy sources to the traditional fuels, its transportation and storage in an efficient manner as well as the effective coupling of production/storage strategy with the end-use. Among these aspects, the hydrogen production is the most important issue since it has major potential for energy intensification. This demands that the existing methods can be reviewed extensively in terms of energy efficiency, environmental concerns, and economics.

Thermal, electrochemical, or biological processes are the main pathways to produce hydrogen. Among these, methane steam reforming (MSR) is the most widely used process in chemical industry. Today, almost all the hydrogen produced by MSR, corresponding over 50% of global production, is used in oil refineries for upgrading fuels and commodities. The efficiency of conventional MSR is 65–75% for the best of the commercial productions. Obviously, any efforts to increase the yield have a significant impact on the H_2-*based* economy. In particular, the traditional process of MSR has undergone modifications in three main areas regarding to diffusional limitations [1], thermodynamic limitations, and catalyst deactivation due to coke formation [2].

Recent advances in fuel cell technologies as well as the integration of various units operation occurring in the process with novel catalysis and separation technologies have triggered efforts in intensified MSR process design. By means of integrated designs and/or operations is possible to increase energy efficiency, reduce the mass and heat transfer resistances and overcoming thermodynamic limitations. Thus, process intensification can favour the design of more compact systems and, consequently, a huge reduction in global size of the plant as well as contribute to reduce greenhouse gas emissions in considerable way.

This thesis presents, therefore, an evaluation of the process integration and intensification engineering aspects by novel membrane technologies to improve the pure hydrogen recovery and production. In particular, this has been realized by using the innovative concept of multifunctional reactors (Membrane Reactors, MRs) in which both separation and reaction are, contemporaneously, carried out in the same equipment. As a consequence, MRs allow to exceed

the mass transfer and thermodynamic limitations and get to high yields with respect to both conventional reforming and shift reactors.

As known, Pd-based membrane technology allows to remove continually and selectively hydrogen producing a pure stream as permeate. When it is combined to a reaction limited by thermodynamic equilibrium (*e.g* reforming reactions), this inherent characteristic assures a higher yield. In fact, the chemical equilibrium is changed towards the products and the thermodynamic limit of a traditional reactor (TREC) is exceeded.

As known, small-scale plants reduce the problems of storage and/or transportation but relatively have poorer investment and operation economics [4]. The ultra-pure hydrogen production on small scale by means of reforming or water gas shift (WGS) reactions in conventional reactors seems to be too expensive and complex due to the high number of equipments required in the traditional MSR process. The integration of a membrane in a conventional reactor can, then, allow a reduction of the total number of equipments, simplification of the hydrogen separation steps downstream of membrane reactor or reduction of the number of shift reactors. In addition, it improves the thermal management in the system [151]. Obviously, potential target is, always, to reduce the cost of hydrogen production from natural gas improving efficiencies over 75% [5**]**. Even in this case, undersized MRs can contribute to guarantee a straightforward and economic small scale hydrogen production.

The presence of carbon monoxide in the reformate stream is a significant problem for a direct use in fuel cells since a few percentage of this gas poisons their catalyst. For this reason, additional steps to reduce CO content are required (*e.g.* methanation, selective oxidation). The water gas shift (WGS) reaction represents a fundamental step in the main industrial routes to produce furthermore hydrogen [3] or for adjusting the CO/H_2 ratio of the syngas stream. Even in this case MRs can contribute to manage effectively the CO presence in the reformate stream by producing pure hydrogen.

From an industrial point of view, MRs technology has not been still applied either to MSR or WGS. Some key technical problems, normally connected to the low Pd-*based* membrane stability at severe operating conditions (high temperature and pressure), have not been still solved. Therefore, drawbacks and advantages can not be deduced by an experience at industrial level and so far as their flexibility or adaptability have been only estimated by theoretical (larger part for MSR reaction) or experimental investigations in systems on bench-scale.

The experimental activity has regarded, particularly, the application in MSR process of a high pressure Pd-*based* MR, on small scale, to realize efficiently and economically both high pure hydrogen recoveries (99.999%) and high conversions (>80%).

As known, in a “conventional” MR, a sweep gas stream on permeate side can be used to increase the driving force through the membrane and favours the conversion. This implies the dilution of the extracted hydrogen and additional costs. Some technological solutions have been studied for example by feeding both the streams (permeate and retentate) in countercurrent to enhance the efficiency of mass transport, as shown in figure **C**. In some case such solutions have not been sufficient to improve the MR performance. The feed pressure represents another important design parameter that can be used to improve the mass exchange through the membrane.

Thus, a theoretical analysis has been carried out and a 2-D model has been developed for MR based on the WGS reaction in high pressure conditions. Differently from MSR, in this case the use of the sweep gas has been considered to manage efficiently temperature hot spots taking place in catalyst bed. This sensitivity analysis has allowed evaluating the role of significant operating conditions such as sweep gas flow-rate and temperature on heat and mass exchange, then, on MR performance (conversion and hydrogen recovery).

For what concern the MSR in a MR, it is preferable to work at high pressures for some main reasons: 1) the natural gas to the primary reformer of a conventional industrial plant is already sent at a high pressure; 2) a high product yield can be accomplished in a reduced reactor volume (fewer palladium membrane surfaces) with a reduction of the MR capital costs [6-13]. The advantage to consider mainly feed pressure to improve the performance of a Pd-based MR employed in MSR instead of a sweep gas has already been theoretically studied by Barbieri *et al.* [14]. Their theoretical analysis shows that by combining the increasing pressure with a high sweep gas flow rate (I=10), the MR performance are improved, figure **a**, whereas in a conventional reactor the increasing feed pressure reduces significantly the conversion, see figure **b**.

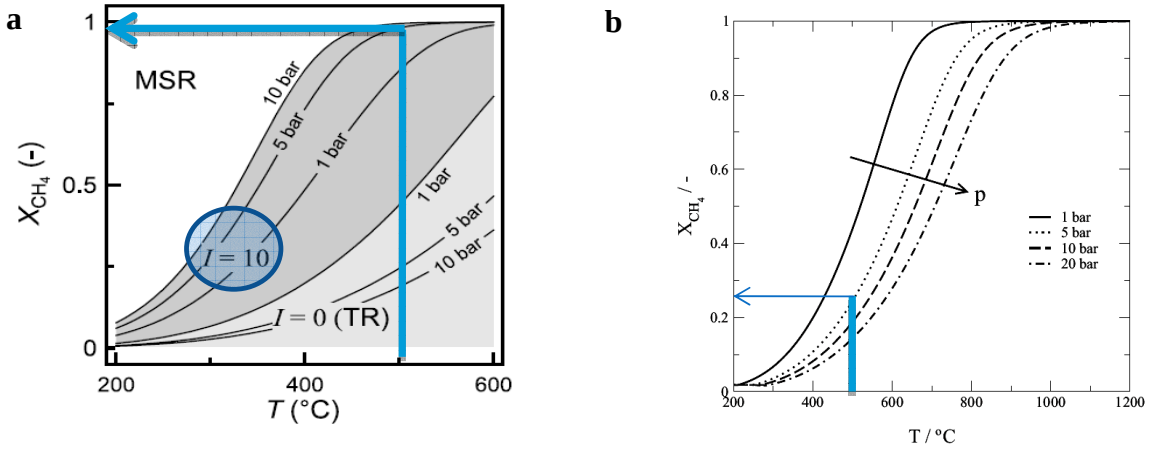

Theoretical trend of methane conversion as a function of temperature at different feed pressure in presence of sweep gas [14]: a) Membrane Reactor ; b) Conventional reactor

Therefore, it is much important to find an appropriate feed pressure range for which its advantageous effect on the pure hydrogen permeation through the membrane counterbalances the negative one on the thermodynamic of reforming reaction. These experimental choices allow combining a low surface area for mass exchange and maximize hydrogen yield with an efficient mass exchange. Thus, a cost-saving in the process could be reached.

By following the indications of the previous theoretical study, an analysis has been carry out to evaluate how the improvement in terms of driving force using only feed pressure could be higher than the one produced by using the sweep gas on permeate side. As showed in table, a five-time increase of the feed pressure value implies a corresponding enhancement of the driving force equal to four-times with respect to the real experimental reference value also indicated in the table. Instead, at fixed feed pressure, a higher sweep gas flow rate (*e.g.* $\rightarrow \infty$) allows only a double increase of driving force.

Table – Theoretical Analysis about pressure effect on driving force

	$P^{reaction}$	$\sqrt{P_{H2}^{reaction}}$	$P_{H2}^{permeation}$	$\sqrt{P_{H2}^{permeation}}$	$\Delta\sqrt{P^{H2}}$	Hydrogen *Driving force* ratio
	kPa	kPa $^{0.5}$	kPa	kPa $^{0.5}$	kPa $^{0.5}$	
Reference	800	18.3	100	10	8.3	
$P^{reaction}$ x 5	4000	41	100	10	31	4
$Q^{sweep} = H_{2,p}$ x 10	800	18.3	10	3.2	15.1	2
$Q^{sweep} \rightarrow \infty$	800	18.3	0	0	18.3	2.2

The study of the effect of pressure, without sweep gas, in MSR is one aspect that has been treated exhaustively in the MRs literature only by means of mono-dimensional theoretical models [14-22]. A large part of them has considered mainly the use of a sweep gas stream on shell side and put in evidence the existence of hydrogen peak inside the catalyst bed of MR [8, 23-28]. This peak is originated by the hydrogen production rate that counterbalances the permeation rate through the membrane as showed in a simplified scheme in the figure **C**. The hydrogen profile is similar to the temperature hot spots taking place during the exothermic reactions in packed bed conventional reactors with external heat exchange. The presence of this peak inside packed bed MR implies a partial use of the mass exchange surface; then, MR results oversized. In this experimental study for MSR, the use of a sweep gas stream on tube side has been avoided to circumvent hydrogen dilution on permeate side. On the other hand, in this case high pressures have been considered to recover successfully pure hydrogen on permeate side and have high methane conversions per-pass. In order to realize experimentally only the side at higher pressure, as evidenced in figure **C**, a self-supported 100 μm-thick Pd/Ag (75/25 wt%)-*based* membranes closed on one end and connected stainless steal tube by "*braze-welding*" have

been inserted inside the catalyst bed. Self-supported membrane is a technical solution that allows avoiding thermal instabilities connected to the sealing between the Pd-*based* membrane and ceramic material support as well as the metallic inter-diffusion processes between Pd-*based* and stainless steel supports.

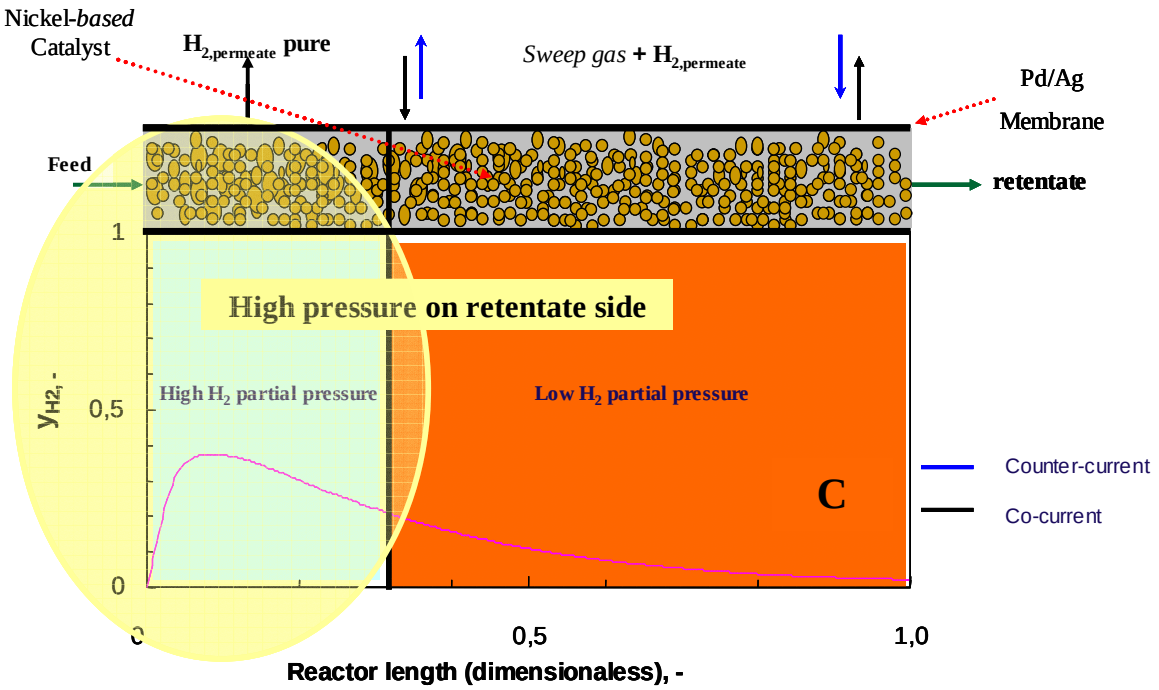

Theoretical profile of hydrogen concentration and different mass exchange modes in the prototype of MR

If hydrogen recovery through the membrane enhances with increasing pressure, the maximum is, nevertheless, a trade-off between the transport propriety (hydrogen separation) and thermodynamic limit which have an opposing pressure dependency in MSR. In this experimental work the antagonist effect of pressure on both equilibrium and H_2 permeation have been also investigated. The use of higher temperatures increase kinetic and permeation rate as well as the equilibrium conversions but the membrane stability can be compromised. Therefore, lower temperatures (fewer 600°C) with respect the industrial operating conditions have been used in this work. At higher pressures, the influence on MR performance of some design parameters such as the membrane area (A_m) and catalyst volume (V_{cat}) ratio combined with the ratio of the methane load (L_s, limiting reagent) in the feed onto membrane area (A_m) has been considered in this study and their effect on the MR performance has been investigated.

In order to mitigate the temperature gradients in exothermic reactions along the catalyst bed in a catalytic reactor a uniform distribution of the catalyst, instead, could not be necessarily optimal. Buchanan *et al.* [33] have studied the problem of the optimum distribution of two catalysts in a wall-cooled non-isothermal packed bed reactor for exothermic reaction of butane oxidation. It

has been compared to the one where a single catalyst was diluted with inert particles to moderate temperature. For what concern in particular the catalyst distribution, most of the theoretical and experimental studies were focused on the radial distribution of the active component in the catalyst pellets. Recently, some studies have revealed that an axially non-uniform catalyst distribution through the catalyst bed length may also affect considerably the process parameters [30, 31]. It was shown that in the case involving first-order homogeneous and heterogeneous reactions in an isothermal reactor, instead, the uniform distribution of the active component along the catalyst bed was optimal [32]. An operative mode to mitigate the magnitude of the temperature hot-spots and, contemporaneously, improve the yield per-pass for the WGS has been established in this work. This aspect has been theoretically investigated and evaluated by dosing an increasing catalyst mass along the MR.

As reported in the literature [2, 29], the methane decomposition tendency to give coke is determined by the ratio (P^2_{H2}/P_{CH4}). Selective removal of the hydrogen by membrane favours also the methane cracking reaction, so that the catalyst activity and MR stability are affected. This could restrict any advantages arising from the use of a MR for MSR. Higher reagents molar ratios are usually employed in the conventional process to reduce the coke formation on the catalyst but this implies the use of a higher steam amount at high pressures. In this study, lower reagents molar ratios (a 2-3 range) than those used in the conventional reformer have been considered. The investigation of the best operating conditions for an optimal running of MR in this range allows to work by a reduced steam amount getting to a significant costs saving. In addition, another objective of the experimental work has been the assessment of the effect of some operating conditions in combination with a proper catalyst distribution on the MR performance to hindrance this insidious effect and preserve the inherent advantages of membrane reactor.

Chapter 1

1.1 Environmental situation

Today, the most of energy power used for our needs is, in large part, obtained by fossil fuels combustion even if a part equivalent to 6% of it is supplied by hydroelectric resources. This energy production generates, mainly, carbon dioxide (greenhouse gas) and heat. Recently, it has been demonstrated how the CO_2 emissions, in the last century, have been the cause for sudden climatic alterations that, as a consequence, are potentially carrying out to wide-ranging effects on the natural environment as well as on human societies and economies. These effects could carry out to the melting of glaciers and, consequently, rising of the sea level, or powerful atmospheric disturbances. These last could carry out still to a reduction of potable water amount as well as the agricultural production causing huge damages to the poorer populations.

1.1.1 Greenhouse Effect

Earth's atmosphere is, yet, composed by a mixture of 78% nitrogen, 21% oxygen, and 1% other gases in which carbon dioxide accounts for just 0.03 - 0.04% and has got a natural temperature control system. In view of this, certain gases can be critical for its thermal stability. Generally, water vapour, carbon dioxide, ozone, methane and nitrous oxide absorb, warming the atmosphere, some of the infrared thermal radiation leaving the earth's surface. These active gases are known as "*greenhouse gases*" because they act as a partial blanket for the thermal radiation and, therefore, their effect is known as the **natural greenhouse effect**, fig. 1a. Without the greenhouse gases Earth's average temperature would be roughly -20°C. On average, about one third of the solar radiation that hits our planet is reflected back to space.

The table, in fig. 1b, lists the main greenhouse gases and their concentrations in pre-industrial times compared to the ones in 1994. Global Warming Potential (GWP) represents an index and a simple measure of the relative radiative effects of different greenhouse gases. It is defined as the cumulative forcing radiative caused by a unit mass of gas as referred to CO_2 or a combination of different gas (CO_2, CH_4, and N_2O) and expressed as CO_2-equivalence for a 100 year time frame [34].

Obviously, both industrial and human activities are causing an increase of greenhouse gas levels in the atmosphere and this effect is producing an overheating of the Earth.

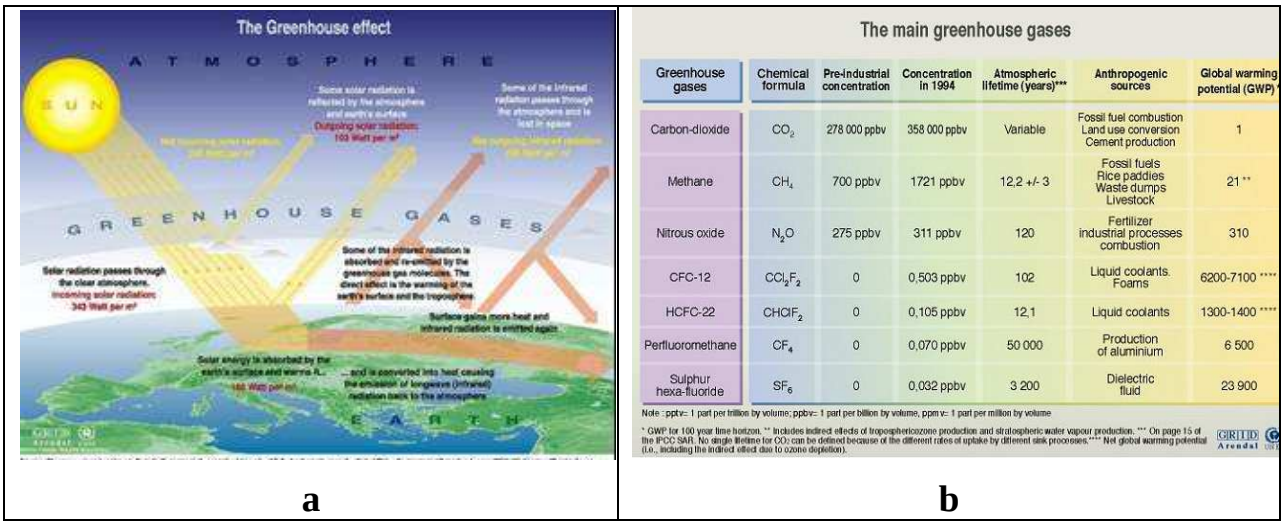

a **b**

Fig. 1 - a) The Greenhouse effect; b) list of the main greenhouse gases and their concentrations in pre-industrial times compared to the ones in 1994 [34]

Fig. 2a shows as Earth's climate has been unstable over the last thousands of years and the direct correlation between carbon dioxide content in the atmosphere and earth's temperature. In fact, fig. 2b indicates as atmospheric CO_2 content has increased from about 280 ppmv (pre-industrial concentration) to about 367 ppmv (at present) [35] in the last 130 years. It is evident that the rapid increase in CO_2 concentrations has been occurring since the onset of industrialization (develop of industrial processes, transport, urbanization) and, then, by economic development that is closely associated with a high energy production.

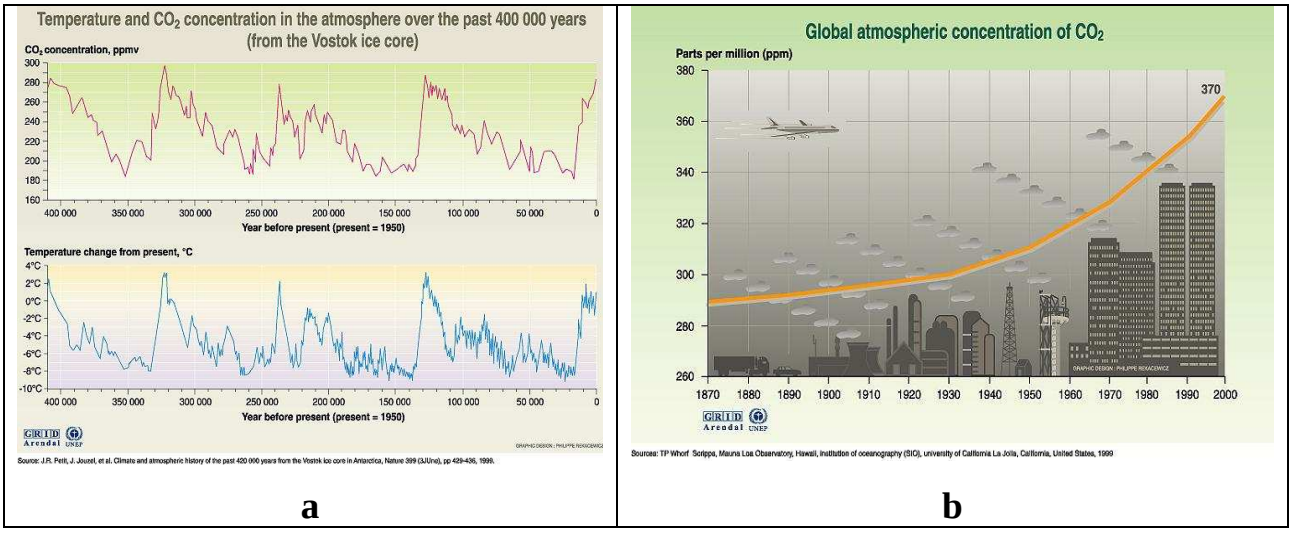

a **b**

Fig. 2 - a) Temperature and CO_2 concentration in the atmosphere [35]; b) Global CO_2 concentration [36]

In addition, non-industrialised countries are increasing their population's standard of living, and this contributes to enhance their greenhouse gas emissions. China, for example, has reached the second biggest level of emissions of GHG in the world after India. Therefore, scientists continue

to make estimates of the potential direct impacts on various socio-economic sectors even if they admit the full consequences could be more complicated because other sectors, indirectly, will be also affected particularly at a regional and local level.

1.2 Potential Supplies for Future Energy

In this part, an overview of the alternative energy sources and the research in the energy field will be illustrated. These aspects are important since they represent a first contribution towards the potential reduction of the negative effects due to the presence of greenhouse gas in the environmental.

1.2.1 Renewable energy growth

There is a great deal of information and enthusiasm today about the development and increased production of global energy needs from alternative energy sources. Solar energy, wind power and moving water are all traditional sources of alternative energy that are making progresses. Figure 3 shows a simulation for the percentage increase expected from 2020 to 2040 in Italy. For example since 2020 world energy consumption could increase by 50% (207 quadrillion BTUs).

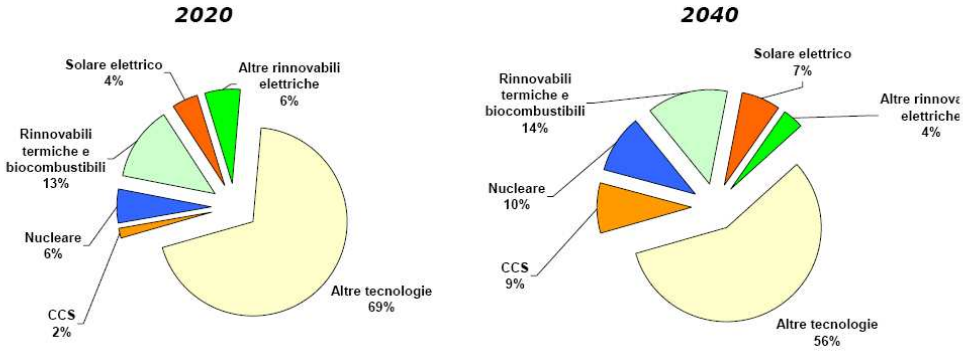

Fig. 3 - A theoretical prediction for a percentage energy growth of renewable sources from 2020 to 2040 in Italy [37].

In a global society, this simply means energy produced from sources unlike from traditional primary (fossil fuels) energy supply. Coal, oil and natural gas are the three kinds of fossil fuels from which our energy needs have mostly depended, from home heating and electricity to fuel for transport. The problem is that fossil fuels are non-renewable. They are limited in supply and, one day, could deplete. Instead, renewable energies have inherent capability to be non-polluting and efficient. From a practical point of view, these sources are able to capture and convert their mechanical power to electricity in the most efficient and productive way. Consequently, they allow reducing global carbon dioxide emissions and adding some flexibility to the energy mix by decreasing dependence on limited reserves of fossil fuels. In Denmark, for example, over 20% of power usage today comes from wind power alone. In Germany, over 6% of total usage comes from wind power (15,000 MW). Currently, US wind energy capacity is around at about 6,500

megawatts (equivalent to the usage of about 1.5 million average American households). In comparison to the US, the EU as a whole has over five times the US capacity, about 30,000 MW [37]. Figure 4, for example, compares resources mix in Europe with the one in Italy for the production of electric power.

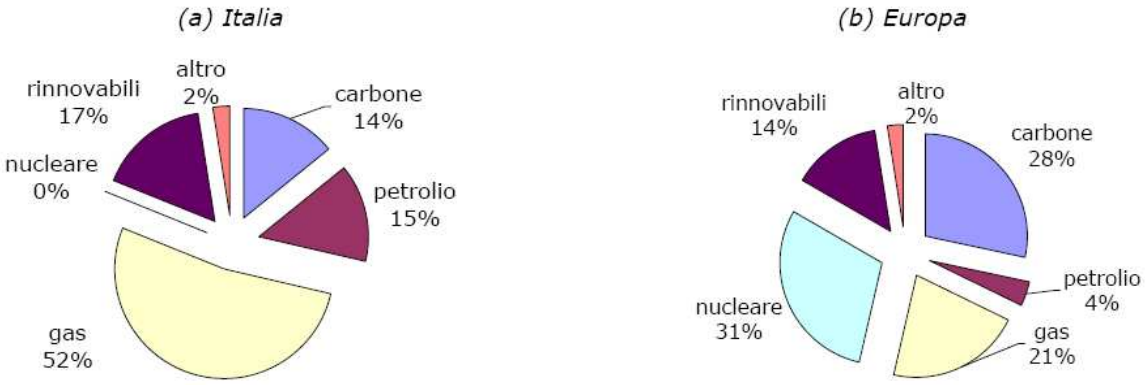

Fig. 4 - Sources mix for electric energy production in Europe and Italy. [37]

In spite of this, they provide only about seven percent (7%) of the world energy needs whereas fossil fuels, along with nuclear energy cover 93% of the world energy resources. This is due to fact all the renewable sources imply very high economic investments (*i.e.* thermodynamic and photovoltaic solar require 20 billions euro in 20 years).

In this contest, the improvement of the energy systems efficiency represents an important parameter since it allows reducing the cost of energy and the amount of fuel needs to produce electricity, respectively. This seems to be, for example, a European task for a 20% reduction of the greenhouse gas emissions in 2020 with respect to the levels in 1990 and an efficient transformation of the energy markets (equipments, buildings and utilities at energy high-yield) [37].

1.2.2 Research in energy field: general aspects and potentialities of the Fuel Cells

The transport sector engraves in relevant way on the expenses of energy (30%) as well as on the greenhouse gas emissions. From technological improvements point of view, the contribution to reduce the consumptions and emissions in the conventional combustion engine is still too low (6%). In addition, this could not still give significant effects in the next future since the expenditures of oil are incompressible and, also, in constant–growing. According to the European Commission suggestions, the use of "*hybrid*" or "*electric*" engines as well as fuel cells-powered engines and hydrogen could entail to realize an environmental-friendly transport system. Fuel Cell-*powered* systems have the potential to update and simplify the way to provide energy power, see figure 5a and b, offering a cleaner and more-efficient alternative to the

combustion of gasoline and other fossil fuels. Moreover, fuel cells show also the attractive potential of decentralizing and democratizing the electricity system as well as reducing costs and lowering the possibility of repetitions of widespread blackouts. The research is in progress, in particular, both in the development of vehicles having a controlled-CO_2 discharge (sustainable mobility) and hydrogen-build up in central to improve and power older industrial plants or produce electric energy. Obviously, critical factor is hydrogen availability.

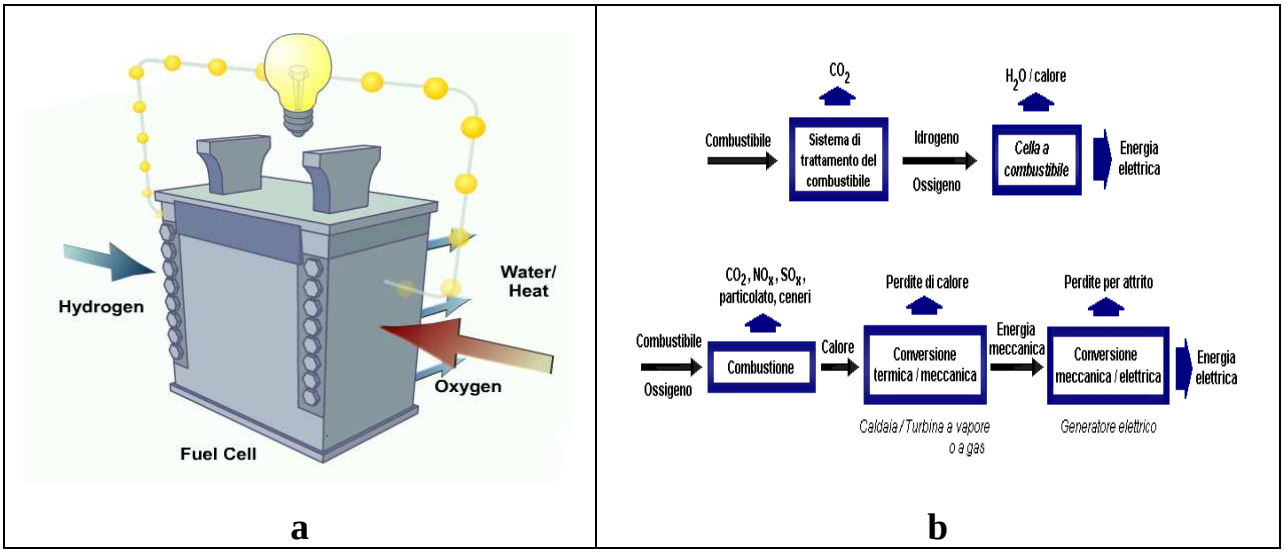

Fig. 5 – a) Basic operation for a Fuel Cell. b) Fuel Cells potentiality for the energy production in comparison with the traditional systems.

But what is a fuel cell (FC)? It is a special device of electrochemical energy conversion. By means of the reaction between hydrogen and oxygen it produces alone a no-polluting waste (water) and energy power with efficiency approximately of 40-50% with no generation of dioxide (CO_2), soot, nitrous oxides with respect to the current internal combustion engines [15], as shown in figure 5a.

At present, hydrogen is still the only suitable fuel for those fuel cells defined of "low-temperature". In addition, to be stable they require a carbon monoxide content in hydrogen feed stream lower than 20 ppm. Other fuels (methanol, methane, liquid petroleum gas, diesel, gasoline, etc.) can be used but they need to be converted into hydrogen before to be supplied to the fuel cell. At the present, some key challenges remain to overcome the hindrances to the complete commercialization of fuel cells and hydrogen infrastructure technologies:

- **Fuel Cell Cost.** The costs of proton exchange membrane fuel cell (PEMFC) engines are still over $3,000/kW [38] which is two orders of magnitude higher than the one officially expected in the late '90's [39].
- **Durability**. Fuel-Cells current technology does not still provide a durability great. Cycle life, storage density, fill-up times, regeneration cycle costs, energy efficiency, and

availability of chemical and metal hydride storage systems need to be evaluated in real-world circumstances.

- **Hydrogen Storage.** In the automotive industry, an efficient storage of hydrogen determines the successful large-scale market introduction. Nevertheless, the most practical way of using hydrogen as a motor fuel is as liquid at high pressure. The problem is a H_2-tank will have three times the size of the gasoline one, liquid hydrogen is cold enough to freeze air and carry out pressure build-up following plugged valves, it gradually evaporates (1.7 percent per day) and, for a car, this is too fast to sit between uses.
- **Hydrogen Production cost and Delivery.** The high cost of hydrogen production, low availability of the hydrogen production systems, and the challenge of providing safe production and delivery systems are all early penetration barriers.

1.3 Conventional Hydrogen production costs and technologies

As previously mentioned hydrogen can be considered the clean fuel of the future since its use allows reducing greenhouse gases (CO_2) and pollutants emissions in the environmental urban and/or in area at high density living [40]. Its employment in the future energy systems contributes overcoming many difficulties linked to the energy production and consume. Unfortunately, all current platforms for hydrogen production are largely based on fossil fuels, relatively energy inefficient.

In today energy supply systems, gasoline, diesel fuel, and natural gas serve as energy carriers. In fact, by the conversion of primary energy sources these carriers are obtained into an energy form such that it is directly transported and delivered to end-users (in industrial, commercial, residential, and transportation areas). Differently, the future sustainable energy supply systems distinguish both electricity and hydrogen as the dominant energy carriers [41]. Governments and industries, particularly in the United States, Japan, and Europe, have been investing heavily in research and development to overcome the technical barriers for hydrogen production, storage, and utilization and realize a sustainable future energy infrastructure based on it. For instance, the development of low-carbon content, low polluting, and lower cost processes is one among targets required.

A fundamental aspect that has to considered for a cost-competitive transportation, energy independence and, therefore, hydrogen-*based* economy is hydrogen and its associated technology has to be comparable to conventional ones to have successful in the commercial marketplace. Then, the primary challenge is to reduce the cost associated with its production, storage and delivery. At the present, even if a suitable method for hydrogen production is established, its cost should result four-time higher than the one required to get gasoline or diesel at the same energy produced [42].

Industry already produces and uses hydrogen on a massive scale [16]. A large-scale production often requires a prohibitive capital investment for the separation and purification processes which significantly drives up the cost of H_2. Over 90% of 0.85 trillion $m^3\ yr^{-1}$ is generated from fossil fuel sources by means of thermo-chemical processes (reforming and oxidation reactions) among which steam reforming of natural gas is mainly used to cover around 30 – 40% of entire production, see Table 1. The total H_2 remaining fraction (8%) is produced through electrolysis of water [49]. It requires electricity that in many countries still is obtained by power plants that, always, use natural gas or coal.

Table 1 - Main processes for industrial hydrogen production [43]

Processes	Hydrogen Yield (% of load)
Semi-rigenerative catalytic reforming	1.2 - 1.7
Continue catalytic reforming	2.3 - 2.6
Steam Reforming	30 - 40
Partial oxidation of methane	~30
Gasification of the residue (when is required complete conversion of hydrogen and CO in the synthesis gas)	15 - 20

Moreover, as figure 6 shows, it produces less hydrogen than the one produced if the electricity is directly fed to the network while fuel is directly conserved to make hydrogen. Consequently, direct conversion of the fuel by reforming seems to be more efficient and cheaper.

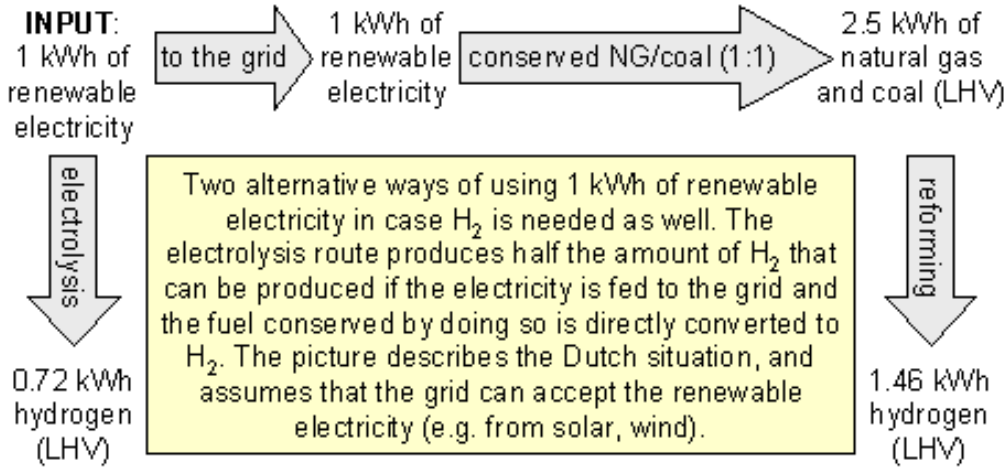

Fig. 6 – Hydrogen production by renewable energy with respect to the one where energy is fed to the grid. The fuel is converted in hydrogen production by MSR [50]

Energy power generated from sunlight, wind and nuclear sources are often used to produce hydrogen by an electrolytic way. Other areas include high-temperature thermo-chemical conversion of biomass, photolytic and fermentative micro-organisms systems, photo-electrochemical systems, and high-temperature chemical cycle water splitting. Although such production systems seem to be the cheapest methods, they have many technological problems. Moreover, they can increase hydrogen cost. Assuming $0.05 per kWh of electricity from, for example, a nuclear power plant during low demand, hydrogen could cost $0.09 per kWh [51]. Hydrogen is currently much more expensive than gasoline primarily due to the massive tax breaks that are given to the oil companies. As an example, table 2 shows the bulk hydrogen cost produced by natural gas as a function of plant size, cost and natural gas (NG) price [44]. At the

same plant cost and size, as the natural gas price increases the hydrogen increases, as well. Instead, if the NG price is fixed, an increase of both plant size and cost reduces the hydrogen cost since it means a large-scale hydrogen production.

Table 2 - Bulk H_2 gas costs, 2004 USD [45]

NG price, $/GJ	Plant Size, tons/day	Plant Cost, $	H_2 gas cost, $/kg
3.5	22	23M	1.8
7.0	22	23M	2.4
15.0	22	23M	4.1
3.5	80	44M	1.2
7.0	80	44M	1.9
15.0	80	44M	3.0
3.5	600	210M	0.7
7.0	600	210M	1.0
15.0	600	210M	2.7

At present, among traditional sources of hydrogen (natural gas, coal, nuclear breeder reactors) only coal begins to compete economically with natural gas even if the generation of liquid H_2 produces at least 8 kg of carbon (29 kg of CO_2) per kilogram of H_2. If a realistic future carbon tax of $0.1/kg is added, coal likely could become uncompetitive [46]. When the cost of natural gas was about $2 per MMBtu (Million Btu) hydrogen was produced at $4/gge. In 2005, the cost of natural gas is rose around $13 per MMBtu increasing proportionally the cost of hydrogen, see figure 7. Liquefaction of H_2 adds some costs, depending on plant size and energy costs [48].

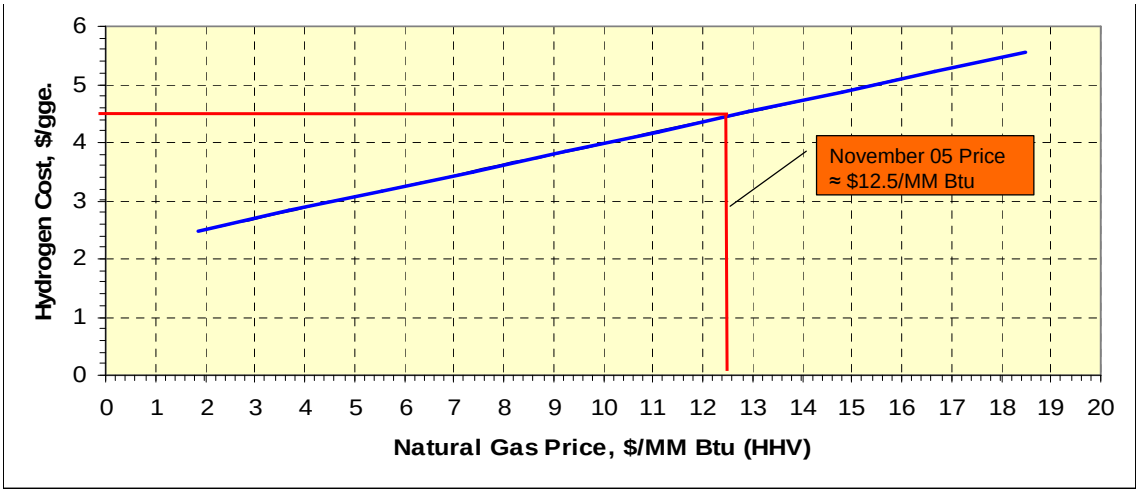

Fig. 7 - Hydrogen Production Cost from Distributed Natural Gas Versus natural gas price [47]

1.4 Additional applications of the Hydrogen

Overall industrial use of hydrogen is about 50 million tons and growing at 4-10% per year [52]. Simultaneously to the employ in fuel cell, hydrogen is used in a number of others industrial applications as ammonia production (62.4%), oil refineries (24.3%), and methanol production plants (8.7%). With respect to earlier years, refineries are now consumers since hydrogen is used for treating and desulphurization of fuels or heavy crude oils [16] see table 3.

Table 3- Hydro-cracking and hydro-treating processes in oil refineries, [43].

Hydro-treating	**Main target for the treatment**	**Consume, kg,$_{H2}$/tons of load**
Gasoline hydro-treating	Elimination of poisons (sulphur and nitrogen) for reforming and isomerization catalyst. Adjustment according to the specifications of sulphur concentration in gasoline	0.5-10.0
Kerosene hydro-desulphurization	Adjustment of sulphur concentration according to the specifications in mid-distillate	1.0-3.0
Diesel fuel hydro-desulphurization	Adjustment of sulphur concentration according to the specifications in mid-distillate	3.0-12.0
Hydro-treating of mid-distillate	Pre-treatment of the feeds in the upgrading processes as FCC (fluid catalytic cracking) and hydro-cracking	5.0-15.0
De-aromatization	Adjustment of aromatic concentration according to the specifications in different oil fractions (e.g. mid-distillate)	3.0-15.0
Hydro-cracking		
Mid-distillate conversion	Conversion of heavy oil fractions by vacuum in light products as GPL, crude gasoline, kerosene, diesel fuel (upgrading of the charge)	15.0-25.0
Hydro-treating and conversion of fuel oils	Reduction of the content for undesired species (metals, sulphur, nitrogen, etc) in fuel oils. Partial upgrading of the residue in feed	10.0-25.0

Today, large-scale H_2 plants are being built close to refineries to balance this huge request [16]. In addition, H_2 is used in asymmetric hydrogenation processes for pharmaceutical products or in the formation of chemical feedstocks needed in the manufacturing of plastics as well as in a small percentage it is employed as a chemical for making fertilizers [53]. Moreover, hydrogen vector is employed in the electric power production; in fact, large centralized hydrogen production plants based on fossil fuels combustion are used to generate syngas required to produce electricity.

1.5 Hydrogen Delivery

A hydrogen-*based* economy requires an infrastructure to deliver hydrogen from the point where it is produced to the point of end-use, such as a dispenser at a refuelling station or stationary power site. Infrastructure includes the pipelines similar to those used to transport natural gas, trucks, storage facilities, compressors, and dispensers involved in the process of delivering fuel. There are some additional problems connect to the hydrogen leakages besides to embrittle some metals used for pipelines. However, the technology of an efficient transport of electric energy may be sufficiently improved without precluding the advantages of hydrogen, except for vehicles. In fact, on-board hydrogen storage for transportation applications continues to be, as previously said, one of the most technically challenging barriers to the widespread commercialization of hydrogen-fuelled vehicles. In some case, different technical solutions are studied such as the use of MRs to produce hydrogen employed in fuel cell.

Chapter 2

2.1 Thermal processes for hydrogen production

Energetically efficient processes for hydrogen production require cost-effective and energy efficient systems for separation and purification. Currently, H_2 can be purified through one (or a combination) of three major processes: 1) pressure swing adsorption (PSA) [54, 55], 2) fractional/cryogenic distillation, or 3) membrane separation [56, 57].

PSA and fractional/cryogenic distillation systems are operation units already used in many large scale plants. Nevertheless, they are not cost-effective and demand much energy for the separation and purification operation of H_2. The third method, membrane separation, is currently considered to be the most promising because of low energy consumption, possibility for continuous operation, dramatically lower investment cost, its ease of operation, and ultimately cost effectiveness.

As already observed, a future energy infrastructure based on hydrogen to have the desired environmental benefits requires that generation of hydrogen occurs by renewable energy sources. But in view of high costs and technical problems does not still completely resolved, the hydrogen production by fossil fuels will continue to play an important role at least in the next decade [58, 59].

2.1.1 Conventional Methane Steam Reforming (MSR) process

Steam reforming of natural gas and light HCs (hydrocarbons) is a process widely used for hydrogen production [60, 61] and presents the highest efficiencies among all commercially available methods [62]. It usually uses natural gas that is a convenient hydrogen feedstock since it has the highest hydrogen-to-carbon ratio among all known-hydrocarbons. Moreover, considering the immense and undiscovered reserves existing around the world it provides near- and mid-term energy security in addition to the environmental benefits. Other reforming processes as bio-ethanol or ethanol steam reforming [63] are used to produce hydrogen. Bio-ethanol is obtained by fermentation of biomass and, therefore, it could represent one of liquid bio-fuels more interesting for its intrinsic safety and uncomplicated handling [17].

However, MSR represents a mature and well-established technology for an industrial production on a worldwide scale of merchant hydrogen that makes it important for the transition to a hydrogen energy economy. Nevertheless, the process is very complicated. A complex energy integration among a high number of process units including reformer, high and low temperature

shift reactors and a preferential oxidation reactor (PrOX) by a network of heat exchangers is required [64]. While MSR plants on large scale are considered the most economic method on the contrary they are not advised for the ultra-pure hydrogen production on small scale owing to outsized number of equipments and the uneconomical downscaling. Small-scale plants eliminate or reduce the problems of storage and transportation but comparatively have poorer investment and operation economics. Many companies are experimenting innovative systems for hydrogen production based on membrane reformers on smaller scale. Membrane reformer designed by Tokyo Gas *Co*. is an example, as showed in figure 8 [65].

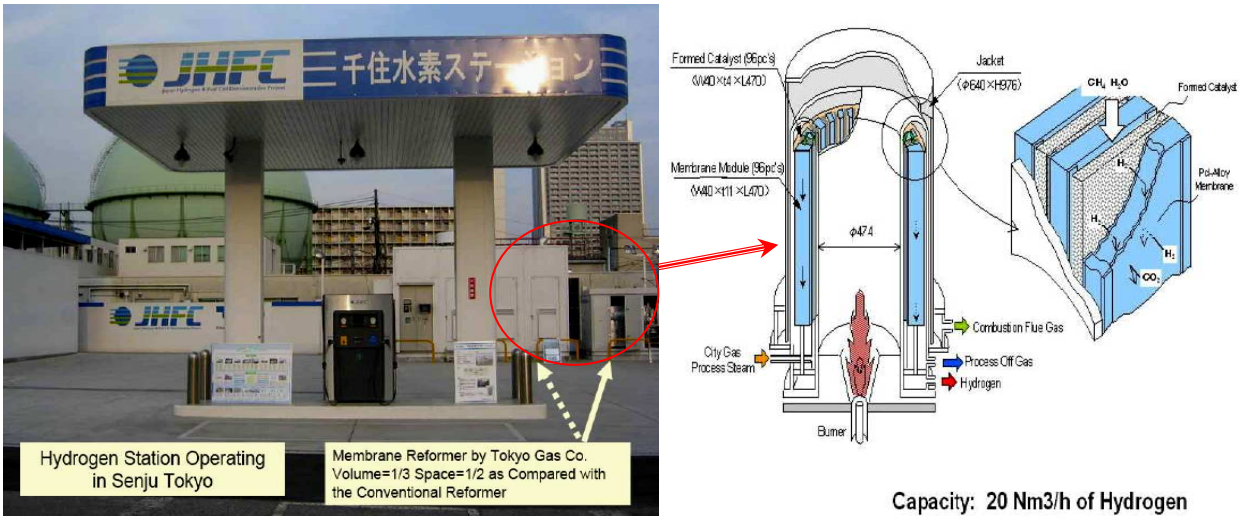

Fig. 8 - Membrane Reformer for H_2 purification *Tokio Gas Co.*[65, 66]

In the endothermic reforming reactions, the conversion is limited by the thermodynamic equilibrium as a result of their reversible character. These reactions produce a net increase in moles and are, then, favored by low pressure. They occur by means of the following mechanism:

Main reactions

$CH_4 + H_2O = CO_2 + 3H_2$ $\Delta H°_{298} = +206$ kJ/mol (1)

$CO + H_2O = CO_2 + H_2$ $\Delta H°_{298} = -41$ kJ/mol (2)

$CH_4 + 2H_2O = CO_2 + 4H_2$ $\Delta H°_{298} = +165$ kJ/mol (3)

Outside reactions

$2CO = CO_2 + C$ $\Delta H°_{298} = -172$ kJ/mol (4)

$CH_4 = C + 2H_2$ $\Delta H°_{298} = +75$ kJ/mol (5)

$CH_4 + CO_2 = 2CO + 2H_2$ $\Delta H°_{298} = +247$ kJ/mol (6)

The steam reforming reactions (1) and (3) occurs in presence of the water gas shift reaction (2), Boudouard equilibrium (4), cracking of methane (5) and methane dry reforming (6). The slightly exothermic WGS reaction prevails only at low temperatures (<400°C). A typical composition of natural gas is shown in table 4.

Table 4 - Typical composition of a natural gas feed.

Component	**Natural gas feedstock used in analysis (a)**	**Typical pipeline composition (b)**	**Typical range of wellhead components (mol%) (c)**	
	mol (%) (dry)	**mol (%) (dry)**	**Low value**	**High value**
Methane (CH_4)	94.5	94.4	75	99
Ethane (C_2H_6)	2.7	3.1	1	15
Propane (C_3H_8)	1.5	0.5	1	10
Nitrogen (N_2)	0.8	1.1	0	15
Carbon Dioxide (CO_2)	0.5	0.5	0	10
Iso-butane (C_4H_{10})	0	0.1	0	1
N-Butane (C_4H_{10})	0	0.1	0	2
Pentanes – (C_5^+)	0	0.2	0	1
Hydrogen sulphide (H_2S)	0	0.0004	0	30
Helium (He)	0	0.0	0	5
Heat of combustion, HHV	53,680 J/g (23,079 Btu/lb)	53,463 J/g (22,985 Btu/lb)	-	-

(a) Taken from SRI, 1994.
(b) Taken from Chemical Economics Handbooks (lacson, 1999) and adjusted to included H2S
(c) Taken from Ulmann's Encyclopedia of Industrial Chemistry, 1986.

Figure 9 is a flow-sheet of the natural gas steam reforming plant. Even if not showed, prior to steam reforming, the natural gas is pre-treated in a hydrogenation vessel in order to convert any sulphur compounds to H_2S. A small amount of hydrogen, which is recycled from the product stream, is used in this step. H_2S is, then, removed in a ZnO catalytic bed. After pre-treatment, both the natural gas and steam are fed to the primary reformer. At the industrial conditions (T = 800 – 950°C e P = 20 - 30 bar), the shift reaction becomes less important therefore the reaction enthalpy is positive (endothermic reaction) and carries on only at higher temperatures [67]. As

said, efficiencies about 65-75% are reached but it is necessary CO_2 capture obtained during the process [5]. Somewhat, these efficiencies are lower for smaller size units.

In the conventional process, natural gas reacts partially with steam on a Ni/Al_2O_3 – *based* catalyst in a heated tubular primary reformer to produce syngas in a H_2/CO ratio equal to 3. It feeds secondary reformer having refractory walls where un-converted methane reacts with oxygen. The most recent industrial configurations allow recovering the heat produced in secondary reformer and re-use it in the primary one. The resulting synthesis gas is cooled and, then, fed to two "*high temperature*" shift (HTS) reactors and, after, to the "*low-temperature*" shift (LTS) one where the water gas shift reaction converts 99% of the CO into H_2. The first two reactors work with Fe_2O_3/Cr_2O_3-based catalysts resistant at high temperatures (300-400°C) while the third works with Cu-based catalyst (200°C) so it allows an improvement of thermodynamic equilibrium [68]. The CO amount present in the hydrogen-rich streams, after their processing in WGS reactors, is close to 1%. In order to eliminate the CO traces different processes are utilized as the preferential oxidation (PrOx), methanation or PSA. However, the methanation implies a lost of hydrogen while the latter requires powerful and, therefore, more expensive compressors [69, 70], see figure 9. In modern hydrogen plants PSA method is used to separate hydrogen from the other components and reach higher quality (99.999% hydrogen purity against 95-98% for scrubbing systems [71]. The PSA off-gas is comprised of CO_2 (55 mol %), H_2 (27 mol %), CH_4 (14 mol %), CO (3 mol %), N_2 (0.4 mol %), and some water vapour. In older plants, CO_2 is subsequently removed by means of a chemical absorption unit. The primary reformer is often fuelled by means of the PSA off-gas, but a small amount of natural gas (4.4 wt% of the total reformer fuel requirement) is used to supply the balance of the reformer duty. The MSR process produces 4.8 MPa of steam which is used by some other processes or facilities. Electricity is purchased from the grid to operate the pumps and compressors.

Notwithstanding MSR occurs with an increase of number of moles, from an industrial point of view, the operation is carried out at high pressures (20-30 bars) in order to reduce the reactor volume [72] as well as the volume for all downstream equipments. This implies that besides high compression costs, the materials have to undergone strong mechanical stress. Moreover, though higher temperatures imply a huge thermodynamic advantage, this adds severe technical problems since the equipments are undertaken at high thermal stresses and the cracking reactions of methane are favoured. Carbon deposition deactivates catalyst surface. On the hot wall of the tube, it obstacles heat exchange towards the reaction zone [73] lowering considerably the temperature close to the wall and carrying out to "*cold-spots*" formation. As a result, only a fraction of combustion heat is used by reforming reaction. By utilizing water amount larger than

the stechiometric value it is possible to take away methane to the cracking reaction and avoid the coke deposition on the catalyst. But this increases the water consume in the plant. A characteristic range for H_2O/CH_4 ratio (H/C) is 2-6 depending from final use of syngas [72]. Modern plants are normally designed for high ratios (4-5) since these carry out at high hydrocarbon conversions [74]. However, by working via a low water amount has a huge advantage since it allows reducing both steam flow rate through the plant and the equipments size [73, 74].

The massive requirement of water, high temperatures and pressures carry out to an exaggerated expenditure of energy besides need to manufacture reformers in more expensive special Chrome-Nickel steel alloys. Low reaction temperatures are most convenient even if thermodynamic conversions of methane result too low to have a large industrial benefit. In addition, a technology allowing higher pressures would make hydrogen, for example the one used in cars, more attractive. As a consequence, the ultra-pure hydrogen production on small scale by means of such a conventional process results uneconomic and too complex for both high number of equipments and difficult scale-down of the plant.

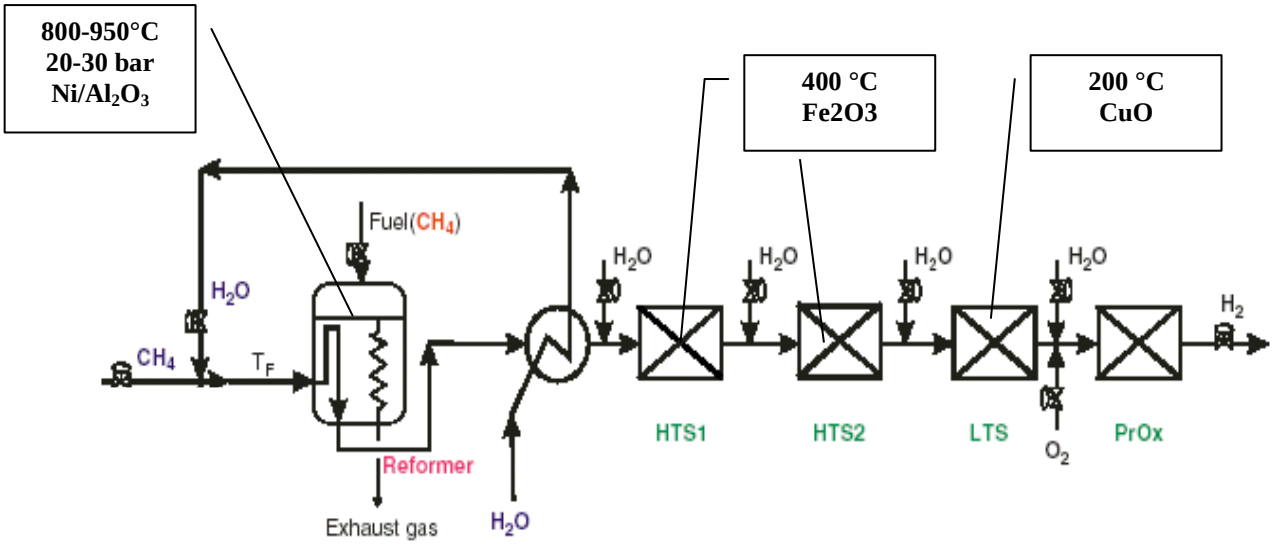

Fig. 9 - Detailed flow-sheet for conventional methane steam reforming process [75].

When small size systems must be realized, a useful approach to reduce operating costs is the use of reactors working at low temperatures and pressures. As previously observed, the operating limit of the temperature is established by the thermodynamic equilibrium value required to get to an appreciable conversion level during the reforming reaction. Moreover, the reaction and heat exchange rate must be optimized to minimize the reactor and plant size. For example, a reforming reactor for fuel cells applications having a 0.4-3 kW of power works at low

temperature (700°C) and pressure (3 bars). This allows reducing the building material cost. The investment cost for these small scale reformers coupled to compact fuel cells is around to 150-180 $/kW to produce from 20 to 200 $Nm^3\ d^{-1}$ of hydrogen every 100 units sold. By means of these reformers yields around 70-80% can be reached [76]. According to Duane *et al.* [77] the initial hydrogen generation from current gas stations based on gasoline will be based on MSR with a hydrogen production capacity of 50-100 $Nm^3\ h^{-1}$ and methane efficiency (or hydrogen to methane yield) of about 2.

2.1.1.1 Catalysts for methane steam reforming reaction

The transformation of methane to hydrogen is a challenging task because methane is extremely difficult to activate. As previously said, among all hydrocarbons the methane molecule has the largest H/C ratio (*i.e.* 4), substantially higher than that of *n*-heptane (*e.g.* 2.3) and much higher than that of a highly condensed poly-aromatic structure. The methane molecule is very stable, with C-H bond energy corresponding to a value of 439 kJ mol^{-1}; hence, it is resistant to many reactants.

The catalysts used in the MSR process are nickel, and all noble metals as ruthenium, rhodium, palladium, iridium, and platinum as the major metallic component. The noble metal catalysts have been used for steam reforming, but the higher cost has made their use prohibitive. Nickel supported on modified alumina (Al_2O_3) is the catalyst widely used for its low-cost and higher activity [18]. The catalytic activity depends on metal amount deposited on the support surface while catalyst properties are dictated by the severe operating conditions such as temperatures in the range of 700-1250 K and steam partial pressures of up to 30 bar. The main barrier of the MSR reaction is thermodynamics, which determines very high conversions only at temperatures above 1170 K. In practice, a significant part of the catalyst loaded into the tubes of the reformer is poorly utilized. For MSR catalysis, kinetic rates are reported and summarized by Xu and Froment [153] or, also, Rostrup-Nielsen *et al.* [78, 79]. These last, for example, have concluded that CH_4 reaction rates are limited solely by C-H bond activation steps and unaffected by the concentration of co-reactants. According to these studies, the following mechanism has been proposed:

$$H_2O(g) + * \rightarrow O*(a) + H_2(g) \quad (7)$$

$$CH_4(g) + 2* \rightarrow CH_3*(a) + H*(a) \quad (8)$$

$$CH_3*(a) + * \rightarrow CH_2*(a) + H*(a) \quad (9)$$

$$CH_2*(a) + * \rightarrow CH*(a) + H*(a) \quad (10)$$

$$CH^*(a) + O^*(a) \rightarrow CO^*(a) + H^*(a) \quad (11)$$

$$CO^*(a) \rightarrow CO(g) + * \quad (12)$$

$$2H^*(a) \rightarrow H_2(g) + 2^* \quad (13)$$

During the methane steam reforming reactions at high temperature on nickel-based catalysts, H_2O reacts with surface Ni atoms, providing adsorbed oxygen and gaseous hydrogen; adsorbed methane dissociates on the Ni surface, forming a methyl group (CH_x) that undergoes further stepwise dehydrogenation steps. They, then, react with the oxygen absorbed on adjacent site to produce CO on the catalyst surface. Other mechanisms suppose that at low temperature (500°C) OH groups are produced by water dissociation reaction and take part actively in the CO_2 formation [80, 81]. Instead, other studies regarding Ni-based catalysts supported on MgO or TiO_2 have taken in evidence the presence of some mechanisms according to which the intermediate CH_x adsorbed on the catalyst surface reacts, directly, with the surface OH groups so that the reforming reaction takes place [82]. Pistonesi *et al.* [74] have carry out a theoretical analysis regarding to the methane interaction with steam on Ni (111) catalyst surface. They have take in evidence that for low H_2O/CH_4 ratios both species are adsorbed on different catalyst sites while CHO group adsorb on atomic Nickel and OHs occupy preferentially a three-coordinate surface site. Instead, at high ratios their antagonist effect on the site reduces the conversion. Hughes *et al.* [83] have carry out a sequence of experimental tests regarding to the investigation of the kinetic for the methane steam reforming reaction in combination with the reverse water gas shift reaction on a commercial nickel-based catalyst ($Ni/\alpha\text{-}Al_2O_3$) in the integral reactor. In this analysis they have neglected the limitations due to the diffusion process. The experimental results confirmed that both CO and CO_2 were the most important products and methane disappearance rate linearly depends on the partial pressure at low product concentrations.

2.1.1.2 Main deactivation mechanisms of catalyst

Catalyst deactivation has important consequences for the design of a process and the manner as it is operated. The nature of the deactivation (sintering, poisoning, coke deposition etc., figure 10) as well as the time-scale determines the type of technology. The possibility of regaining lost catalyst activity, and the speed of deactivation are technical and economic factors that determine process options. For example, the process configuration, reactor type, and mode of operation of an industrial process can be influenced by the deactivation of the catalyst [84]. Figure 10 shows

some deactivation mechanisms on the catalyst surface that can occur during the heterogeneous reactions. Among these the main deactivations processes are sintering and coke deposition.

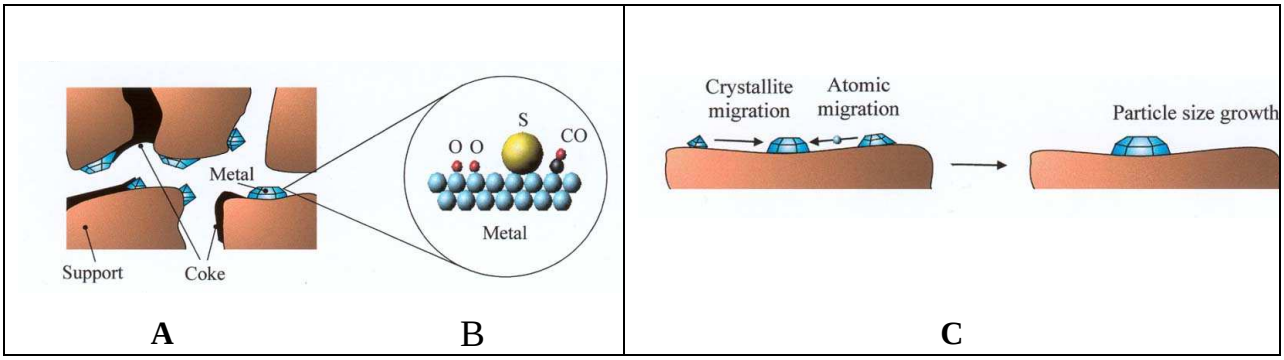

Fig. 10 - Deactivation mechanisms: A) **Coke formation**, B) Poisoning, C) **Sintering** of the active metal particles [85].

2.1.1.2.a Catalyst Sintering

As both figure 10**C** and the following detailed figure 11 show, the sintering is the loss of active surface of the catalyst due to crystal growth of the active phase. In the case of supported metal catalysts, reduction of the active surface area is provoked via agglomeration and coalescence of small metal crystallites into larger ones.

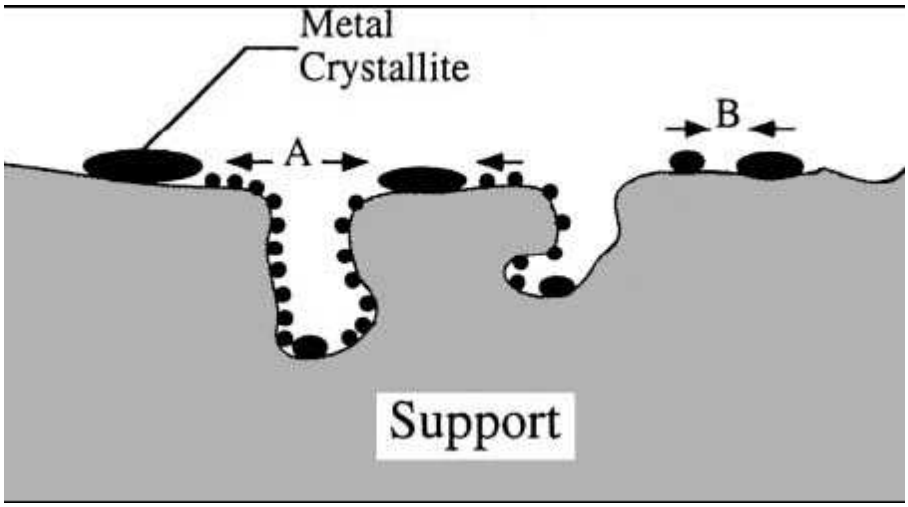

Fig. 11 - Two conceptual models for crystallite growth due to sintering by (A) atomic migration or (B) crystallite migration.

In general, *sintering* processes are kinetically slow (at moderate reaction temperatures) and difficult to reverse. They increase exponentially with the reaction temperature increasing (*i.e.* >500°C) and are accelerated by the presence of water vapour. *Sintering* can enhance, in a significant way, kinetic rate and limit coke formation. Two different models have been proposed for *sintering* process: 1) metal atoms migrating from one crystallite to another (atomic migration

model or *Ostwald ripening*), figure 11**A**; 2) migration of the crystallites along the surface followed by collision and coalescence of two crystallites (crystallite migration model) [86], figure 11**B**. The driving force for this process is the surface energy.

2.1.1.2.b Coke formation

In the production of H_2 from methane by means of reforming reaction, at low temperatures, the activated Ni catalyst is covered by a hydrocarbon layer which degrading slowly into a polymeric film blocks the nickel surface. There are three different well-defined morphological structures for the deposited carbon [78]:

1. **whisker-like** carbon;
2. **encapsulating** carbon;
3. **pyrolitic** carbon.

For instance, at high temperatures the pyrolysis of higher hydrocarbons produces ***pyrolytic coke*** which encapsulates the catalyst particles [76]. ***Whisker carbon*** is the most common and the most destructive form of carbon produced in steam reforming reaction over nickel catalysts.

Under MSR conditions nickel carbide is not stable. Therefore, carbon nucleates in the form of filaments with a small Ni particle at the top of each fiber and grows at a constant rate after an induction period [78, 87-88] by following this mechanism:

$$CH_4 + * \rightarrow CH_x* \quad (14)$$

$$\begin{aligned} CH_x* &\rightarrow C_\alpha \searrow \\ &\rightarrow C_\beta \leftrightarrow [C, Ni]_{\text{bulk, dissolution}} \rightarrow \text{Carbon Whiskers} \end{aligned} \quad (15)$$

$$CH_x* + OH_y*(a) \rightarrow CO*(a) + H*(a) \quad (16)$$

$$CO*(a) \rightarrow CO(g) + * \quad (17)$$

$$2H*(a) \rightarrow H_2(g) + 2* \quad (18)$$

Such growth of filaments dirties the metallic surface (deactivation), blocks both the catalyst pores and voids among catalyst particle besides generate a mechanical break-up of the catalyst support [2, 89]. The formation of carbon, either dissolved in or deposited on the nickel, requires the polymerization of monatomic carbon species (C_α) whereas their gasification implies necessarily the transformation in carbon species C_β, figure 12. Obviously, the formation of different species demands more surface sites. Because the MSR requires the dissociation of methane to form a carbonaceous intermediate, coke formation would be characterized by an

ensemble of surface sites which number is larger than that necessary for the reforming reaction. Then, by controlling the number of sites in a given ensemble it may be possible to minimize coke formation during the reforming reaction [76].

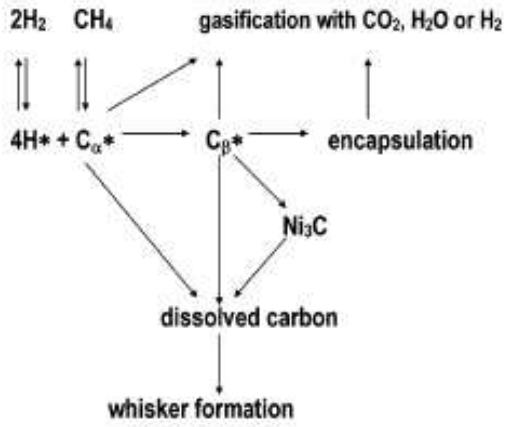

Fig. 12 - Carbon formation and gasification routes during the steam reforming of methane [76].

For high temperatures MSR reaction in a traditional reactor, deactivation of supported metal catalyst by means of carbon deposition is a very severe problem. Several approaches can be followed to minimize coke formation on Ni or other metal surfaces: 1) Ni particles size control and 2) the addition of small amounts of dopant [90]. However, carbon formation is avoided when the concentration of carbon dissolved in the nickel crystal is smaller than that at equilibrium or when the steady state carbon activity is smaller than one. In fact, it is decreased if the adsorption of steam or CO_2, the rate of the surface reaction is enhanced or the rate and degree of methane activation and dissociation are decreased.

In the MSR process, the reduction of CO content in the mix downstream of the reformer is carried out by means of three WGS reactors. This reaction is a well-know exothermic reaction, with equilibrium constant increasing in reverse order with the temperature, see equation (2). It is one of the most important industrial reactions that can be used to produce hydrogen, *e.g.* for ammonia synthesis, adjust the hydrogen-to-carbon monoxide ratio of the synthesis gas and detoxify gases [142]. A larger number of metals (Fe, Cu, Zn, Cr, Co, Ni), metal oxides and mixed oxides have been proposed and patented to catalyze the WGS. In industry, Fe_3O_4-Cr_2O_3 and $CuZn/Al_2O_3$ are being used exclusively [117]. The Fe_3O_4-Cr_2O_3 catalysts are used, as previously observed, at 300-400°C where the equilibrium affects the composition of the product. Therefore, in industry, this reaction is often run in two stages to ensure the total conversion of carbon monoxide to carbon dioxide. The catalyst used in the second stage is $CuZnO/Al_2O_3$ which is active at 200–250°C.

Chapter 3

3.1 A novel technology for Hydrogen Separation: Membrane systems

In the latest years, the environmental problems derived from the use of fossil energy sources as well as the increment of fossil fuels price are addressing towards the development of new technologies for a more clean and economic energy production [17]. As previously considered, high-purity hydrogen is required for fuel-cell operation to reduce as possible greenhouse gas emissions. But a large amount of gaseous or liquefied hydrogen is not easy to storage both stationary and on-board transport applications. Moreover, the CO concentration in the hydrogen fuel stream should be controlled to a very low value that is usually less than 20 ppm when polymer-electrolyte type fuel cells are operated.

Instead of carrying hydrogen, advanced systems as Membrane Reactors (MRs) can be combined to the polymer fuel cells so fuels like natural gas are directly converted in high-purity hydrogen.

The issues related to MRs entail choice of a suitable membrane for a given product quality and throughput required. For a given membrane material, it is important to assess the effect of feed quality and operating condition on the stability and robustness of membrane. Other important factors that must be considered are: the mass transport characteristics through the membrane material, purity of the hydrogen required and the pressure at which it is obtained. The improvement in the performance of MRs, as for industrial applications, needs to integrate these aspects both from design and operation point of view within the MSR reactor. In an integrated framework, the result is the compatibility of the separation of H_2 by the membrane with the rate of production.

In a long term operation at industrial level, the integration of H_2 transport membranes with reformers opens new possibilities for highly efficient and low-cost pure hydrogen production [91]. Obviously, the scale of many of these potential processes may demand that some of membrane operations involve sizable membrane reactor volumes and surfaces, thus necessitating potentially higher capital costs.

Apart from electro-chemical catalytic reactions in the fuel cells which work at low temperature, high temperature and chemical harsh environment are generally encountered for reforming reactions. These two factors strongly favour the inorganic membrane use for MRs applications. Consequently, the membranes manufacturing is a key factor to increase commercial availability of MRs so far as they still need optimization and new developments.

3.1.1 Inorganic Membranes

There are at least four types of inorganic membranes [16]:

1. ***Precipitated oxides*** onto mesoporous support. By producing small particles and packing them tightly together on top of mesoporous support one can produce a pore structure with <20 Å micropores. The drawbacks for these membranes are that they are subject to surface chemistry of oxide, delamination, and superficial defect. Moreover, heating such material above and below their preparation temperature can often cause collapse or change in the pores size. In addition, these membranes can not be easily scaled to larger membrane devices.
2. ***Zeolites***. The growth of zeolite layer occurs by a stack of zeolite crystals in soldier-like array. The drawbacks are that the absorption of components changes with the temperature, so the perm-selective characteristics of the membrane can change too.
3. ***Carbon based membranes*** are obtained by decomposition of an organic material at high temperatures that produces a dense layer having a microporous sieving network. They can be used to recovery hydrogen from targeted refinery streams. However, it is still difficult to realize microcracks-free and strong carbon membranes by means of a continuous process. This limits their application at an industrial level.
4. ***Dense metal membranes*** have had a great deal of attention because they are commercially available in a variety of compositions. Unfortunately, there are only a limited number of applied separations by perm-selective membranes as, for example, Pd-*based* or Ag–*based* alloys for hydrogen or oxygen separation, respectively. Development of these membranes has been limited by manufacture capability and availability of a wide composition of alloys and cost.

Membranes that selectively transport atomic hydrogen are vital to the hydrogen economy since they allow purifying hydrogen fuel streams in a simple way.

3.1.1.1 Transport in palladium-based membranes. Theoretical aspects

Hydrogen permeation is a complex mechanism said "*Solution-Diffusion*" that starts by the hydrogen molecules adsorption from gaseous bulk to the palladium surface of the upstream metallic layer. These molecules separate in atoms to the interface gas-metal and, subsequently, solubilize in metallic bulk. They diffuse in the metallic bulk up to the downstream palladium surface. At this interface gas-metal, these atoms rearrange to form, again, hydrogen molecules that reach the gaseous bulk by desorbing (figure 13).

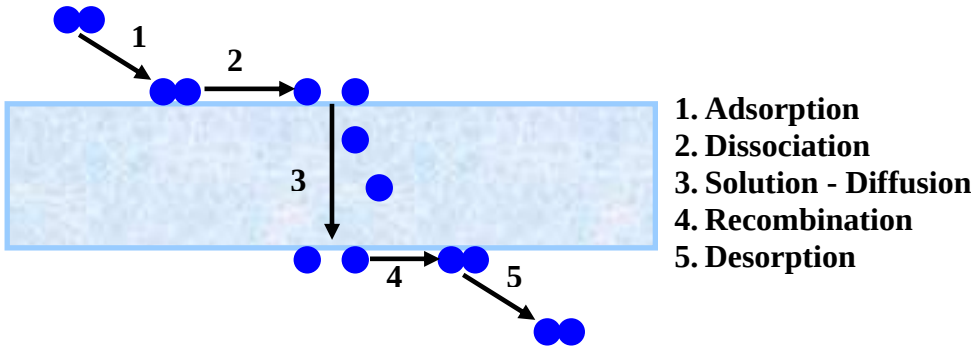

Fig. 13 – "Solution-Diffusion" mechanism in a palladium-based membrane.

The following theoretical expression describes the earlier process [24]:

$$J_{H_2} = \frac{D_{H2}}{\delta} \cdot \left(c^{n}_{H_2,ret} - c^{n}_{H_2,perm} \right) \qquad (19)$$

where $\mathbf{J_{H2}}$ is fickian hydrogen flux (mol m^{-2} s^{-1}) and $\mathbf{D_{H2}}$ is the hydrogen diffusion coefficient through the membrane (m^2 s^{-1}), **δ** is the membrane thickness (μm), $\mathbf{c_{H2,ret}}$ is the hydrogen concentration in the metallic bulk on retentate side (upstream side in mol m^{-3}) and $\mathbf{c_{H2,perm}}$ is, instead, the hydrogen concentration on permeate side (downstream side in mol m^{-3}) while **n** is a exponent that can oscillate from 0.5 to 1. When bulk diffusion is the rate-limiting step, the permeation rate through the palladium-*based* membranes is controlled by the diffusion in metallic lattice and the hydrogen transport obeys the Sieverts' law [19]:

$$c_{H_2} = K_s \cdot \sqrt{P_{H_2}} \qquad (20)$$

This represents the relationship between hydrogen concentration in metallic bulk ($\mathbf{c_{H2}}$) close to the surface directly exposed to gas stream and hydrogen partial pressure (*i.e.* retentate or permeate side) and is valid if hydride phase (**H/Pd**) is **α** and hydrogen concentration in the metallic bulk is low, see figure 14. In practical applications, the pure palladium membrane is restricted since hydrogen embrittlement can be caused by the phase transition from **α** to **β** palladium hydride at temperatures below 573 K and pressures below 2 MPa [19], figure 14. By effect lattice expansion, micro-cracks result inside the bulk metal. Moreover, these phase changes are very dependent from pressure and temperature. Thus, in many cases the operating temperature of the pure Pd membrane must be kept strictly above 573 K to avoid hydrogen embrittlement. Instead, the critical temperature for **α** → **β** phase transition is dependent on the operation pressure. For example, Elkina *et al.* [92] found that for a 25 μm thick Pd foil, the **α/β** phase transition temperature was 478 K when the H_2 feed pressure was set at 5.1 bar, and the

transition temperature decreased to 457 K when the H_2 feed pressure was decreased to 3.4 bar. The use of palladium alloy reduces the embrittlement hazardous since critical temperature is increased over 573 K. Moreover, in presence of definite metal alloying concentrations an enhancement of hydrogen permeation rate is obtained in comparison with the pure palladium behaviour. For what concerns the Pd/Ag alloy it reaches a maximum around 25 wt. % [3, 19].

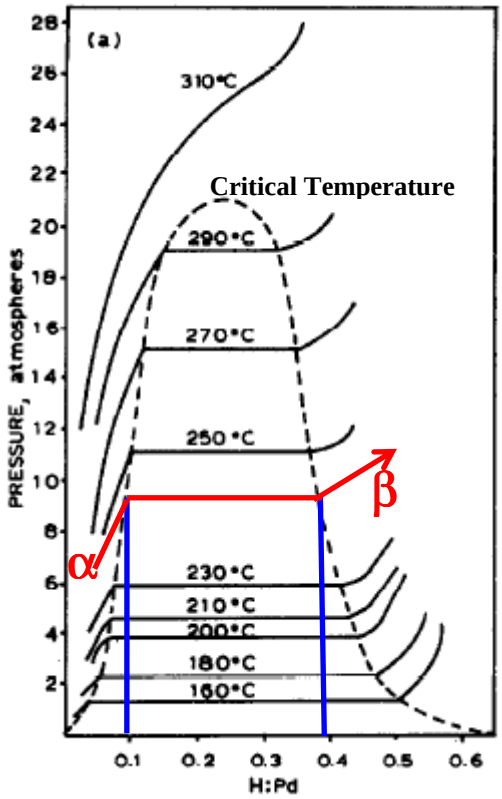

Fig. 14 - Phase transition from α to β palladium hydride at temperatures below 573 K and pressures below 2 MPa.

When the earlier expression is introduced in the hydrogen flux equation, it generates the following expression according to the Sieverts' law:

$$J_{H_2} = \frac{D_{H_2} \cdot K_s}{\delta} \cdot \left(P_{H_2,ret}^{0.5} - P_{H_2,perm}^{0.5} \right) \qquad (21)$$

where $\mathbf{Pe_{H2}}$ is obtained as product of hydrogen diffusion coefficient ($\mathbf{D_{H2}}$) and solubility constant ($\boldsymbol{K_S}$) in accordance to Sieverts' law. It represents an important parameter that characterizes inherently the palladium-*based* metallic membrane and it is called "hydrogen permeability" in (mol m m^{-2} s^{-1} $Pa^{-0.5}$). The ratio between hydrogen permeability and the membrane thickness is said, instead, "hydrogen permeance" (mol m^{-2} s^{-1} $Pa^{-0.5}$). The permeation rate or hydrogen flux is inversely proportional to the thickness of the membrane if, as previously mentioned, bulk diffusion is the rate-limiting step. It is usually valid for thick membranes. The exponent **n**

assumes the value equivalent to 0.5. The inverse dependence to the thickness will change (*e.g.* by the **n** value) if other transport steps become limiting. In fact, deviation from Sieverts' law (**n** > 0.5) have been often reported for the membranes with thickness about few microns since surface processes (dissociative adsorption, absorption, recombinative desorption and bulk metal-to-surface transition) may become the rate-controlling step for permeation through the membrane under this condition [93-95].

3.1.1.2 Membranes preparation methods. Outlines

The most important technique used to deposit palladium on either ceramic or metallic supports, both required to strength the membrane, is *electroless plating* [96]. However, other techniques can be also utilized as *electroplating* [97], *chemical vapour deposition* [98] and *cold rolling* and *annealing* technique [99] each one having appropriate characteristics. Zhang *et al*. [100] have synthesized by means of a modified *electroless plating* method palladium membranes, on ceramic tubular supports, having high efficiencies. These membranes could be potentially applied to the enrichment of the hydrogen streams coming from ammonia cracking. Shu *et al.* [58], instead, have prepared different Pd/Ag alloy asymmetric composite membranes utilizing *electroless plating* method followed by thermal treatment with hydrogen. They accomplished Pd-*based* alloy development by overcoming the *Tamman* temperature during the thermal treatment (*i.e.* ***Tamman*** temperature corresponding to half the melting temperature and is considered the point at which *sintering* starts in ceramics materials). These membranes were utilized in a reactor to carry out the MSR. At different experimental conditions, they reached an increase of methane conversion in less severe temperatures and pressures conditions. Tong *et al.* [101] have synthesized by means of *electroless plating* technique Pd-based membranes on porous stainless steel tube. These membranes have a thickness of 10 μm. However, in order to avoid the development of micro-defects on palladium film surface, they deposited also ZrO particles inside the pores. Experimental tests evidenced that the permeation rate was controlled by the surface diffusion in the pores. Dittmeyer *et al.* [102, 103] have tested different composite palladium-*based* membrane preparation methods on both ceramic (*electroless plating*) and stainless steel supports (*electroplating, chemical* e *physical vapor deposition, high velocity oxy-fuel spraying*) for dehydrogenation reactions. Further and more innovative improvements are realized continually on materials and structures supporting selective metallic film as *e.g.* porous glasses, ceramic and stainless steel substrates, as well as on nano-structured carbide. Among diverse substrates studied, porous stainless steel is the most favourable for large-scale applications since it is resistant to the corrosion and, additionally, the value for its thermal

expansion coefficient is close to the one for the palladium. Therefore, mechanical and thermal stresses between different materials at contact are minimized. The main drawback is the interdiffusional process of metals, making up the support, in the Pd-*based* membrane at high temperatures.

3.1.2 Basic configurations of Membrane Reactors

Many research efforts have been devoted to the MRs in combination with studies on catalysis, membrane science and chemical engineering. In such an "integrated" system, the membrane is used as an active contributor in a chemical transformation for increasing the reaction rate, selectivity and yield. The concept of combining membranes and reactors is being explored in various configurations which can be classified in three main groups, related to the role of the membrane in the process:

1. ***Extractor*** where the selective removal of a reaction product increases the per-pass conversion by shifting the reaction equilibrium compared to conventional fixed-bed reactors;
2. ***Distributor*** (or selective enhancer) where the controlled addition or selective permeation of reactant limits side reactions;
3. ***Active contactor*** where the controlled diffusion of reactants to the catalyst can lead to an engineered catalytic zone.

New emerging applications (MRs with separate feed of reactants, catalytic filters and traps, slurry MRs, etc.) have been recently investigated which do not require membrane perm-selectivity to gases and, therefore, appear to be closer to industrial success [3].

3.1.2.1 Technological problems in MRs

The most difficult and common aspect regards the seal between the membrane and the rest of reactor unit that becomes a process limitation determined by materials incompatibility. For example, it is difficult to fix palladium alloys to steel or ceramic walls since coefficients of thermal expansion are different enough that on temperature cycling the seals can weaken and fail destroying the membrane layer.

As previously said, the current development of MRs is limited by not having membrane materials highly permeable and being able to manufacture membrane systems having productivities acceptable for the chemical industry. Productivity of a reaction is limited by the amount of surface area available to the permeation process. From a practical point of view,

differently from a catalyst particle, selective membrane material has to have no real micro-porosity and this implies a very limited surface area for gas permeation. A way to circumvent this limitation could be, for example, to manufacture membrane systems having particular pattern flow (*e.g.* cross-flow channels) which favour the contact between the gas and surface area. But, actually, this is difficult to be realized. In addition, thickness slows down the transport of permeating species if the membrane has not a sufficient permeation rate. For instance, the reaction products (*i.e.* H_2) must find their way to the walls and permeate the membrane without first being swept away in the retentate stream. For what concern the hydrogen, it must desorb from the surface of the catalyst, and reach the membrane. Here it is dissociated, in accordance with the typical mechanism in palladium membranes, at a feed rate so to have sufficient time for the permeation.

One of the clear hurdles in the development of inorganic membranes in catalytic membrane reactors appliances is the life of the membranes (thermal, chemical and mechanical stability) in addition to the ability to repair it during the operation. While, regarding to on bench-scale applications this means to replace the membrane, from a commercial-scale point of view this is an unacceptable technical solution for higher operating cost.

The other important issues of concern are the catalyst deactivation and control of the reactor configuration. Significant developments have been carried out in various reactor configurations under both kinetic [6, 104] and equilibrium conditions [14, 105]. These studies were aimed at determining the effect of various parameters such as reaction temperature and pressure, steam to methane ratio, sweep gas flow rate, and the operating mode (co-current or counter-current) on the overall performance. But they did not consider evaluation of membrane area and energy requirements that definitely affect the fixed and operating costs of the plant specifically in an integrated framework with other processes. Recently, Bottino *et al.* [106] proposed a model for non-adiabatic industrial MSR under equilibrium conditions to study the effect of operating parameters on these two important aspects. Their investigations revealed that temperature profile plays a significant role in process economy and development of thin and permeable membranes is a key issue for improving the performance of large industrial plants.

3.1.2.2 Pd-*based* Membrane Reactors. State-of-the-art

During an equilibrium-limited reaction (*e.g.* reforming and water gas shift), by removing selectively and continuously hydrogen through the membrane the chemical equilibrium shifts towards the products. Thus, it is possible to get to high methane conversions and exceed

thermodynamic equilibrium limitation of a traditional reactor (TR). Figure 15 shows the operation of a typical membrane reactor.

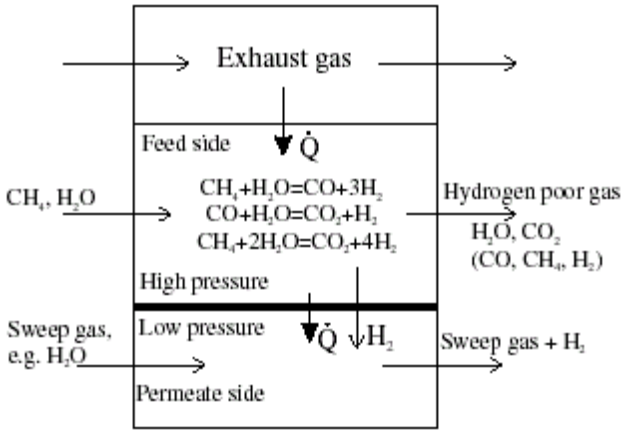

Fig. 15 - Common flow-sheet of a membrane reactor with sweep gas according to Johannessen *et al.* [107]

As an attractive technique able to carry out in single equipment two different unit operations, MR is integration of a hydrogen perm-selective Pd-based membrane in a conventional reformer.

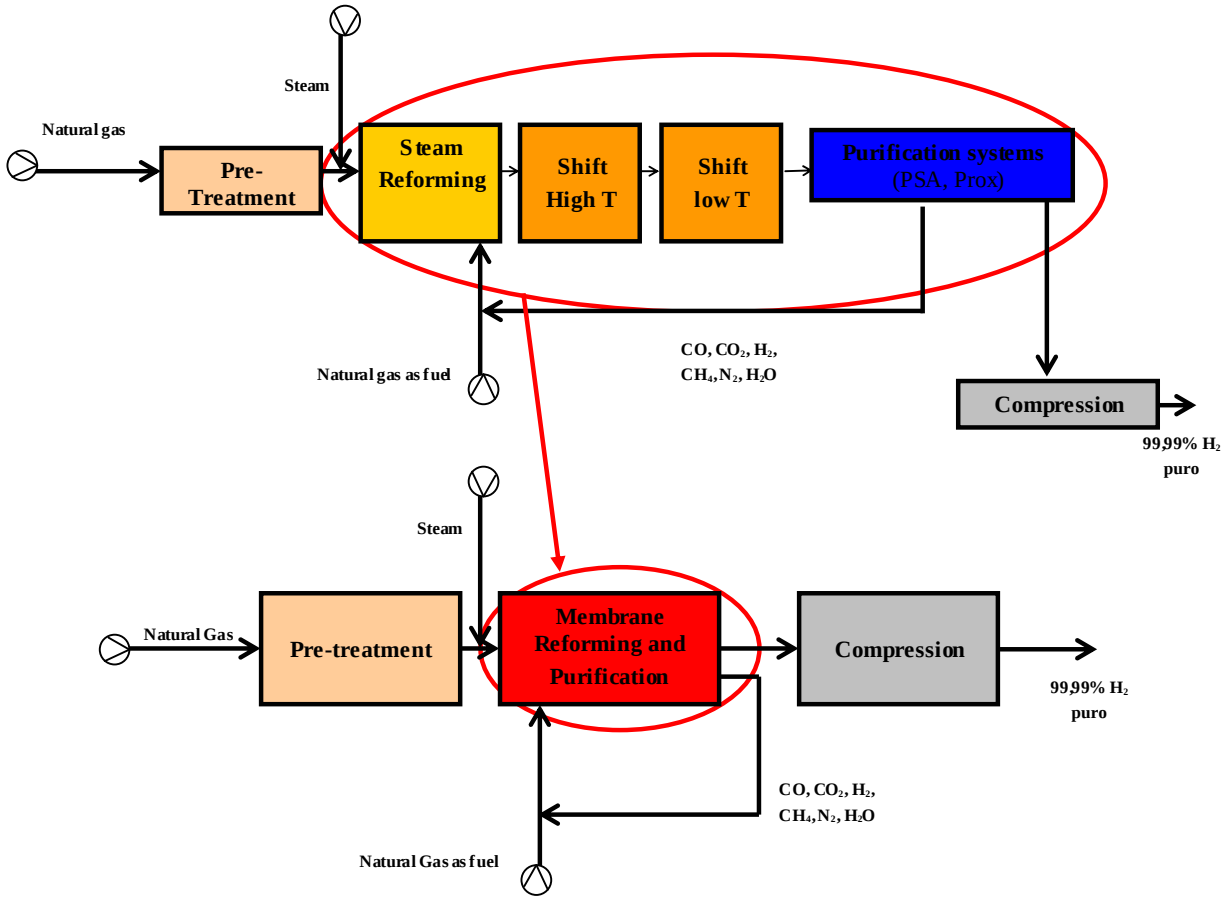

Fig. 16 – Process intensification and process integration by membrane reactors in MSR process.

This satisfies, contemporarily, both the requirement to recover pure hydrogen and reach high yield at less severe operating conditions and higher overall energy efficiencies. In the steam reforming, the membrane reactor can generate a high pressure retentate stream that is more concentrated in CO_2, and in some cases, at a low CO content. This adds huge advantages since it makes easy CO_2 capture as well as simplifies steps for water gas shift reaction.

Due to MR, a high degree of process integration and intensification can be accomplished. In fact, a MR allows to reduce the number of process units as well as the total required reactor volume (or the membrane surface), then the load to the downstream separation steps, maintenance costs and to simplify the heat management in the process [151].

All this, for example, determines an economic scale-down of steam reforming process and its simplification. As mentioned, small-scale plants reduce the problems of storage and transportation besides to have poorer investment and operation economics even in stationary applications. Thus, the future technology aims at the design of compact, easy to use, and highly integrated MSR plants for power generation, specifically, for both stationary and on-board fuel cell applications. Figure 16 shows the scale-down for the reforming, shift and separation steps, respectively [152]. For all these reasons, MRs can guarantee a straightforward and economic small scale hydrogen production.

For innovative applications of MRs, it is necessary to combine appropriately the hydrogen amount produced during the reaction to that removed through the membrane. It is important to evaluate accurately the flow-rates for different operating conditions in order to determine the hydrogen amount produced. Moreover for an optimal combination between steam reforming reaction and membrane, another parameter has to be necessarily taken into consideration: hydrogen permeance coupled to the required membrane surface area. However, from an industrial point of view for reforming reaction, the need to work in more severe operating conditions can further enforce the employment of MRs having high thermal, mechanical and chemical stability.

The first attempt to apply palladium-*based* MRs for this kind of reaction was accomplished by Oertel [7]. Bredesen *et al.* [108] have analysed a MSR process by using metallic membranes. They obtained that reforming reaction by membranes becomes interesting only if electricity cost is very low and the hydrogen selectivity of the membranes is next to 100%. Chen *et al.* [25] have investigated the hydrogen production by means of steam reforming of liquid hydrocarbons utilizing nickel-based catalysts in packed bed reactors with palladium membranes. The experimental results showed the membranes produce an efficient separation and hydrogen recovery even if a higher reduction of methane conversion is achieved. Shu *et al.* [58] have

prepared diverse asymmetric palladium/silver-*based* membranes to use in a MR for MSR reaction. At different operating conditions, they have obtained an increase of conversion in less severe conditions of temperature and pressure by virtue of the hydrogen extraction through the membrane. In fact, at 136 kPa, 500°C and a feed molar ratio equal to 3 methane conversion was 1.4 times higher in MR than in a conventional reactor. Tong *et al.* [8] have studied MSR reaction by using palladium-*based* membranes in the temperature range of 500-550°C. They were able to get to high methane conversions. In particular, they evaluated the performance of two different MRs having thickness of 11 and 8 μm, respectively. By these experimental results, MRs gave the same methane conversion since catalytic activity to produce hydrogen was not sufficient to counterbalance the shift of the equilibrium by means of membrane. In addition, they have confirmed that both a high catalyst activity and high permeation through the membrane are required to reach a high methane conversion in high space velocity conditions. Willms *et al.* [26] have showed a nickel-*based* catalyst in a MR was efficient to allow a high pure hydrogen recovery by steam reforming reaction of methane. When the temperature increased from 450°C to 600°C, the MR performance improved progressively. By investigating hydrogen permeation through palladium-*based* membranes and MSR in isothermal conditions, Kleinert *et al.* [67] have obtained methane conversions over 96%. Experimental results have put in evidence that high conversions can be reached with a lower coke formation by working at a low feed molar ratio, at high temperatures (>800°C) and a feed pressure around 170 kPa (1.7 bar).

For what concern the experimental study of high pressure in a MR, Lee *et al.* [98] have investigated the antagonistic effects of pressure on reaction equilibrium and permeability in a MR for the catalytic dry-reforming of methane reaction. In the same way as steam reforming of methane, it produces a net increase in moles and is disfavoured by high pressures. The studies were carried out at non-equilibrium conditions in an MR with a hydrogen-selective ceramic membrane and a packed-bed reactor at various pressures (1-20 atm) and temperatures (873 and 923 K) using a Rh/Al_2O_3 catalyst. Because of the concurrent and selective removal of hydrogen from the reaction zone in the MR, the rate of hydrogen separation increased with increasing pressure while the conversions of the reactants decreased. The maximum was due to a trade-off between a transport property (hydrogen separation) and a thermodynamic quantity (hydrogen production) which had opposing pressure dependencies. Hacarlioglu *et al.* have studied both theoretically by means of a model [109] and experimentally [110] the effects of temperature and pressure on the MSR in a membrane reactor with a hydrogen permeable silica-*based* membrane at various temperatures (773-923 K) and pressures (1-20 atm) using a commercial $Ni/MgAl_2O_4$ catalyst. In particular, from an experimental point of view, the author has found that the

conversion of methane was improved significantly in the MR by the counter-current removal of hydrogen at all temperatures and allowed product yields higher than those obtained in equilibrium conditions. Also in this case, they noted that high pressure has a positive effect on the hydrogen yield since it increases driving force for the hydrogen permeance. The hydrogen yield reached a constant value, at 20 atm and 923 K, and higher by 108% than that obtained at the equilibrium. Chen *et al*. [111] have investigated an ultra-thin, high performance composite palladium MR for MSR reaction under the following working conditions: temperature 723–823 K, pressure 300–900 kPa, gas hourly space velocity (GHSV) 4000–8000 ml g^{-1}_{cat} h^{-1}, steam-to-carbon feed ratio (S/C, mol/mol) 2.5–3.5 but with sweep gas on shell side. The results indicated that selective removal of H_2 from reaction zone produced methane conversions much higher and CO selectivity significantly lower than those obtained in a traditional reactor under thermodynamic control. For instance, 98.8% methane conversion and over 97.0% of the selectivity to CO_2 are obtained. The much higher performance of MR was attributed to the combination of hydrogen ultra-permeable Pd-*based* membrane, highly active catalyst for MSR with counter-current sweep gas flux design. Tong *et al.* [112] have investigated steam reforming of methane over a ruthenium catalyst at 500°C in a membrane reactor equipped with a palladium membrane supported on a porous stainless steel tube. Hydrogen is selectively permeated through the membrane. The methane conversion significantly exceeds the equilibrium value, which is low at 500°C. The selectivity to carbon monoxide by-produced in the reaction is lower than that expected from the equilibrium. Thus, although the equilibrium conversion decreases with an increase in the reaction pressure, the conversion with the MR can increase because the hydrogen separation is promoted by the pressure increasing. The catalytic activity is resulted an important factor to produce a sufficiently high methane conversion and it is enhanced at a high reaction pressure. Tsuru *et al*. [113] have investigated both by means of a simulation and experimentation the hydrogen production by steam reforming of methane using catalytic membrane reactors. The MR simulation, using an isothermal and plug-flow model with selective permeation, was carried out to evaluate the effect of perm-selectivity on MR performance (methane conversion and hydrogen yield) at 10 atm and 500°C. Increased performance for the production of hydrogen was experimentally obtained with an increase in reaction-side pressure up to 500 kPa which agreed with the theoretical simulation.

For what concerns the study of catalyst distribution to improve the MR performance in the MSR process, Caravella *et al.* [149] have developed a numerical model of a permeative-stage MR for hydrogen production to investigate, at various temperatures and membrane thicknesses, the importance of the catalyst and membrane area axial distribution on the reactor performances.

They have shown that a higher conversion than in conventional membrane reactors can be achieved. The main result of this analysis is a much higher maximized recovery factor (+21% ca.) than the conventional MR.

Much interest towards the water gas shift (WGS) reaction assisted by MR has been also evidenced in literature. Seok and Hwang [143] evaluated the performance of the WGS reaction by using Vycor glass coated with ruthenium (III) cloride trihydrate. The reaction was carried out under various operating conditions of temperature, pressure and feed composition. The highest CO conversion obtained was 85% (equilibrium value 99.9%) at relatively low temperature (430 K) and at a permeate rate of 0.64 cm^3 min^{-1}. Complete conversion (100%) was obtained by Kikuchi *et al.* [144] and Uemiya *et al*. [145] at 673 K using a double tubular type MR, in which the inner tube consisted of a thin palladium film. An important application of the WGS assisted by MR is the tritium recovery process from tritiated water coming from breeder-blanket fluids of the fusion reactors. The hydrogen isotopes separation at low concentration level in gaseous mixtures is a typical problem of the fusion reactor fuel cycle since the tritium produced in the breeder needs a proper extraction process to reach the required purity level. Yoshida *et al.* [146] carried out experimental and theoretical studies regarding a catalytic reduction method for application to the tritium recovery process from tritiated water in fusion reactor system. They demonstrated that this method allows the tritium recovery from tritiated water with a high conversion value (>99.99%) at a relatively low temperature.

Chiappetta *et al.* [147] have investigated in non-isothermal and non-adiabatic conditions both mass and heat transport by a theoretical model as well as the effect of working temperature, pressure, sweep flow rate, molar feed ratio on the MR performance for the exothermic WGS reaction. In addition, they analysed the inherent safety aspects of a MR at different working conditions by using the HAZOP technique. Always Chiappetta *et al.* [131] have carried out a sensitivity analysis to define the role of some variables on the performance of a MR for maximizing the system efficiency. The behaviour of MR has been investigated by means of a 2-D mathematical model applied to the WGS. By depending on operation feed pressure, a specific choice of both sweep gas flow rate and temperature can limit the occurring of dangerous temperature hot spots without compromising the performance of the system. The catalyst distribution coupled with an efficient heat exchange across the membrane has been investigated as well. It can be considered as a technical solution adequate to control temperature *hot-spots* along the MR.

In terms of process intensification (PI), Chiappetta *et al*. [148] have carried out a theoretical analysis regarding the potential of integrated membrane systems to recover hydrogen at a very

high purity level (with CO content lower than 10 ppm), suitable for fuel cell applications. Both polymeric and palladium separators as well as Pd-*based* MRs have been investigated. They have concluded that as a low driving force is available (*e.g.* 5 atm), the combination that seems to be the most convenient assumes that the syngas mixture is first fed to the two-stage polymeric membrane unit, then the permeate stream is further treated in a palladium separator while the retentate streams are processed in two palladium MRs. On the contrary, at 10 atm a single polymeric stage followed by a palladium separator and palladium-*based* MR represents the most adequate solution because a comparable membrane surface is combined to lower compression power and H_2 losses. Brunetti *et al.* [150] have investigated WGS in a Pd-alloy MR by means of a non-isothermal mathematical model using, as main parameter, Damköhler's number (*Da*), the ratio of characteristic times of flow rate and reaction, in a temperature range of 220–320°C with no sweep gas. In this work a feed pressure ranging 200–1500 kPa has allowed a good H_2 recovery index (up to 95%) as well as a retentate stream rich (up to 80%) in CO_2. In addition regarding the process intensification strategy, they employed both volume and conversion *index* as simple tools for the analysis of MRs for H_2 production and CO_2 separation.

3.1.2.3 Coke formation effect on MR performance

Catalyst deactivation represents a technical as well as an economic factor since it may have effects on the performance of a given type of reactor and, hence, the economics of the process. Consequently, different reactor technologies and process configurational choices are possible. The exiting relation between catalyst deactivation, process design and operation has carried out to the development of novel technologies that counterbalance the problems set by the same deactivation of the catalyst. They open the possibility to the novel catalysts application or the use of unconventional conditions that can lead to a more economic or improved process.
The metallic nickel is a catalyst for both endothermic methane reforming and cracking reactions that are characterized by an increase of number of moles, as equations (22)-(24) show:

$$CH_4 + 2H_2O = CO_2 + 4H_2 \qquad \Delta H°_{298} = + 165 \text{ kJ/mol} \qquad (22)$$

$$2CO = CO_2 + C \qquad \Delta H°_{298} = - 172 \text{ kJ/mol} \qquad (23)$$

$$CH_4 = C + 2H_2 \qquad \Delta H°_{298} = + 75 \text{ kJ/mol} \qquad (24)$$

At a low temperature is more difficult to form carbon by CO disproportionation (23) since the yield in CO is low in comparison to CO_2.

In a conventional reformer, temperatures, gas compositions and catalyst activity can influence both direction and kinetic rate for methane cracking reaction, see figure 17.

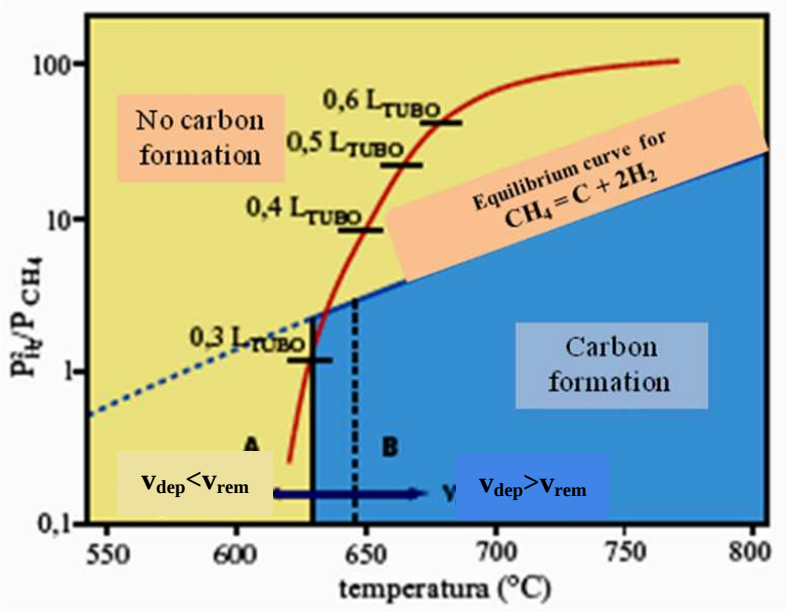

Fig. 17 – Trend of the composition vs. temperature for a conventional MSR reformer [43]. Solid line represents the composition-temperature profile inside the traditional MSR reformer tubes.

Moreover, methane decomposition is a weakly endothermic reaction and evolves, as already said, with an increase of number of moles. That means it is not promoted by a high pressure but only by a high temperature. As a result, by working at low temperatures, high pressures and high reagents molar ratios this gives the opportunity to hinder methane decomposition and allows to a conventional reformer to work in no carbon formation zone, even though at low methane conversions. Instead, in an MR the continue hydrogen extraction through the membrane can increase the carbon deposition rate (v_{dep}) with respect to carbon removal rate (v_{rem}) widening the carbon formation zone (**blue zone**) also in less severe temperature conditions when a low reagents molar ratio is combined to a low pressure.

In MRs, this is a pervasive problem because both phenomena reduce the MR stability in the time. In addition, it has been experimentally observed that the carbon formation has the most probability to occur close to inlet of the MR where the methane has a high concentration in presence of fresh catalyst. Wagner e Froment [114] defined by their experiments a *threshold constant* for methane decomposition which equation is the following:

$$K_\tau = \exp\left(-\frac{9573}{T} + 11.62\right), \; bar \qquad (25)$$

They established a criterion coming from the “Principle of Equilibrated Gas” that states the formation of carbon can be envisaged if the equilibrium between reagents and products on the catalyst surface is reached. MSR is a reaction that proceeds quickly; therefore, the gaseous species reach quickly the equilibrium on active sites of the catalyst surface. Consequently, the gaseous reagents can have a tendency to make carbon deposition. This criterion is described by means of the $\mathbf{V_{CH4}}$ parameter which is defined as:

$$V_{CH4} = \frac{P_{H2}^2 / P_{CH4}}{K_\tau} \tag{26}$$

$\mathbf{P_{H2}}$ and $\mathbf{P_{CH4}}$ represent the hydrogen and methane partial pressure inside the MR, respectively. Precisely, as $\mathbf{V_{CH4}}$ is less than one the carbon deposition will occur on active surface of the catalyst. Of course, this limit is only experimental and not thermodynamic [29].

In addition, by effect of the methane decomposition, the carbon formation has the most likelihood to occur in a zone closer to inlet of MR where reagents flow rate is highest and the hydrogen one is lowest. As a result, by effect of the continuous hydrogen removal through the membrane $\mathbf{V_{CH4}}$ value can be furthermore reduced. This means that the hazard of carbon formation is enhanced during reforming reaction [29]. The above mentioned criterion has been utilized in order to evaluate/estimate qualitatively the entity of the carbon formation in MR during reaction tests. Thus, $\mathbf{V_{CH4}}$ values represent an assessment for the carbon formation tendency on catalyst surface and if they assume a value less than one coke will be present on catalyst surface with consequent breakdowns of the catalyst. However, as previously said, the carbon formation is thermodynamically restrained by a high applied pressure.

Chapter 4

4.1 Experimental details

For an evaluation of palladium-*based* inorganic membrane perm-selective properties as well as membrane reactors performance, an experimental plant has been realized.

4.1.1 Laboratory bench-scale experimental plant

Such a experimental plant, see figure 19, is composed by a furnace to supply the energy necessary to uphold the endothermic reforming reaction in MR. The feed pressure inside the membrane system is finely-tuned (*Metering gauge pressure*, *Spriano*) and changed by means of a back pressure controller (*Swagelok*) that is placed downstream of MR. On retentate line, a cooler, a heat exchange and dryer (silica gel) have been placed to have the complete reduction of the non-reacted water content in the stream prior to the Gas Chromatograph (*GC6890N NetworkGC System, Agilent*). The distillate water, as one of the reagents, is fed to MR by means of HPLC pump (*P680 HPLC Pump, Dionex*) whereas pure methane gas is, instead, fed by means of mass flow controller (*Brooks Smart Mass Flow, Brook Instruments B.V.*). Both are perfectly mixed in the furnace by setting a smaller bed of glass spheres previous to the catalyst bed and membrane, figure 18.

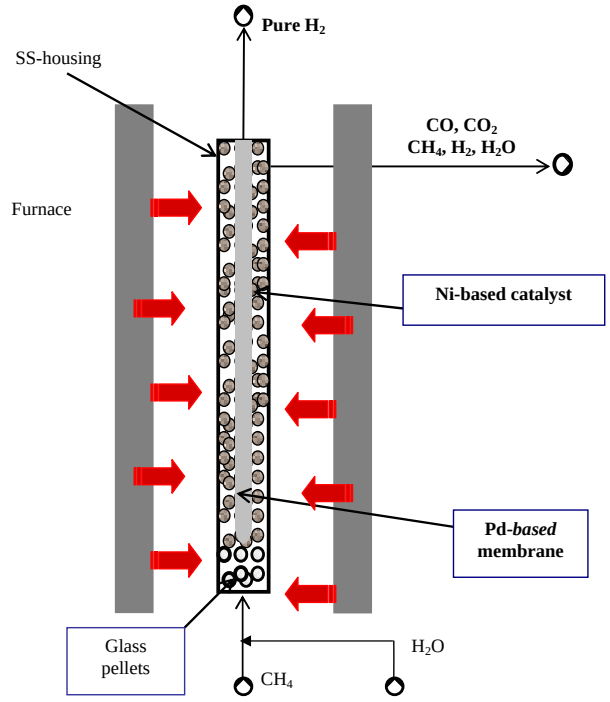

Fig. 18 - Scheme of Membrane Reactor used in this experimental work

The MR temperature is measured by means of a thermocouple (*type K*) placed in contact with external part of housing. The retentate line is heated by means of a heating tape and controlled by temperature controller (*Digi Sense Temperature Controller*). This allows avoiding the condensation of steam inside the tube prior to the back pressure controller. Both permeate and retentate streams are alternatively fed to GC for the analysis. By this testing, it is possible to evaluate both the extracted hydrogen amount in the permeate stream and the methane concentration in the retentate stream, respectively. As a result, both hydrogen recovery and methane conversion can be estimated.

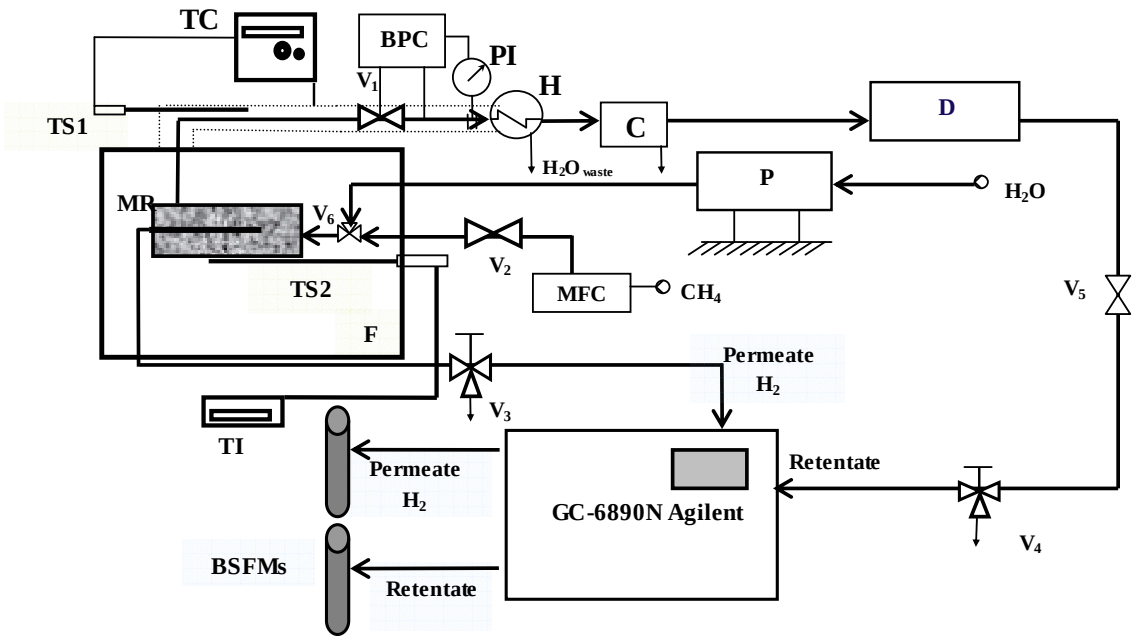

Legend

MR	**Membrane Reactor**
C	**Cooler**
D	**Dryer**
H	**Heat exchanger**
F	**Furnace**
P	**HPLC Pump**
BPC	**Back Pressure Controller**
MFC	**Mass Flow Controller**
BSFMs	**Bouble-soap flowmeters**
PI	**Gauge Pressure Indicator**
TS1, TS2	**K-type thermocouples**
TI	**Temperature Indicator**
TC	**Temperature Controller**
V_1, V_2, V_5	**On-Off valves**
V_3, V_4, V_6	**Three-ways On-Off valves**
……..	**Heating tape**

Fig. 19 Experimental plant flow-sheet for steam reforming reaction of methane.

The hydrogen selective Pd/Ag-*based* commercial (*GoodFellow Industries*, Ltd) membranes used in this experimental work have a thickness equal to 100 µm. Figure 20 shows Pd/Ag-based membrane used during the characterization experimental tests of perm-selective properties by pure gas.

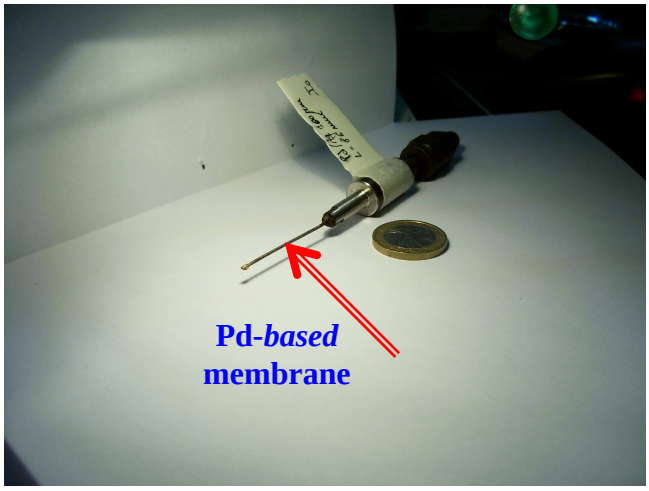

Fig. 20 – A view of palladium-based membrane

They were closed on one end whereas the other, from which the permeated hydrogen goes out, was brazed-weld to stainless steel tube (internal diameter 1.6 mm), as shown in figure 21.

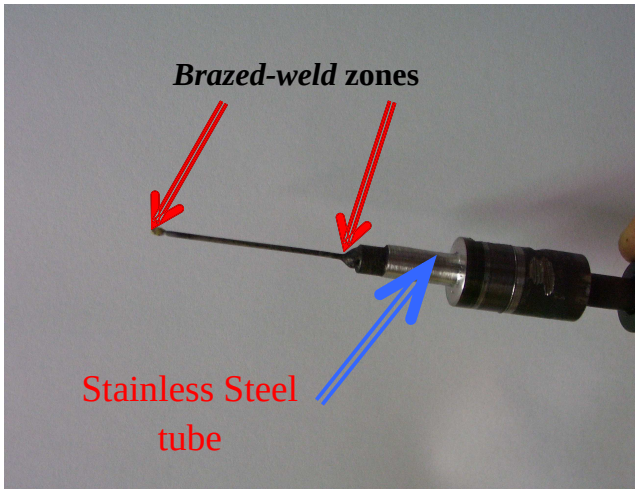

Fig. 21 – *Goodfellow*'s Pd/Ag-based membrane brazed to the tube.

The operating conditions used during the characterization and permeation tests are indicated in table 5.

Table 5 – Operating conditions

Feed composition	Pure H_2
Temperature	360-560°C
Feed pressure	200 – 600 kPa
Permeate Pressure	100 kPa
No sweep	

Before the permeation tests, the membrane module has been checked to gas leakage. At room temperature, the system was kept for six hours under a high driving force (8.5 bara) in nitrogen atmosphere. During this period, no nitrogen permeation was observed through the membrane as well as no inert gas leakages through the whole system. The membrane was, then, placed within the catalyst bed in a *tube-in-tube* configuration with the stainless steel tubular housing, see figure 18.

Each membrane was pre-heated in nitrogen atmosphere and kept under a slight (2 bara) trans-membrane pressure up to the achievement of the temperature required. No nitrogen permeation was evidenced through the membrane. This was necessary to estimate during the heating, eventually, gas leakages due to either cracks in the *braze-welding* parts or defects through the membrane. Then, at this reaction temperature, further tests were carried out by nitrogen also at the working pressure required for the characterization. This allowed evaluating the total selectivity of the membrane towards hydrogen. At this high pressure and temperature both measurements by bubble-soap flow meter and Gas Chromatograph were continually carried out to confirm the absence of inert gas on permeate side during the heating up to the required reaction temperature. In fact, no evidence of inert gas N_2 or helium (used in substitution) has been revealed on permeate side.

Four different MRs have been manufactured, as shown in table 6, each one characterized by means of different length, catalyst amount and design parameters.

The experimentally investigated reaction is, obviously, the catalytic *methane steam reforming* reaction. The operating conditions used during reaction tests are showed in table 7. In figure 22, the bench-scale MR used in tests for MSR is showed.

Table 6 – Design parameters for different MRs.

Membrane Reactors	**A_m/V_{cat}, $cm^2\ cm^{-3}$**	**L_s/A_m, $cm^3\ cm^{-2}\ min^{-1}$**
MR1	0.42	11.6
MR2	2.1	11.6
MR3	2.1	8.4
MR4_catalyst distributed	10	2-3

Table 7 – Operating conditions

Temperature, °C	500 - 600
Feed Pressure, kPa	600 - 800
Permeate Pressure, kPa	100
m (H/C)	2 - 3
GHSV, h^{-1}	1200 - 6400

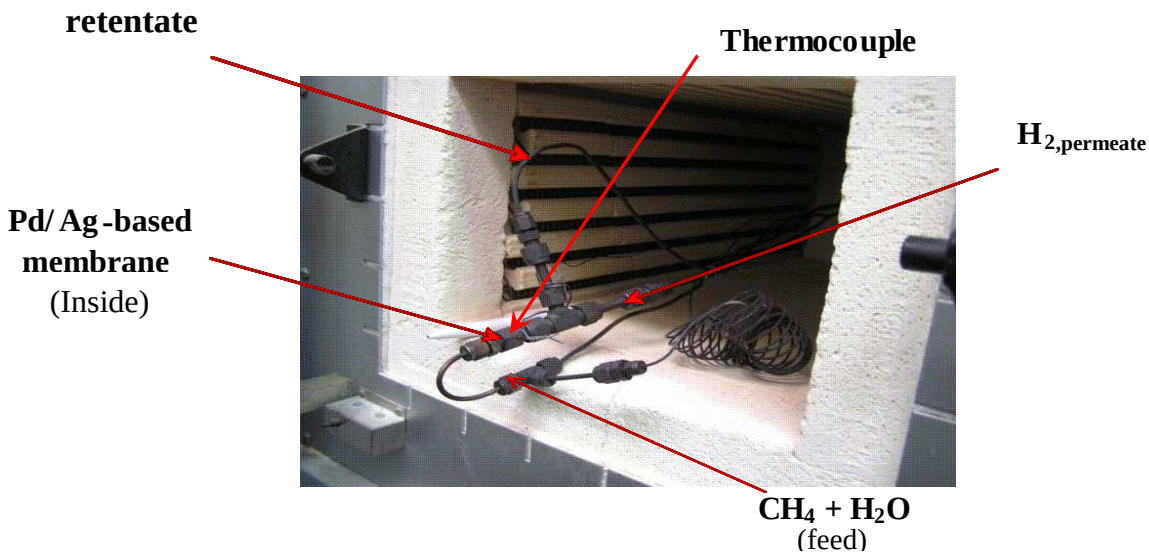

Fig. 22 – A view of the MR for steam reforming of methane,

Fundamental variables used to describe the MR performance are methane conversion (the same equation is used for WGS reaction referred to the CO):

$$CH_4 \text{ Conversion} = 1 - \frac{F_{CH_4}^{Retentate}}{F_{CH_4}^{Feed}}, (-) \quad (27)$$

and the H_2 Recovery *Index* that corresponds to the amount of hydrogen recovered through the membrane with respect to its global production:

$$H_2 \text{ Recovery } Index = \frac{F_{H_2}^{Permeate}}{F_{H_2}^{Permeate} + F_{H_2}^{Retentate}}, (-) \quad (28)$$

In addition, the design parameters used to improve the MR performance are:

$$\frac{L_s}{A_m}, [cm^3\ cm^{-2}\ min^{-1}] \quad (29)$$

that compares the extraction ability of the membrane represented by accessible surface area with residence times spend to produce hydrogen inside the MR characterized by the limiting reagent flow rate (L_s).

A typical parameter required for the development of a competitive and efficient MR [3] is the ratio between membrane surface area and the catalyst volume necessary to uphold the equilibrium reaction (*i.e.* MSR or WGS):

$$\frac{A_m}{V_{cat}}, [cm^2\ cm^{-3}] \quad (30)$$

4.1.2 *Braze-welding* process

In this section, a braze-welding procedure is exposed since it has been used to weld the palladium-*based* membrane to the stainless steal tube on permeate side and close it on one end.

Generally, it is used to produce joints of excellent strength in steel, in cast iron, and in copper and some copper alloys. In braze welding process, the filler metal always has a melting point well below the melting point of the base metal, then, the base metal is never melted. The basis for the braze-welding process is that both brass (*i.e.* an alloy of copper and zinc) and bronze (*i.e.* an alloy of copper and tin) will flow onto properly prepared surfaces of higher-melting-point metals or alloys to form a bond or molecular union which has excellent strength. The base metal is never melted but it is merely raised to the temperature at which the filler metal will tin (*i.e.* form a smooth film) on the surface of the joint. Although the temperatures involved are much lower than those required for the fusion welding of steel, braze welding is primarily an oxy-acetylene process.

The filler metal used for most braze welding is a copper alloy containing roughly 60% copper, 40% zinc, and small amounts of tin, iron, manganese, and silicon. For bronze-surfacing a filler metal of slightly different composition, designed to achieve greater hardness at some sacrifice in ductility, is Silicon-bronze, which contains only copper and silicon (no zinc), and phosphor bronze (a copper-tin alloy) are also sometimes used for braze-welding steel. Braze welding technique requires:

1. Preparation and mechanical cleaning of the joint.
2. Proper tinning of the joint surface.
3. Complete fusion between layers of weld metal.

Braze welding is faster than fusion welding, since the heat input required is much less. The rod normally used for braze welding has a melting point of about 875°C. In the braze welding of steel, the base metal must be heated only to a temperature of about 900°C, rather than to a temperature of more than 1500°C. When it is used on steel, braze welding reduces distortion of the base metal due to forces of contraction and expansion. At 500°C, steel and cast iron are nearly as strong as they are at room temperature (20°C). Any bronze lost a great deal of its strength at 500°C.

4.1.3 Activation procedure of Ni-*based* catalyst used in MSR

A commercial Ni-based catalyst (31% Ni, 39% NiO, 11% Al_2O_3 and 19% SiO_2) has been used in this work.

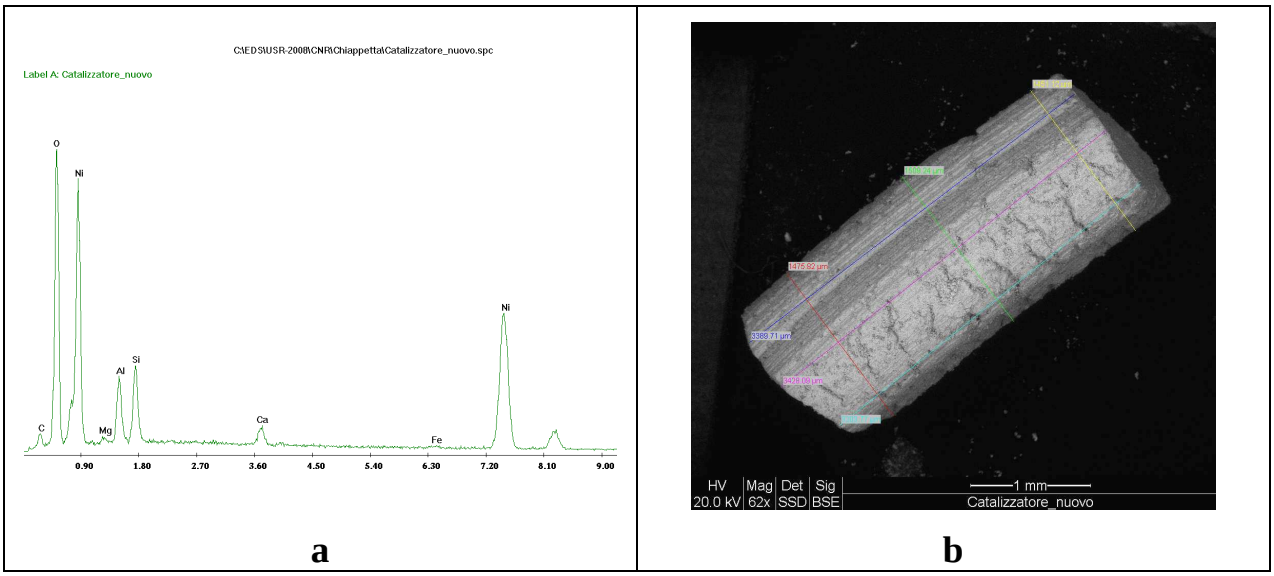

Fig. 23 – An EDX and SEM analysis, respectively, of a fresh catalyst particle.

It contains 60 wt.% of nickel distributed on a surface area equal to 160 $m^2\ g^{-1}$. The catalyst particle has a cylindrical geometry and its corresponding diameter was approximately 1.5-2 mm

and length 3-5 mm. It is black and odorless. This catalyst is stabilized by means of CO_2 to avoid hazardous transport procedures. Figure 23a shows an EDX analysis whereas figure 23b represents a SEM photo of a fresh catalyst particle (prior to the steam reforming reaction). Figure 24, instead, is a SEM magnification of a fresh catalyst surface zone.

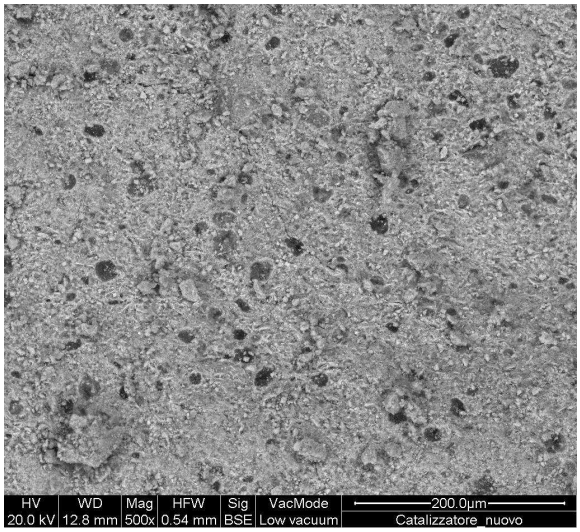

Fig. 24 – Superficial magnification of a fresh catalyst pellet.

When it is placed in the reactor, generally it is cut in smaller cylinders in order to have the length equivalent to the diameter (1.5-2 mm) and, therefore, obtain a homogeneous packaging inside the module. However, by effect of stabilization process by means of CO_2, it can not be used just as it is. In order to eliminate all CO_2 absorbed on active sites of the Ni-*based* catalyst, this last requires a pre-activation process in which the catalyst is heated at a temperature over 150°C. According to the experimental procedure and since the desorbing rate of CO_2 increases with the temperature, the system has been heated, in presence of a nitrogen stream, (about 40 cm^3(*STP*) min^{-1}) up to a temperature 262°C. This process carries on for 2 h. Once this temperature has been reached, the system is left for one hour in nitrogen atmosphere. During this step, the outlet stream from the reactor (retentate side) is analysed by means of a Gas-Chromatograph (GC) to verify the progressive reduction of the CO_2 content. After one hour, the temperature is again increased up to 350°C. This is necessary to avoid the embrittlement phenomenon since a Pd-based membrane is present in the reactor and hydrogen is fed to the reactor. Hydrogen creates a reducing atmosphere essential to obtain metallic nickel. In addition, it allows activating/conditioning the membrane by keeping the system under a slight trans-membrane pressure (1 barg). The amount of hydrogen is progressively increased from 10% to 100%, every 15 min, while, at the contrary, the nitrogen is decreased by an analogous amount. Also in this

case, the stream is analysed to the GC and the operation takes 2 hours. This step is concluded when the CO_2 concentration is under 0.5% (not investigated by GC). The whole process takes about 6 hours.

4.1.4 Theoretical model for WGSR-*based* MR

A sensitivity analysis has been developed in order to define the role of some variables on the performance of a MR and for maximizing the system efficiency as well as hydrogen recovery. The behaviour of a MR has been investigated by means of a 2-D mathematical model. It considers, for heat and mass transport, the only convective term in the axial direction and the diffusive term in the radial direction, neglecting the axial dispersion. These axial dispersive effects due to the conversion of the reagents have been neglected by selecting an appropriate ratio of catalyst bed length to particle size (L_r/d_p). The value calculated for this ratio is equal to 180; it meets the criterion concerning the minimum L_r/d_p ratio to limit significantly the axial dispersion in a reactor [48-50]. The radial convective flow is neglected because the membrane has a dense selective layer. In this way it is possible to simulate simultaneously the chemical reaction and the hydrogen separation through the membrane, taking into account both fluid dynamics and heat transfer inside the reactor. With respect to the MSR reactor, the reagents are fed to the lumen of the tubular reactor in parallel mode with a sweep gas that flowing in the shell side extracts the product from the reaction zone through the Pd-*based* membrane. The catalyst bed is considered inside the lumen differently from MR for reforming reaction. The membrane is considered completely selective for the hydrogen and also in this case is self-supported. All species involved in the process have been considered as ideal gases and for their physical properties (*e.g.* viscosity, density, specific heats and so on) an average value as a function of temperature and composition has been assumed. The reaction system has been represented by a continuous single-phase model (**pseudo-homogeneous**) which uses the effective transport concept to formulate the fluxes of heat and mass in the radial direction superimposed on the transport by overall convection (plug flow type). Therefore, the resulting 2-D differential equations written in steady state for the lumen side with the appropriate boundary conditions are the following:

$$u_s \cdot \rho_g \cdot Cp_{mix} \frac{\partial T}{\partial z} = \frac{1}{r}\frac{\partial}{\partial r}\left(r \cdot \lambda_{er} \frac{\partial T}{\partial r} \right) + \Re_i \cdot \left(-\Delta H(T)\right) \tag{31}$$

$$v_z \frac{\partial c_i}{\partial z} = \frac{1}{r}\frac{\partial}{\partial r}\left(r \cdot D_{i,r} \frac{\partial c_i}{\partial r} \right) + \Re_i \tag{32}$$

B.C.1

$$\forall z,\ r = 0$$

$$\frac{\partial c_i}{\partial r} = 0;\quad \frac{\partial T}{\partial r} = 0 \tag{33}$$

B.C.2

$$\forall z,\ r = R$$

$$-D_{i,R}\frac{\partial c_i}{\partial r} = P_e\left(\sqrt{P_{H2,ret}} - \sqrt{P_{H2,perm}}\right) \tag{34}$$

$$-\lambda_{er}\frac{\partial T}{\partial r} = h_w\left(T - T_w\right) + J_{H2}Cp_{H2}\left(T - T_w\right)$$

B.C.3

$$\forall r,\ z = 0 \tag{35}$$

$$\mathbf{c_i = c_{i,0}} \qquad \mathbf{T = T_0}$$

As to boundary conditions, concentration and temperature gradients have been set equal to zero on the reactor axis (**symmetry condition**), while hydrogen diffusive flux at membrane surface is expressed by Sieverts' law [19, 24]. The temperature change in radial direction is the sum of the heat transferred across the metallic layer and the enthalpy associated with the hydrogen permeation. The concentration of the species and the temperature on both lumen and shell sides are known at the inlet of the MR. Heat and mass 1-D differential equations written in steady state for the shell side are the following:

$$u_{s,perm}\cdot\rho_{g,perm}\cdot Cp_{mix,perm}\frac{dT}{dz} = h_w\left(T_w - T\right) + J_{H2}Cp_{H2}\left(T_w - T\right) \tag{36}$$

$$u_{s,perm}\frac{dc_{H2}}{dz} = \frac{A_m}{V_r}P_e\left(\sqrt{P_{H2,ret}} - \sqrt{P_{H2,perm}}\right) \tag{37}$$

B.C.4

$$\forall r,\ z = 0 \tag{38}$$

$$\mathbf{c_{H2} = 0} \qquad \mathbf{T = T_{0,perm}}$$

The equation (36) considers that the temperature on the shell side can change also for effect of the sensible heat of the permeating hydrogen. This contribution is more significant as much as the permeating flow rate through the membrane increases. Hydrogen permeability obeys to

Arrhenius' law with temperature. The sweep gas stream fed to the shell side of the MR does not contain hydrogen.

The partial differential equations have been discretised by means of an *orthogonal collocation* procedure at finite elements giving a set of ordinary differential equations solved by 4th order *Runge-Kutta* method. The collocation points, representative of mean compositions for each component and the temperature in radial direction, have been determined by using a Legendre polynomial. The *orthogonal collocation* has already been applied to solve, in a reduced computation time also in fixed bed reactors, complex energy and mass balances, where non-linear terms are present [115].

Experimental values of membrane thickness and hydrogen permeation rates [116] have been utilised in the computer code. The Temkin's kinetic expression [117], considered for the water gas shift reaction, is the following:

$$\Re_i = \frac{k_c \cdot P_{feed} \cdot (1-\varepsilon) \cdot c_{tot} \cdot \left((y_{CO} \cdot y_{H2O}) - \left(\frac{(y_{H2} \cdot y_{CO2})}{Keq} \right) \right)}{(a_k \cdot y_{H2O} + y_{CO2})}; \qquad \text{kmol m}^{-3}\,\text{s}^{-1} \qquad (39)$$

where:

$$k_c = 6.0 \cdot 10^{11} \cdot \exp(-26800/(R_{gas} \cdot T)); \qquad \text{atm}^{-1}\,\text{s}^{-1} \qquad (40)$$

$$a_k = 2.5 \cdot 10^{9} \cdot \exp(-21500/(R_{gas} \cdot T)); \qquad - \qquad (41)$$

$$R_{gas} = 1.987 \qquad \text{cal mol}^{-1}\,\text{K}^{-1}; \qquad (42)$$

This expression was experimentally confirmed for a Cu-Zn-Cr low-temperature catalyst assuming an oxidation-reduction mechanism and no diffusive control for a grain size of 0.1-1 mm [117]. It fits better the experimental data in MRs with respect to Langmuir-Hinshelwood model, as indicated in literature for isothermal conditions [118, 119].

Preliminary experimental tests, previously carried out in a similar bench-scale MR in non-isothermal conditions at 110 kPa, have shown the presence of a maximum in the temperature profile. In this work for the spherical pellets of catalyst, which are packed inside the tubular membrane, a unitary efficiency has been assumed (no internal and external transport resistance). The pellets size of the catalyst does not affect the fluid dynamics of the system and the gas velocity in axial direction is independent on the radial position. The latter assumption is equivalent to neglect the pressure drops along the reactor due to the wall friction [115]. The catalytic bed depth has been assumed equal to the membrane length. For practical purposes

radial Peclet (**Pe_r)** has been assumed to lie between 8 and 10; from this dimensionless number the effective radial diffusion has been evaluated. In packed bed reactors, the effective heat conductivity, λ_{er}, decreases strongly close to the wall as a consequence of an additional resistance due to changes in the packing density and flow velocity. In table 8 the main parameters used in this work as *base case* are summarized.

Table 8 - Modelling parameters as a reference

Geometric and physical parameters	**Value**
Axial length of the catalyst bed, cm	15
Inside diameter of membrane, cm	1
Thickness of Pd/Ag film, μm	70
Average particle diameter, mm	0.815
Heat capacity of gas mixture in lumen side, kJ kg^{-1} K^{-1}	1.5
Heat capacity of gas mixture on shell side, kJ kg^{-1} K^{-1}	1.1
Hydrogen heat capacity, kJ kg^{-1} K^{-1}	14.5
Wall-heat transfer coefficient, kJ m^{-2} $s^{-1}\cdot K^{-1}$	1.6
Effective radial thermal conductivity, kJ $m^{-1}s^{-1}$ K^{-1}	0.000297
Operating conditions	**Value**
Pressure on shell side, kPa	110
Inlet feed temperature, K	600
Limiting reagent flow rate (CO), mol min^{-1}	$1.17\cdot10^{-3}$
Steam sweep gas flow-rate, mol min^{-1}	$1.17\cdot10^{-2}$
Sweep factor (sweep gas flow-rate/ limiting reagent flow rate)	10
Feed molar ratio, H_2O/CO	1
Bed voidage fraction (internal porosity of catalyst), ε	0.3

Chapter 5

5.1 Results and Discussion

5.1.1 Membrane reactors for hydrogen production

An important question in membrane reactor-MSR process is the compactness of the reactor. As it is well known, palladium is very expensive. Then, the reduction of membrane surface area considerably decreases the MR manufacturing costs. Since nickel-*based* catalysts are very active and efficient [78], MSR is usually carried out at high space velocities that results in a compact industrial reactor.

5.1.1.1 Characterization and permeation experimental tests

Each membrane was pre-heated in nitrogen atmosphere up to the testing temperature. During the permeation tests of the selective palladium-*based* membrane, pure hydrogen was fed to the outside of the capillary membrane tube. Fluxes of hydrogen through the membrane were determined, at every temperature and for different feed pressures, by means of a bubble-soap flow meter (500µl) placed to the open end of the tube. Before of each test, the membrane system was kept at testing temperature and pressure for one hour to get to the stationary state. The pressure at a controlled flux was measured after stabilization.

Prior to permeation and characterization tests at every temperature, the Pd-*based* membranes underwent a conditioning process where they were kept under pressure in hydrogen atmosphere for two hours. As previously mentioned, the hydrogen permeation measurements have been performed in the temperature range of 360-560°C and in the pressure range of 200-600 kPa, with no sweep gas on shell side. Experimental tests in presence of nitrogen have been carried out both to check the membrane system to the gas tight and the integral perm-selectivity towards hydrogen of the Pd-alloy membranes.

The hydrogen transport into the Pd – *based* membrane obeys to the Sieverts' law as shown in figure 25a, for 100 µm-thick Pd/Ag-*based* membrane having 8.5 cm of length. For each different temperature, the hydrogen flux through the membrane increases as the hydrogen *driving force* increases confirming to a linear dependence in accordance with the Sieverts' law (*i.e.* correlation factor 0.99±0.01). Figure 25b shows the membrane stability in the time since the hydrogen flux both before and after reaction tests is unchanged.

Different gas present in the hydrogen streams influence the permeselective properties of Pd-*based* membranes. In particular, the presence of CO decreases the hydrogen permeance since it blocks the active sites on membrane surface [120]. A 10% hydrogen flux decrease is obtained at 250°C whereas at 350°C its influence on palladium-*based* membrane permselective capacity is highly reduced [121]. Gielens *et al.* [122] have studied both the CO_2 and steam influence on the H_2 behaviour during the permeation through the Pd-*based* membrane having high flux. By this investigation is shown that thinner membranes suffer much more the inhibitor effects with respect to the thicker ones. After eighty hours of operating tests, a 70% reduction of hydrogen flux has been evidenced at 623 K. Barbieri *et al.* [123] have investigated the CO effect on perm-selective membrane properties for commercial Pd/Ag-*based* membranes. The aim was to estimate the effective membrane surface area for mass exchange necessary to compensate this hydrogen flux reduction through the membrane. Experimental results on our membrane reactors have evidenced that the CO formation during steam reforming of methane is very low. Moreover, since these membranes must work at high temperatures, they will suffer few reductions of their performance by effect of both steam and CO_2.

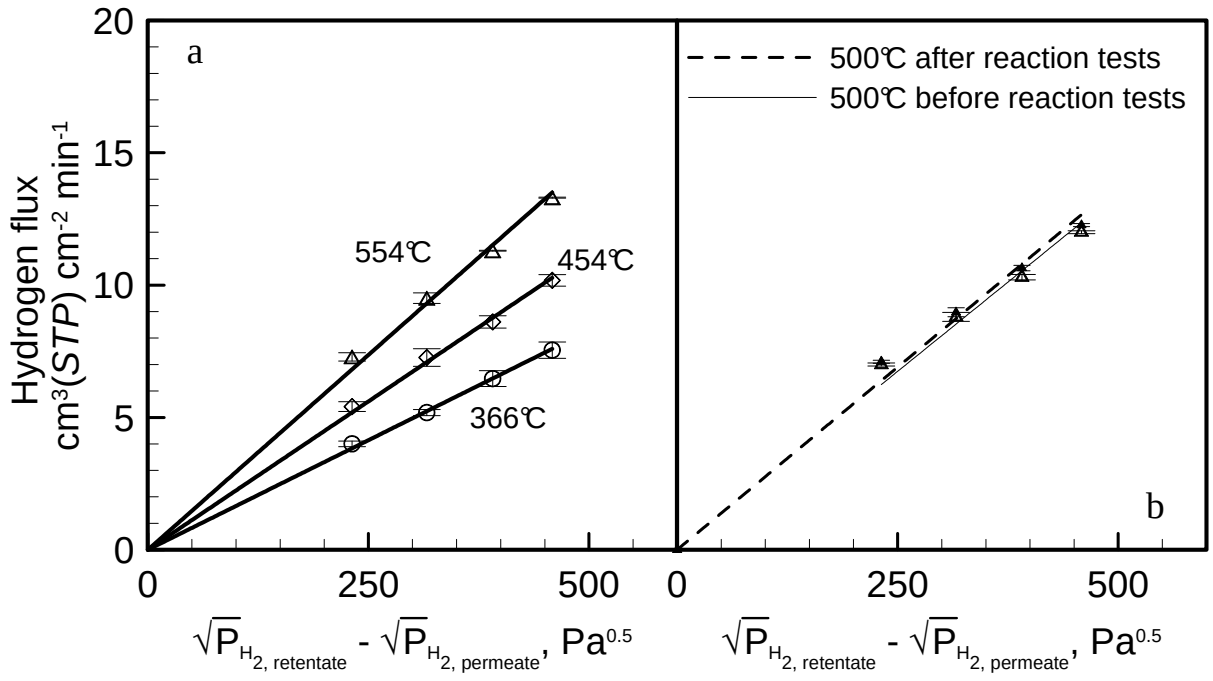

Fig. **25** - Hydrogen flux as a function of the hydrogen driving-force through the Pd-*based* membrane.

The hydrogen permeability increases as a function of the temperature, at each fixed driving force. The hydrogen permeability, see equation (43) has been obtained:

$$Pe_{H_2} = 154 \cdot exp\left(\frac{-13.44\ kJ\ mol^{-1}}{(R_{gas}T)}\right),\ [nmol\ m\ m^{-2}\ s^{-1}\ Pa^{-0.5}\ ] \qquad (43)$$

It indicates that the hydrogen transport is an activated process in agreement to Arrhenius' law, figure 26.

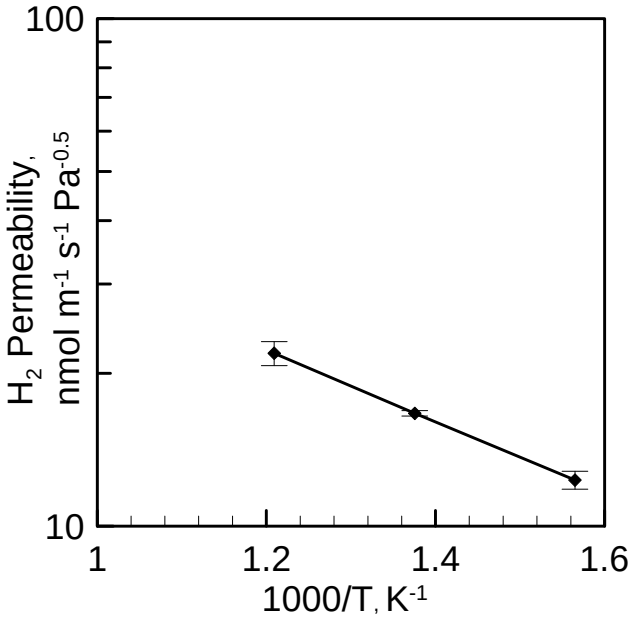

Fig. 26 – Hydrogen Permeability as a function of the temperature.

This expression is well-matched with some experimental expressions reported in literature such as, for example, the extracted one from Buxbaum's experimental work figure 27 [124].

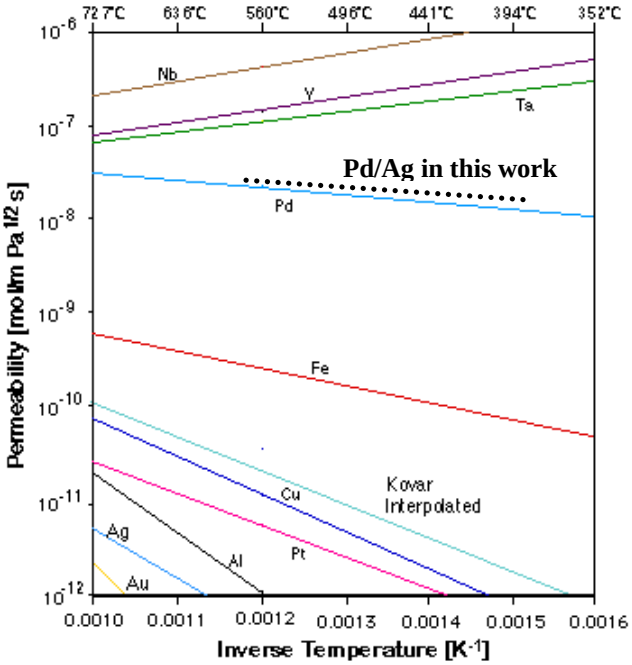

Fig. 27 – Hydrogen permeability (mol m m^{-2} s^{-1} $Pa^{-0.5}$) in aluminium, copper, iron, gold, kovar, niobium, palladium, platinum, silver, tantalum, titanium, and vanadium.

or, in particular, Scura *et al.* [123], Koffler *et al.* [125], Tosti *et al.* [126], Li *et al.* [127] as table 9 shows:

Table 9 – Parameters of the experimental H_2 permeability expression compared to the ones present in literature

Apparent Activation Energy, kJ mol^{-1}	**Pre-exponential factor, nmol m m^{-2} s^{-1} Pa$^{-0.5}$**	**Permeability$_{H2}$ (554°C), nmol m m^{-2} s^{-1} Pa$^{-0.5}$**	***Reference***
15.7	220	22.5	[123]
13.4	**154**	**22.0**	***This work***
12.0	109	19.0	[126]
5.5	44.7	20.2	[125]
9.18	109	27	[127][1]

[1]Pd–25%Ag alloy membranes with thickness of 15–50 μm for the temperature range of 400–650°C using pure hydrogen [127]

The stability of Pd-*based* membranes is reduced when membrane temperature is higher or the membrane is thinner. Li *et al.* [127] have found that hydrogen selectivity for 10 μm Pd membrane obtained by *electroless plating* considerably decreased over 10-20 h period at 550°C, whereas it remained stable for more than 1000 h if it is operated at 450°C or lower. The actual temperature needs to be constrained for practical processes, as MRs applied to MSR, even though MSR is thermodynamically favoured by high temperature. It is advised to operate these systems at about 550°C or lower with Pd-*based* membranes thickness of 25 μm (or thicker) in order to achieve appropriate membrane life [58, 128].

5.1.1.2 Membrane Reactor *MR1*.

This MR works at low membrane surface area with respect to catalyst volume**.** Figure 28 shows the dependence of the methane conversion from the gas hourly space velocity (GHSV). GHSV represents the reagents flow rate effect on traditional reactor performance. Therefore, by working at a high GHSV value means to make worse and worse the performance since the residence times are reduced. The same considerations are applicable onto an integrated system as membrane reactor since, as for traditional reactor, it represents the effect of reagents feed flow rate on the performance of MR. A 77% increase of the GHSV involves a 25% reduction of the methane conversion. Even if MR performance is worsening, since the residence times are reduced, the system works by exceeding the traditional reactor equilibrium conversion (TREC).

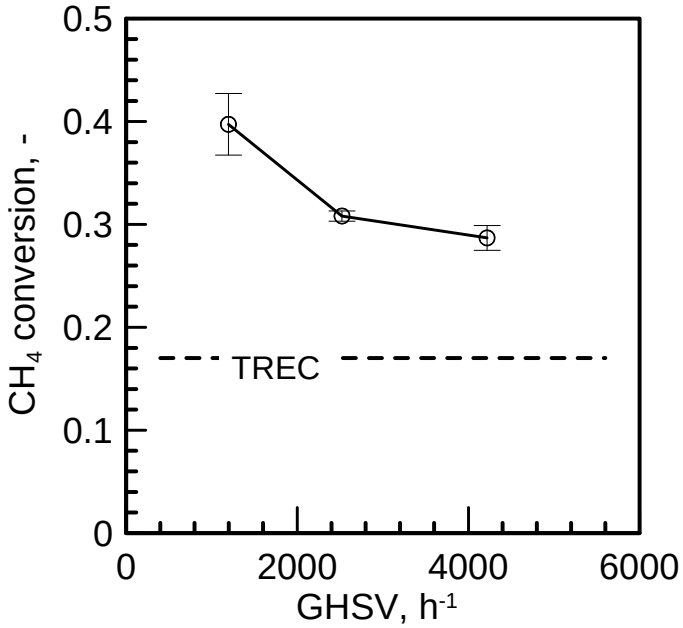

Fig. 28 - Methane conversion vs. GHSV compared to the equilibrium conversion for a traditional reactor (TREC, *dotted* line). Operating conditions: 500°C and 600 kPa, reagents molar ratio equal to 3. Design parameters: A_m/V_{cat} of 0.42 cm^2 cm^{-3} and L_s/A_m of 11.6 cm^3*(STP)* cm^{-2} min^{-1}, length 8.5 cm.

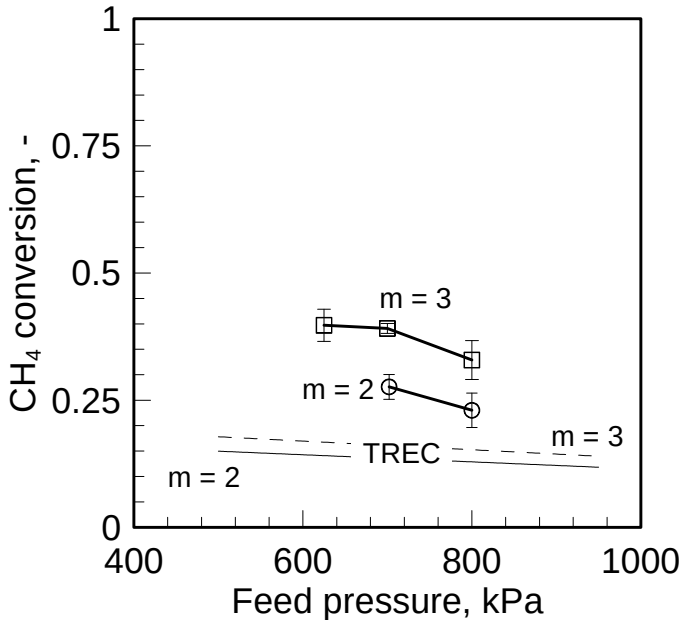

Fig. 29 - Methane conversion vs. feed pressure at two different reagents molar ratio. Operating conditions: GHSV = 1200 h^{-1}. Design parameters: A_m/V_{cat} = 0.42 cm^2 cm^{-3} and L_s/A_m = 11.6 cm^3*(STP)* cm^{-2} min^{-1}, length 8.5 cm.

Fig. 29 shows that a feed pressure increase reduces methane conversion at each reagents molar ratio, at 500°C. In particular at m=2, the membrane reactor performance worsen even if MR operates over the TREC.

Figure 30a shows the dependence of the H_2 *Recovery Index* from reaction temperature at different feed pressures.

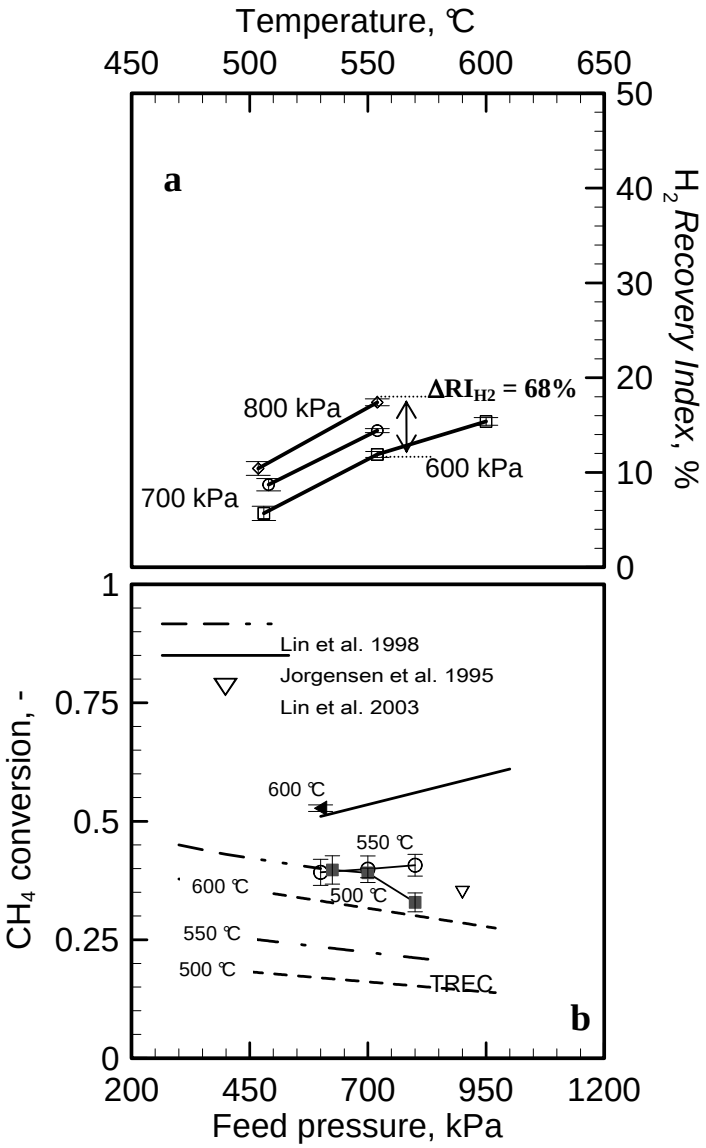

Fig. 30 – a) H_2 *Recovery Index* vs. reaction temperature at different Feed pressures value and b) Methane conversion vs. Feed Pressure at different reaction temperatures compared to TREC curve (dotted lines). Operating conditions: GHSV = 1200 h^{-1}, reagents molar ratio equal to 3. Design parameters: A_m/V_{cat} of 0.42 cm^2 cm^{-3} and L_s/A_m of 11.6 cm^3*(STP)* cm^{-2} min^{-1}, length 8.5 cm.

At each temperature, the feed pressure increases the driving force through the membrane and, then, it allows a higher hydrogen recovery. For example, at 550°C, by increasing the feed pressure up to 800 kPa the hydrogen recovery achievable is 16% that is four-times higher than the one at 600 kPa (*e.g.* corresponding to a 68 % increase). In addition, it has been estimated that a 10% increase of the temperature leads to a twofold enhancement of the hydrogen recovery at both 600 kPa and 800 kPa. Figure 30b shows the methane conversion as a function of feed pressure by working at the lowest GHSV value (1200 h^{-1}). At each temperature, the MR operates

by exceeding the TREC. In particular, at 500°C, the methane conversion decreases as pressure increases according to Lin's experimental trend [10]. The authors worked at 900 kPa, in presence of a sweep gas on shell side, by using a 10 μm-thick composite palladium membrane. They obtained, at 720 kPa and 500°C, a 35% methane conversion by employing a membrane surface sixty-time greater than the one utilized in our MR. At the same operating conditions, our MR has reached a 32% methane conversion. At 500°C, the increasing pressure does not allow getting to a high CH_4 conversion since permeation rate is not sufficient to counterbalance the concurrent negative effect of both slow kinetic rate and low equilibrium conversion. This condition does not guarantee an efficient production and separation of hydrogen through the membrane. Moreover, MR presents a poor membrane surface to extract all the hydrogen produced (low A_m/V_{cat} ratio) even at high residence times (low GHSV value). Therefore, differently from that occurs to the higher temperatures, the conversion decreases as a whole. At 550°C, the trend is reversed and, at 800 kPa the maximum CH_4 conversion achievable is 44%. At higher temperature, feed pressure favors methane conversion since both kinetic and permeation rate increase. In fact, by increasing the feed pressure, the hydrogen permeation rate counterbalances the negative effect resulting by thermodynamic limitation.

The stresses localized, during the heating and cooling step, have contributed many times to the break-down of palladium-*based* membrane, see figure 31.

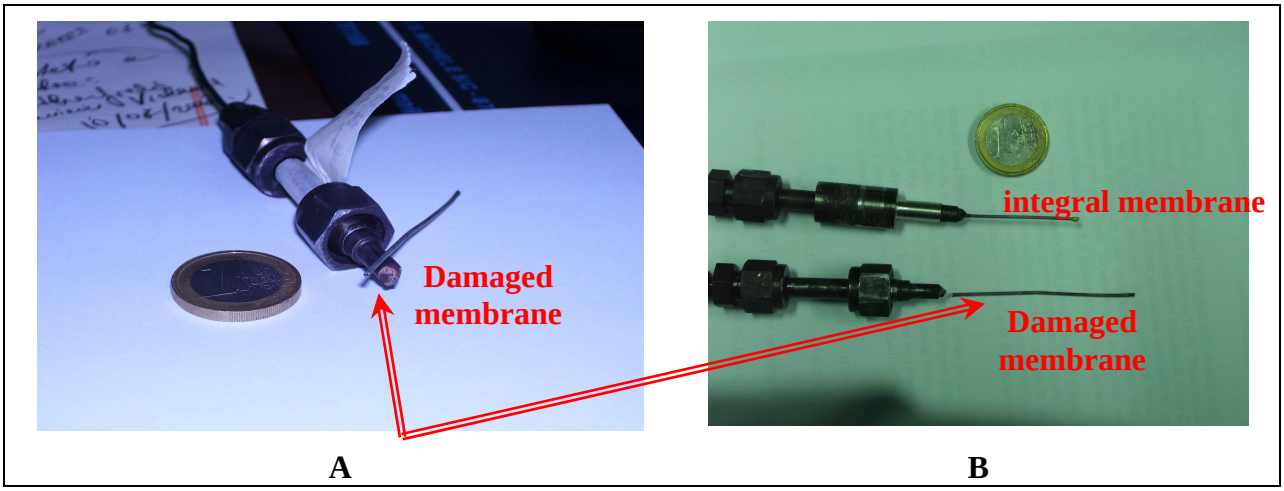

Fig. 31 – MR after a programmed cycle of experimental tests at 600°C. Breaking in braze-welded points.

At 600°C and 600 kPa, the result accords to the Jørgensen's one [129] which carried out experimental tests by using a sweep gas, a ratio A_m/V_{cat} ten-times higher and L_s/A_m six-times lower than the values considered for our experimental work. At 600°C, higher methane conversions are reached but the membrane is compromised, as shown again in figure 31.

As above mentioned, *MR1* presents inadequate design parameters since a ratio equal to 0.42 cm^2 cm^{-3} means that a surplus of catalyst is placed in reactor with respect to the needed membrane surface.

Figure 32 shows the methane conversion as a function of reaction temperature. As for the previous experimental results, at every temperature and fixed feed pressure methane conversion results higher than TREC. The pressure positively influences both the kinetic and permeation rate through the membrane. The trend accords to Basile *et al.* [27]. They have carried out experimental tests at 136 kPa, in presence of inert sweep gas on shell side of the palladium membrane. Membrane surface area was twenty-times higher than the one used in this work (A_m/V_{cat} = 9.1 cm^2 cm^{-3}) with an L_s/A_m ratio equivalent to 0.4 cm^3 cm^{-2} min^{-1}.

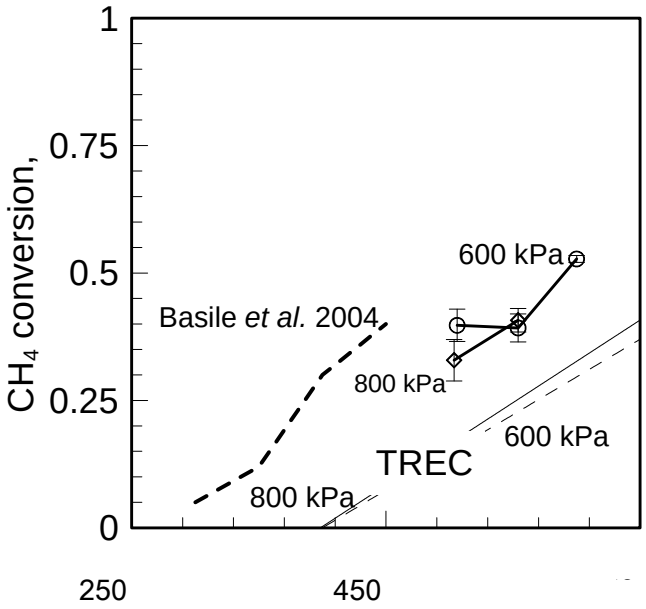

Fig. 32 - Methane conversion vs. reaction temperature compared to the equilibrium conversion for a traditional reactor (TREC, dotted line) at two different feed pressures. Operating conditions: GHSV = 1200 h^{-1}; reagents molar ratio equal to 3. Design parameters: A_m/V_{cat} = 0.42 cm^2 cm^{-3} and L_s/A_m = 11.6 cm^3*(STP)* cm^{-2} min^{-1}, length 8.5 cm.

In a membrane reactor, the continuous and selective hydrogen extraction carries out at higher methane conversions than the TREC and counterbalances the opposite effect of an increasing GHSV value.

In figure 33, the hydrogen recovery increases as feed pressure increases at fixed temperature and reagents molar ratio equal to 3. A higher permeation rate occurs as the reaction temperature increases at fixed feed pressure. A 10% increase of the temperature (from 550°C to 600°C) allows to enhance hydrogen recovery of the 21% whereas, instead, by increasing the temperature from 500°C to 600°C entails a 68% increase of the recovery at lowest feed pressure. At 800 kPa,

a 10% increase of temperature (from 500°C to 550°C) carries out an 88% increase of recovery. Obviously, at 500°C a feed reagents molar ratio equal to 2 reduces further the hydrogen recovery at each feed pressure value since hydrogen is slowly produced and its amount in retentate is lower.

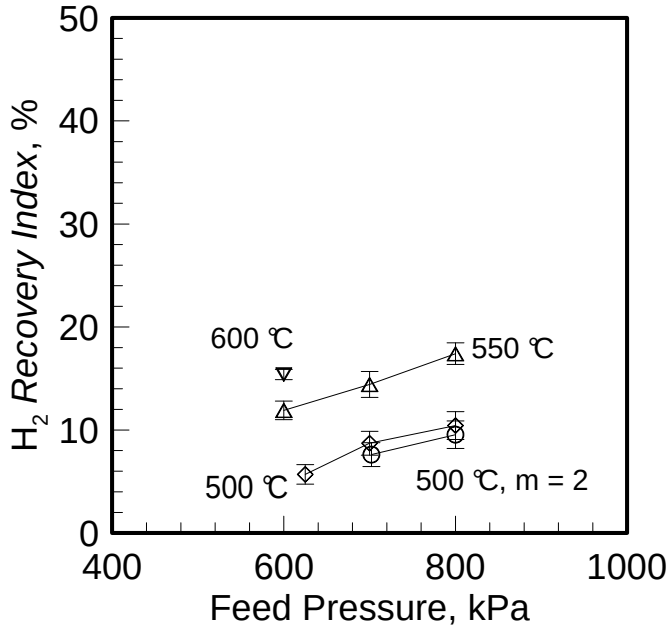

Fig. 33 - Hydrogen Recovery *Index* vs. feed pressure at different reaction temperatures. Operating conditions: GHSV = 1200 h^{-1}. Design parameters: A_m/V_{cat} = 0.42 cm^2 cm^{-3} and L_s/A_m = 11.6 cm^3*(STP)* cm^{-2} min^{-1}, length 8.5 cm.

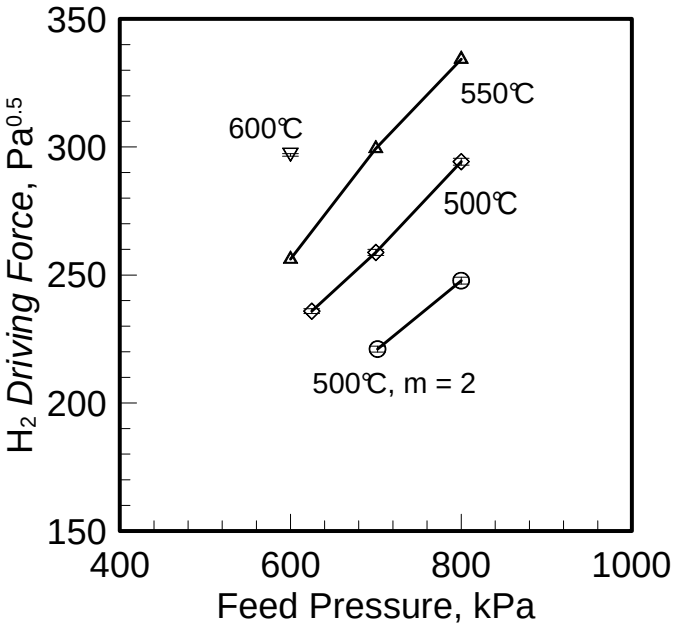

Fig. 34 - Hydrogen driving force vs. feed pressure at different reaction temperatures and reagents molar ratio. Operating conditions: GHSV = 1200 h^{-1}; m = 3. Design parameters: A_m/V_{cat} = 0.42 cm^2 cm^{-3} and L_s/A_m = 11.6 cm^3*(STP)* cm^{-2} min^{-1}, length 8.5 cm.

In confirmation of that previously said, figure 34 is showed. According to Sieverts' law, hydrogen driving force increase with the feed pressure in MR, at every temperature and a reagents molar ratio equal to 3. At a fixed feed pressure, the temperature increases the driving force whereas a reagents molar ratio less than three reduces the driving force values. In MRs, the combined effect of both temperature and pressure favors a larger hydrogen recovery as well as methane conversion. A 10% increase of temperature allows a 20% increase of driving force, at every feed pressure value since it influences the hydrogen permeability in according to Arrhenious law.

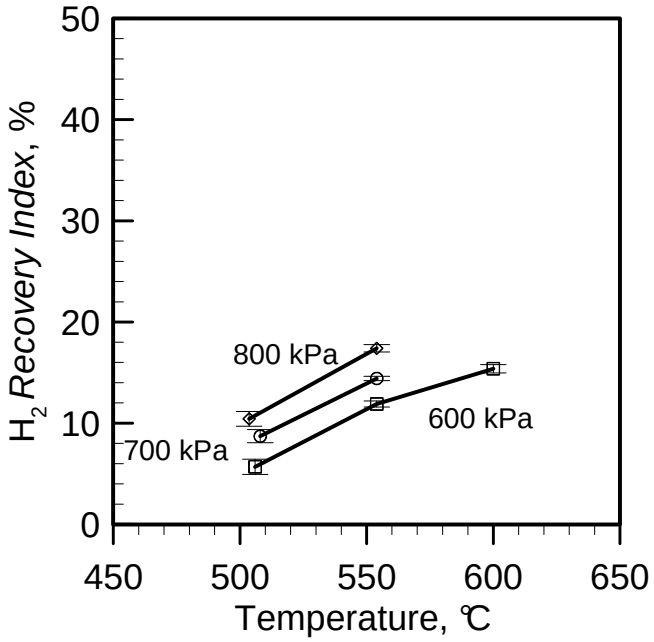

Fig. 35 - Hydrogen Recovery *Index* vs. reaction temperature at different feed pressure. Operating conditions: GHSV = 1200 h^{-1}, m = 3. Design parameters: A_m/V_{cat} = 0.42 cm^2 cm^{-3} and L_s/A_m = 11.6 cm^3*(STP)* cm^{-2} min^{-1}, length 8.5 cm.

Instead, the trend of hydrogen recovery at different feed pressures with reaction temperature is showed in figure 35 (or figure 30a). This figure confirms undoubtedly all the conclusions stated in figure 34. In fact, the hydrogen recovery is favored, at every temperature, by increasing driving force as well as at a fixed driving-force it increases with temperature, as also figure 36 shows. In this case, the trend between H_2 Recovery *Index* and driving force can be considered approximately linear since hydrogen absorption and desorption as well as the diffusion on the catalyst surface can interfere hindering transportation process towards the membrane surface.

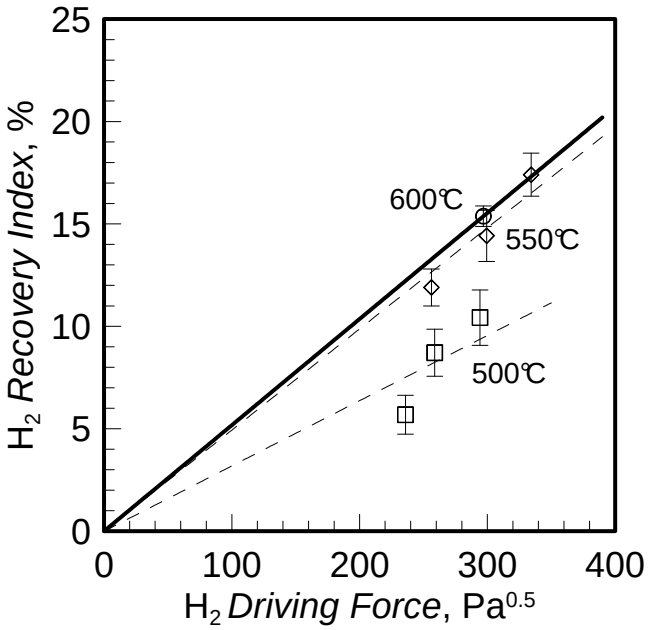

Fig. 36 - Hydrogen Recovery *Index* vs. hydrogen driving force at different reaction temperature. Operating conditions: GHSV = 1200 h^{-1}, ragents molar ratio equal to 3. Design parameters: A_m/V_{cat} = 0.42 cm^2 cm^{-3} and L_s/A_m = 11.6 cm^3*(STP)* cm^{-2} min^{-1}, length 8.5 cm.

5.1.1.3 Membrane Reactor *MR2*

This MR is characterized by a high membrane surface area with respect to catalyst volume. As said, membrane permeability and the thermodynamics of MSR reaction are promoted by higher temperatures; on the contrary membrane stability is preserved by lower temperature conditions. In fact, during the experimental tests, the membrane has been many times compromised at 600°C, figure 31; differently it resulted more stable at 550°C. Hence, as a trade-off solution, during the experimental study a temperature of 550°C has been chosen subsequently according to Grace *et al.* [130]. In fact, they conclude for all MRs in which the MSR is combined to the hydrogen permeation a good trade-off temperature to preserve the membrane is 550°C.

In this section, an MR (*MR2*) having a membrane length equal to 60 mm, catalyst mass of 0.884 g, L_s/A_m ratio equal to 11.6 cm^3*(STP)* cm^{-2} min^{-1} and A_m/V_{cat} ratio equivalent to 0.42 cm^2 cm^{-3} has been investigated. As shown in the previous section, for the same L_s/A_m constant ratio and reaction temperature, a lower hydrogen recovery (16%) has been obtained at an A_m/V_{cat} ratio equal to 0.42 cm^2 cm^{-3}. This means that in presence of a large volume of catalyst a larger hydrogen amount has been produced. At a fixed hydrogen driving force, palladium membrane surface is not able to counterbalance this production by recovering hydrogen. The membrane presents a low hydrogen permeation rate in addition to an inadequate surface area for the mass exchange. By increasing the membrane surface area with respect to the reduced catalyst volume, it is possible to improve the MR performance.

In this second case, then, the MR works by a high membrane surface area with respect to catalyst volume. In fact, the A_m/V_{cat} ratio is five-times higher than the previous one. This produces a 50% increase for methane conversion and a similar improvement of H_2 recovery, as shown in the figure 37.

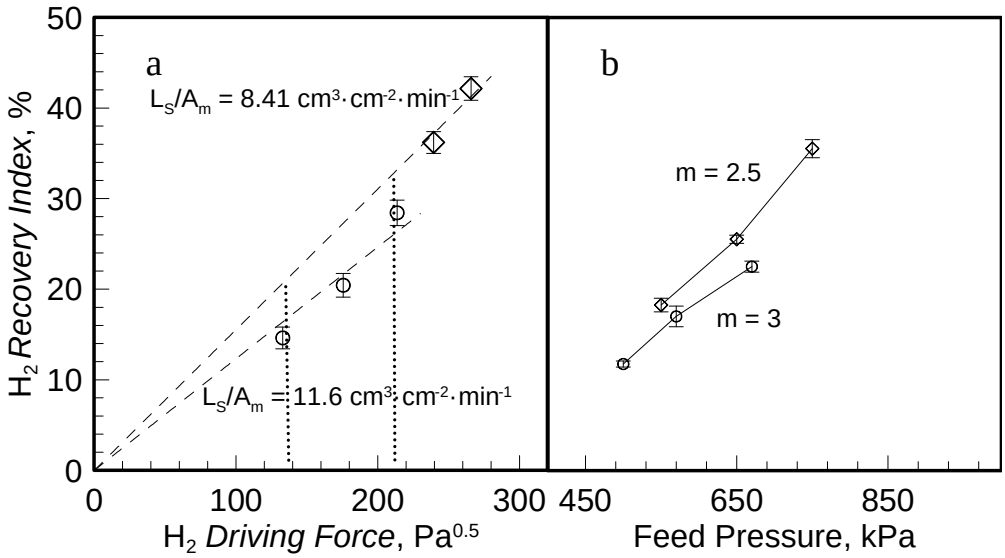

Fig. 37 – Hydrogen recovery versus both (**a**) H_2 driving force and (**b**) feed pressure. Operating conditions: GHSV = 4200 h^{-1}. Design parameter: A_m/V_{cat} = 2.1 cm^2 cm^{-3}.

As figure 37a is compared with figure 36, at the same reaction temperature, L_s/A_m ratio and driving force (equal to 320 $Pa^{0.5}$), a 16% hydrogen recovery is obtained at 0.42 cm^2 cm^{-3} whereas a 32% value is, instead, reached at 2.1 cm^2 cm^{-3}. Figure 37a shows as the effect of L_s/A_m ratio determines a significant influence on the MR performance. A 27% reduction of L_s/A_m value entails a 50% increase of hydrogen recovery at the lowest driving force value (140 $kPa^{0.5}$). This means that MR places more membrane surface at disposal of the hydrogen extraction with respect to the methane amount fed. The same percentage reduction carries out a moderate increase (40%) of the highest driving force value (210 $kPa^{0.5}$) since at a high pressure the hydrogen recovery is high even if reforming reaction is not thermodynamically favored.

Figure 38a shows as at a lower reagents molar ratio increase, at a fixed feed pressure, the hydrogen recovery since dilution effect on the reagents is decreased. Hence, the hydrogen partial pressures into MR are increased and the maximum H_2 recovery achievable is 28% at 760 kPa. As figure 38b shows, the methane conversion increases as the feed pressure increases at each different reagents molar ratio in feed. At each feed pressure, it achieves methane conversion values higher than the previous ones for *MR1*. When reagents reach the catalyst surface, a production of hydrogen higher than the one at m = 2.5 is reached. In fact, CH_4 conversion equal to 52% at m = 3 is obtained.. However, even if the yield of MR is not particularly high, the

methane conversion presents average values two-times greater than the thermodynamic equilibrium ones (TREC) at m = 3 as well as a 55% increase is obtained at m = 2.5 and 760 kPa.

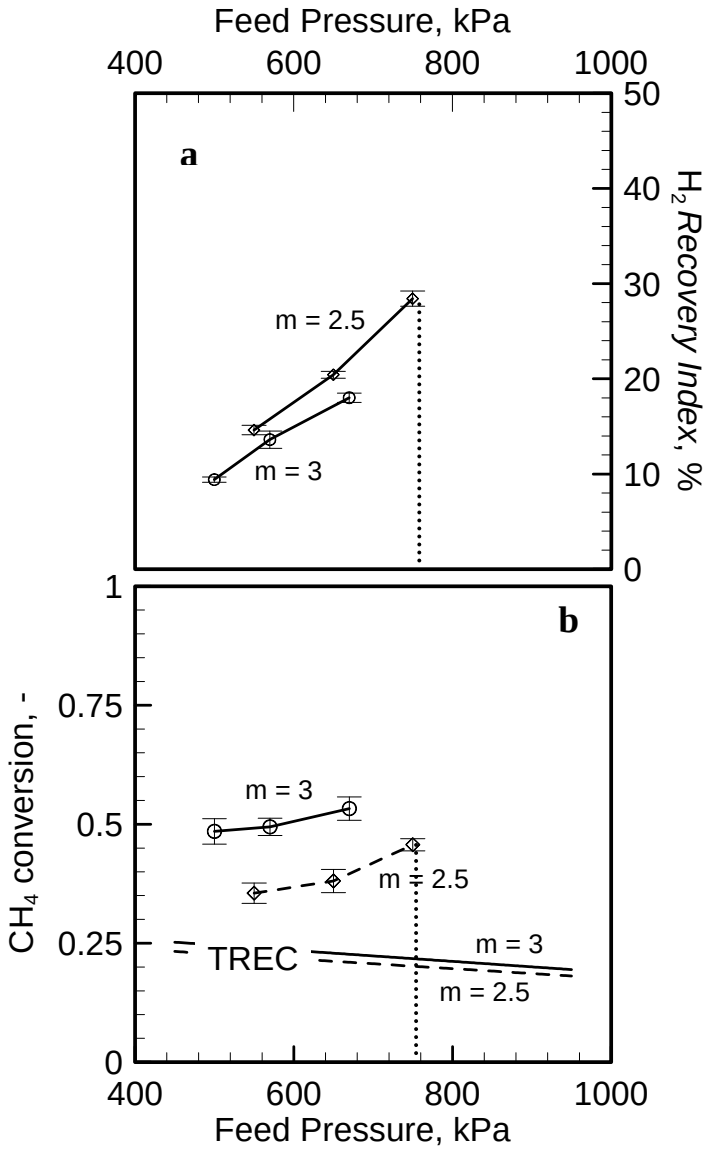

Fig. 38 – a) H_2 *Recovery Index* and b) Methane conversion as a function of Feed Pressure at two different reagents molar ratios compared to the TREC curve (solid and dotted lines). Operating conditions: 550°C and 4200 h^{-1}. Design parameters: A_m/V_{cat} of 2.1 cm^2 cm^{-3} and L_s/A_m of 11.6 cm^3*(STP)* cm^{-2} min^{-1}, length 6.0 cm.

5.1.1.4 Effect of L_s/A_m ratio on MR performance

With respect to earlier results, a reduced methane feed flow rate (L_s) with respect to membrane area has been considered. It points out that a low amount of methane reacts in presence of a higher membrane surface. In addition, high A_m/V_{cat} ratio has been still considered in order to keep a high extractive capability of the membrane in comparison to the productive capability of the catalyst.

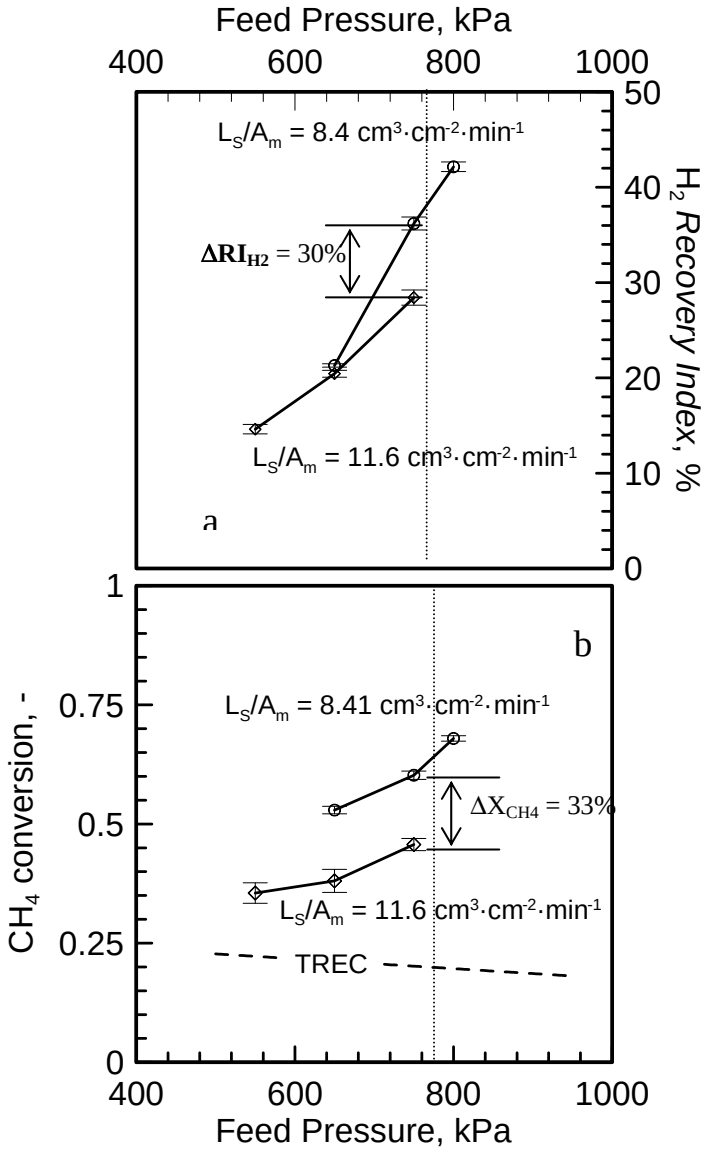

Fig. 39 – a) H_2 *Recovery Index* and b) Methane Conversion as a function of the Feed Pressure at two different L_s/A_m ratios compared to the TREC curve (dotted lines).
Operating conditions: GHSV = 4200 h^{-1}; T = 550 °C, reagents molar ratio equal to 2.5.
Design parameters: A_m/V_{cat} = 2.1 cm^2 cm^{-3}

A high hydrogen recovery improves the methane conversion. A low methane flow rate in feed (*i.e.* load) with respect to membrane surface offers to the hydrogen a sufficient residence time to be extracted from the reaction mixture allowing high methane conversion values. At A_m/V_{cat} = 2.1 cm^2 cm^{-3}, available for the reforming reaction, a reduction of limiting reagent flow rate means that an amount of methane reacts in presence of a higher mass transport surface (membrane surface area). At the same hydrogen driving force or feed pressure, this carries out to a higher hydrogen recovery (*i.e.* methane conversion) as showed in figures 39a and 39b. A 27% reduction for L_s/A_m carries out about a mild-30% increase for both CH_4 conversion and H_2 Recovery.

5.1.1.5 Membrane Reactor *MR3*

This MR works at lowest catalyst volume and methane flow rate in comparison to membrane surface area.

In view of the previous experimental results, this MR is characterized by a membrane length of 3.5 cm, a ratio A_m/V_{cat} = 2.1 cm^2 cm^{-3} and L_s/A_m = 8.4 cm^3(*STP*) cm^{-2} min^{-1}.

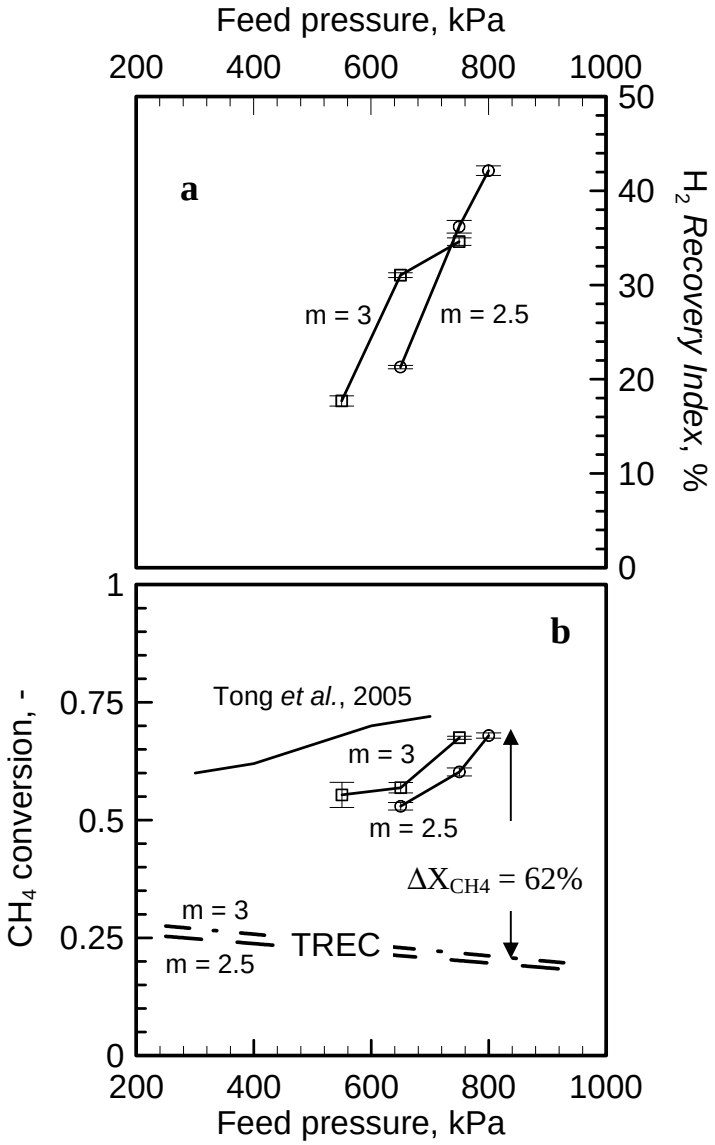

Fig. 40 - a) Hydrogen Recovery and b) Methane Conversion as a function of Feed Pressure at different molar ratios compared to TREC curves. Operating conditions: GHSV = 4200 h^{-1}; T = 550 °C. Design parameters: A_m/V_{cat} = 2.1 cm^2 cm^{-3}; L_s/A_m = 8.4 cm^3(*STP*) cm^{-2} min^{-1}; membrane length = 3.5 cm.

As shown in figure 40, the hydrogen recovery as well as methane conversion increase as a function of the feed pressure. A methane conversion corresponding to the 68% was reached at 800 kPa and m = 2.5. By removing continuously and quickly the produced hydrogen from the reaction zone, in high pressure operating conditions, a methane conversion approximately three-

time higher than the thermodynamic equilibrium value in a conventional reactor (*e.g.* a mid-62% percentage difference) has been achieved at lower reagents molar ratios. The hydrogen recovered on permeate side is 43% with respect to the amount produced and about three-times higher than the one in *MR1*. With respect to this latter MR (*MR2*), at 650 kPa methane conversion increases of the 20% for m = 3 and 50% for m=2.5, respectively. The results are in agreement with Tong and Matsumara's experimental work [20] in which the reaction tests were carried out, however, in presence of a sweep gas stream by using both a A_m/V_{cat} ratio of 3.8 cm^2 cm^{-3} and value of GHSV equal to 3360 h^{-1} (feed pressure range of 100-700 kPa) as well as by using a 11 μm-thick Pd/Ag-based membrane.

Figure 41 confirms that has been previously said. In fact, by doubling approximately (*e.g.* a 76% percentage increase) the value of L_s/A_m ratio, for example at 800 kPa, methane conversion decreases of a value equal to the 30% whereas hydrogen recovery, instead, decreases of a value equal to the 44%, figure 42. In the same catalyst volume, a higher methane load in the feed produces a large amount of hydrogen that is not extracted quickly by palladium membrane for its low permeation rate (*i.e.* low hydrogen recovery). Even if higher GHSV values are reached in MR, a methane conversion 2.5-time higher than TREC (X_e) is obtained.

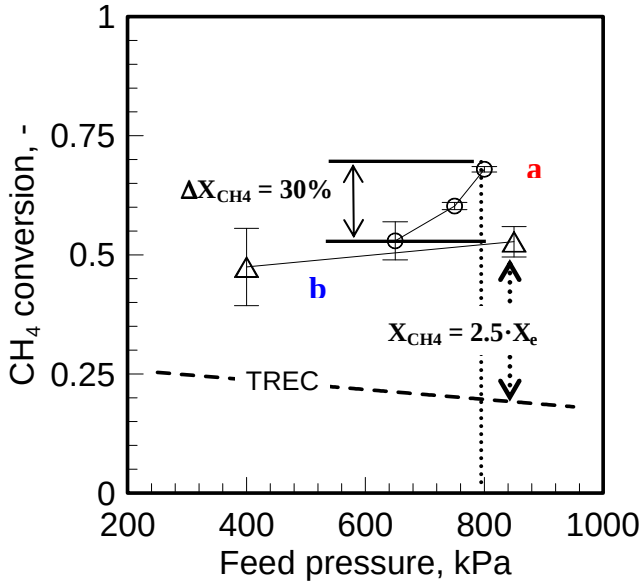

Fig. 41 - Methane Conversion as a function of Feed Pressure at two different values of L_s/A_m ratio compared to TREC curves. Operating conditions: m = 2.5; T = 550 °C. Design parameters: A_m/V_{cat} = 2.1 cm^2 cm^{-3}; membrane length = 3.5 cm. a) GHSV = 4200 h^{-1}; L_s/A_m = 8.4 cm^3(*STP*) cm^{-2} min^{-1}. b) GHSV = 6400 h^{-1}; L_s/A_m = 14.8 cm^3(*STP*) cm^{-2} min^{-1}.

As feed pressure increases both hydrogen recovery and methane conversion increase, see figure 42. At higher L_s/A_m ratios, this means that an upgrading of the membrane reactor performance, with 100-μm thick Pd/Ag membrane, can be reached if the feed pressure is still further increased.

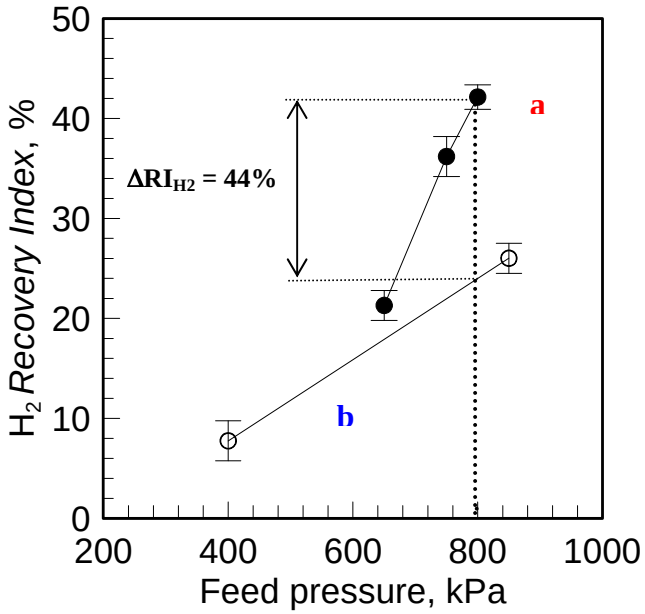

Fig. 42 - Hydrogen recovery *Index* as a function of Feed Pressure at two different values of L_s/A_m ratio. Operating conditions: m = 2.5; T = 550 °C. Design parameters: A_m/V_{cat} = 2.1 cm^2 cm^{-3}; membrane length = 3.5 cm. a) GHSV = 4200 h^{-1}; L_s/A_m = 8.4 cm^3(*STP*) cm^{-2} min^{-1}. b) GHSV = 6400 h^{-1}; L_s/A_m = 14.8 cm^3(*STP*) cm^{-2} min^{-1}.

5.1.1.6 Membrane Reactor *MR4*. Effect of the catalyst distribution

With respect to the previous membrane reactors, *MR4* has a catalyst volume distributed along the axial direction as figure 43 shows. The opportunity to tune the catalyst [131] along the MR has been established by setting a lower catalyst mass where the reaction rate is important (close to inlet) and a higher catalyst amount in the zone where the increase of the conversion is became less significant (close to outlet). This choice guarantees an improvement of the MR performance because it imposes to the reagents to react progressively along the reactor in contact with an increasing amount of catalyst. Thus, the ***whiskers-like*** coke formation and, then, the collapse of the catalyst support can be limited. The same results have been obtained by means of a theoretical model by Caravella *et al.* [149] for the MSR.

The produced hydrogen amount in the catalyst bed increases progressively in the membrane reactor so as methane conversion per-pass. In the first part of membrane reactor (I), the produced hydrogen amount and its partial pressure are too low since conversion per-pass, referred to this catalyst volume, is low. In addition, hydrogen is exposed at a lower membrane surface area and, as a consequence, the recovery is low.

In the second part of MR (II), the hydrogen amount, and then, partial pressure are enhanced by the continue occurrence of reforming reaction (increase of the methane conversion per-pass). The produced hydrogen adds to the one previously generated and not entirely extracted. Thus, it

has a higher partial pressure and being exposed at higher membrane surface area, the recovery is a little bit higher than the preceding one but not still enough.

In the third part (III), the reagents already in some measure converted are in contact with the highest catalyst volume and, then, they produce a higher conversion per-pass (*i.e.* high "partial" residence time). Hydrogen presents a high partial pressure with respect to the previous parts and although it has a low permeation rate, hydrogen is in presence of a reduced membrane surface. Therefore, it is not sufficiently extracted through the membrane. As a consequence, most of the hydrogen remains in the retentate stream. The total hydrogen recovery does not result higher than the one with no-distributed catalyst figure 43**.**

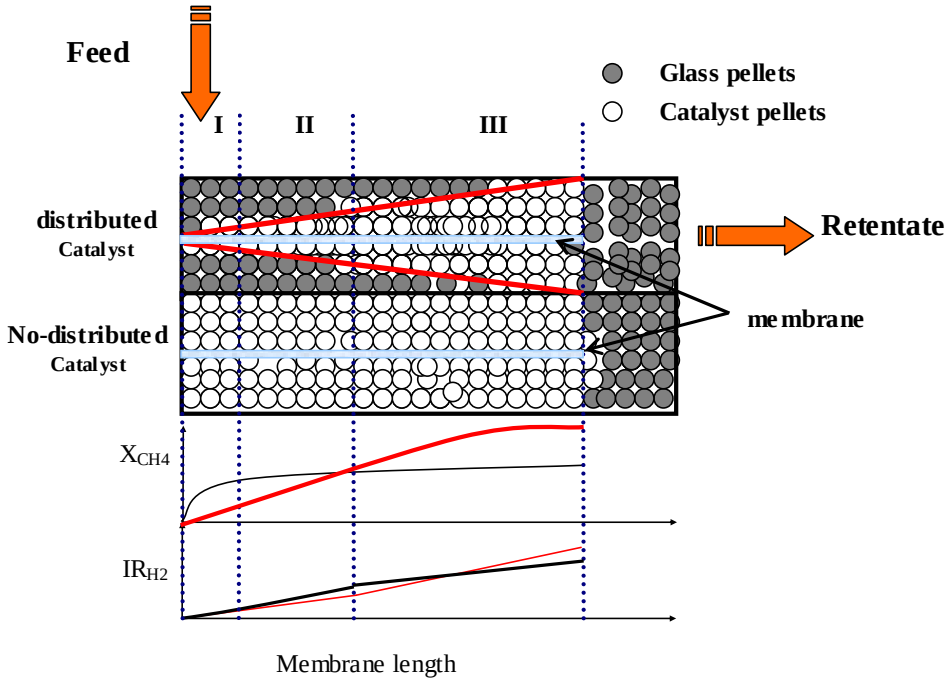

Fig. 43 - A qualitative evaluation of methane conversion and hydrogen recovery profiles inside of non-distributed catalyst bed (**black line**) in comparison with the distributed one (red line) during the MSR reaction.

In this case it has been decided to increase the ratio A_m/V_{cat} = 10 cm^2 cm^{-3} in order to improve the material exchange through the membrane compared to the catalyst amount necessary to uphold the reforming reaction. Moreover, the effect of the L_s/A_m ratio has been analyzed to evaluate if the time spent by the limiting reagent in catalyst bed is enough so that the membrane extracts produced hydrogen.

In figure 44, the dependence of hydrogen recovery and methane conversion by the feed pressure is showed and both increase as feed pressure increases at every feed molar ratio. Obviously, as feed molar ratio increases much steam is present in the reaction zone. It allows producing more hydrogen. At high pressure (*e.g.* 700 kPa), the thermodynamic equilibrium conversion of a TR is

four-time less than chemical conversion in MR (*i.e.* 94%). The produced hydrogen is quickly extracted through the membrane by effect of a higher driving force. This forces the shift of chemical equilibrium towards the products. The presence of a higher catalyst amount in a zone, at the end of membrane, where the reagents are partially converted (zone III, figure 43) assures a higher methane conversion even due to the presence of the membrane. Hydrogen recovery (*i.e.* 46%) will be a little bit higher than the one obtained in the MR previously tested (*MR3*) since hydrogen is in presence of an membrane surface inadequate for the complete extraction.

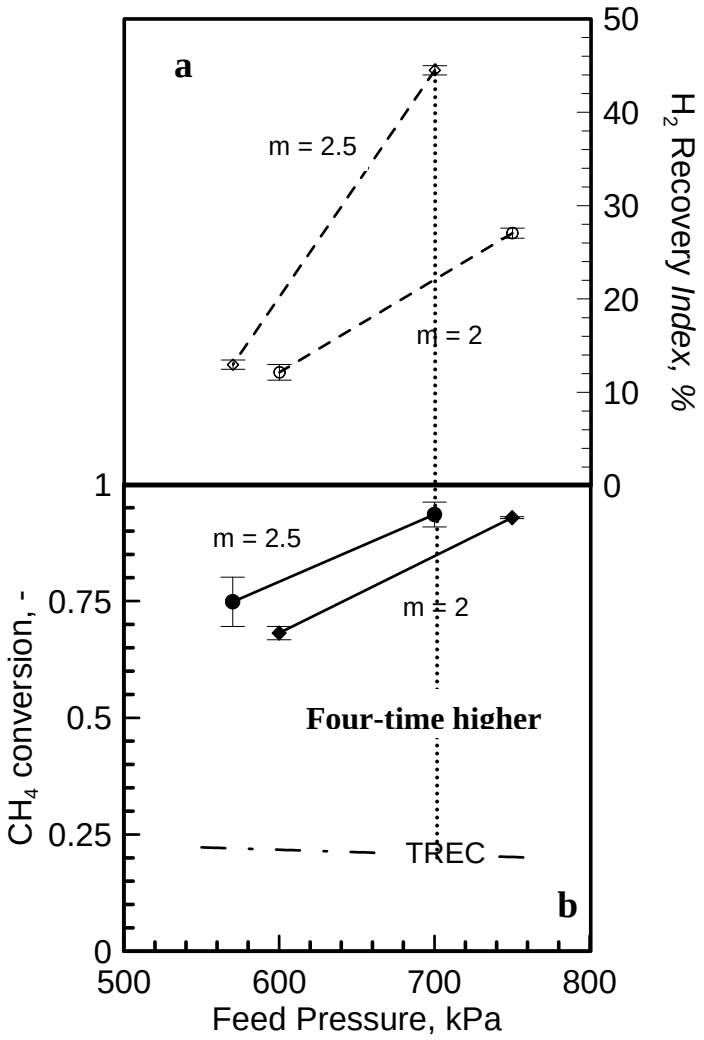

Fig. 44 – a) Hydrogen recovery *Index* and b) methane conversion as a function of Feed Pressure at two different values of reagent molar ratios. Operating conditions: T = 550 °C. Design parameters: L_s/A_m = 2 cm^3 cm^{-2} min^{-1}; A_m/V_{cat} = 10 cm^2 cm^{-3}; Distributed catalyst mass.

Figure 45 shows the same earlier conclusions. By confirming how previously said, both methane conversion and hydrogen recovery increase as feed pressure increases. Obviously, high conversions are reached at a higher reagents molar ratio. With respect to TREC, MR presents methane conversions about three-times higher at each reagents molar ratio.

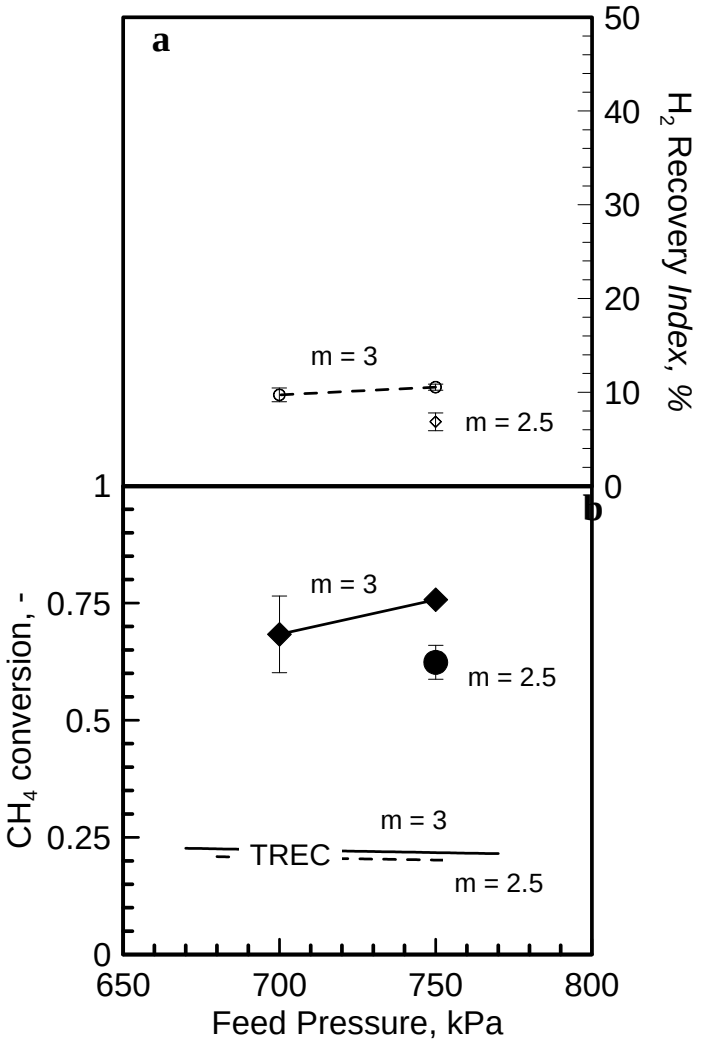

Fig. 45 - a) Hydrogen recovery *Index* and b) methane conversion as a function of Feed Pressure at two different values of reagent molar ratios. Operating conditions: T = 550 °C. Design parameters: L_s/A_m = 3 cm^3 cm^{-2} min^{-1}; A_m/V_{cat} = 10 cm^2 cm^{-3}; Distributed catalyst mass.

By increasing the L_s/A_m ratio, figure 46, methane conversion is lower than the previous one since the residence time is reduced (*i.e.* high GHSV). The less hydrogen amount produced during the MSR is not able to permeate efficiently the membrane (*e.g* lower driving force). If it combined to the low residence times, these operating conditions reduce considerably the hydrogen recovery (*i.e.* about 80%).

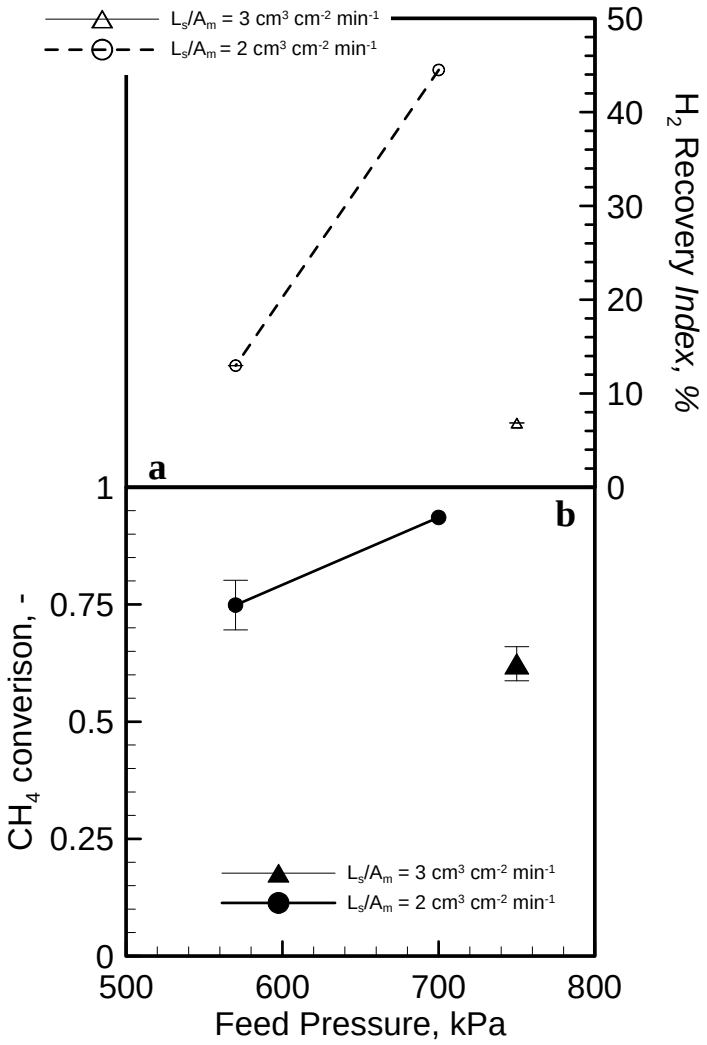

Fig. 46 - a) Hydrogen recovery *Index* and b) methane conversion as a function of Feed Pressure at two different values of L_s/A_m ratios. Operating conditions: m = 2.5; T = 550 °C. Design parameters: A_m/V_{cat} = 10 cm^2 cm^{-3}; Distributed catalyst mass.

In figure 47, the performance for *MR3* at m = 2.5 have been compared to the ones for *MR4*. At 700 kPa, a 25% increase of hydrogen recovery and 42% increase of methane conversion are possible, respectively. Instead, in comparison to the TREC a four-time increase for methane conversion is obtained.

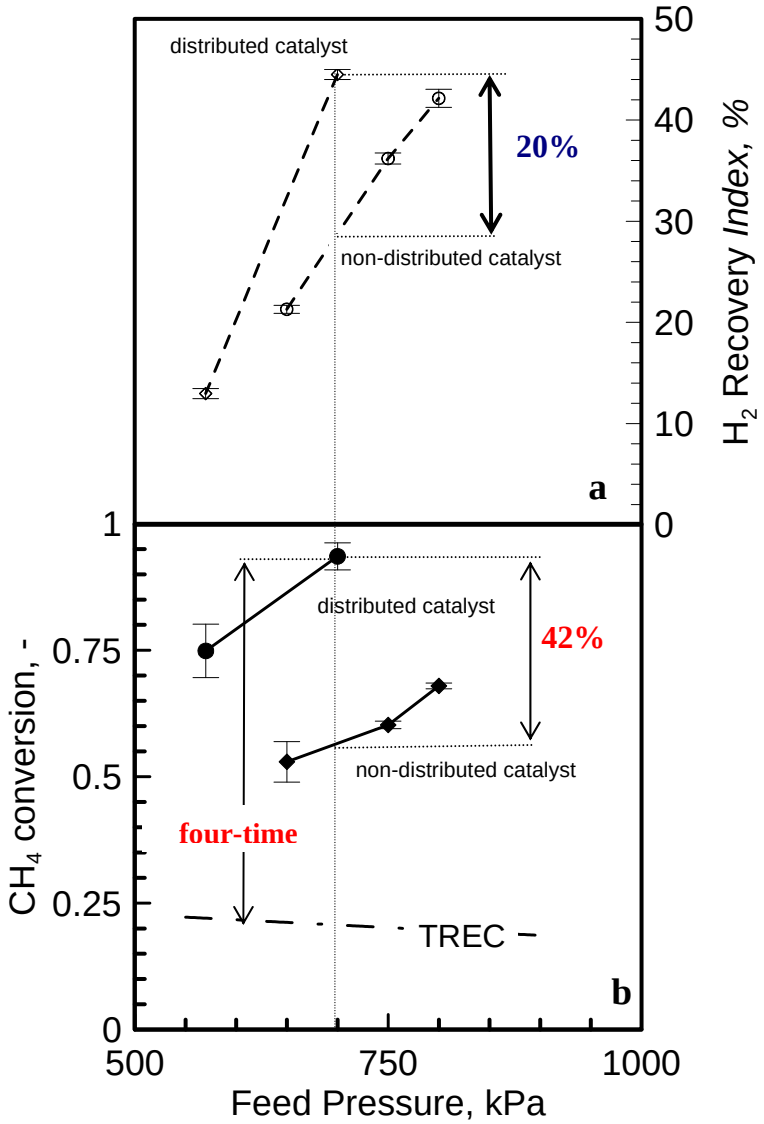

Fig. 47 - a) Hydrogen recovery *Index* and b) methane conversion as a function of Feed Pressure at two different catalyst distribution mode. Design parmeters: (distributed) A_m/V_{cat}= 10 cm^2 cm^{-3}; L_s/A_m = 2 cm^3 cm^{-2} min^{-1}; (non-distributed) A_m/V_{cat}= 2.1 cm^2 cm^{-3}; L_s/A_m = 8.4 cm^3 cm^{-2} min^{-1}

Table 10 compares the experimental results obtained in this work with those of literature. It is possible to observe as, by choosing properly both operating conditions and design parameters, higher methane conversions are reachable in MR by working without sweep gas in presence of a 100 μm-thick membrane and distributed catalyst.

Table 10 - Comparison of the performance and design parameters for different MRs.

Reference	δ μm	A_m/V_{cat} $cm^2\ cm^{-3}$	L_s/A_m $cm^3\ cm^{-2}\ min^{-1}$	Sweep (sw) flow rate /Temperature/feed pressure	Conversion, %
[132]	11	1.31	1.27	sw/523°C/100 kPa	82
[129]	100	3.8	1.9	sw/500°C/600 kPa	61
[11]	20	3.2	4	sw/500°C/136 kPa	85
[8]	11	3.8	14.7	sw/527°C/700 kPa	70
[27]	50	9.1	0.4	sw/450°C/136 kPa	40
[21]	10	0.92	3.73	sw/500°C/100 kPa	51
This work	**100**	**10**	**2**	**no-sw/550°C/700 kPa**	**94**

5.1.1.6a Coke deposition effect

Carbon deposition increases with the depth of the catalyst bed and a higher CH_4 partial pressure in the feed [133]. It is important to consider that catalyst fractions in the fixed bed reactor located at different lengths operate under a diverse local reaction atmosphere. These differences become even more pronounced in the case in which a membrane removing H_2 from the reaction medium is present. Thus under the conditions used, a higher carbon deposition at the end of the catalytic *non-distributed* bed due to the occurrence of cracking of methane is expected. In the case of a *non-distributed* catalyst bed, even if an excess in the reactant H_2O is presents, it is not able to act as “moderator” of the cracking of methane. By the forcing of hydrogen extraction, high amounts of low-reactivity deposits are obtained. Moreover, whereas conditions at the initial part of the fixed bed inside the MR resemble those existing in a conventional reactor, catalyst particles located at the end of the catalytic bed will operate under more unfavourable conditions due to the lack of hydrogen and high CO_2 concentration.

The coke reduction occurs since a catalyst bed distribution arranged in an increasing mode along the membrane reactor put available of the reagents, step-by-step already converted a catalyst amount more and higher. In this way, it is possible to favour the water spill over since at the end of the catalyst bed OH groups will have available more support for the spill-over whereas methane molecule adsorbed on the catalyst surface will have available more nickel amount. Thus, steam reforming is more favoured with respect to the cracking.

Figure 48 shows experimental results for the coke deposition for *MR1*. The selective and continue extraction of hydrogen through the palladium membrane shifts the chemical

equilibrium of the methane decomposition reaction towards a high carbon formation increasing the risk of the carbon deposition. In fact, at m = 3, the V_{CH4} values are less than one. In this case, they increase as feed pressure increases. By combining a high reagents molar ratio to high feed pressure, it is possible to reduce tendency to carbon deposition since coke formation is hindered. Differently, at a stechiometric reagents molar ratio (m=2), higher and higher feed pressure increases higher and higher the V_{CH4} values decrease according to the conventional reformer behavior in the same operating conditions.

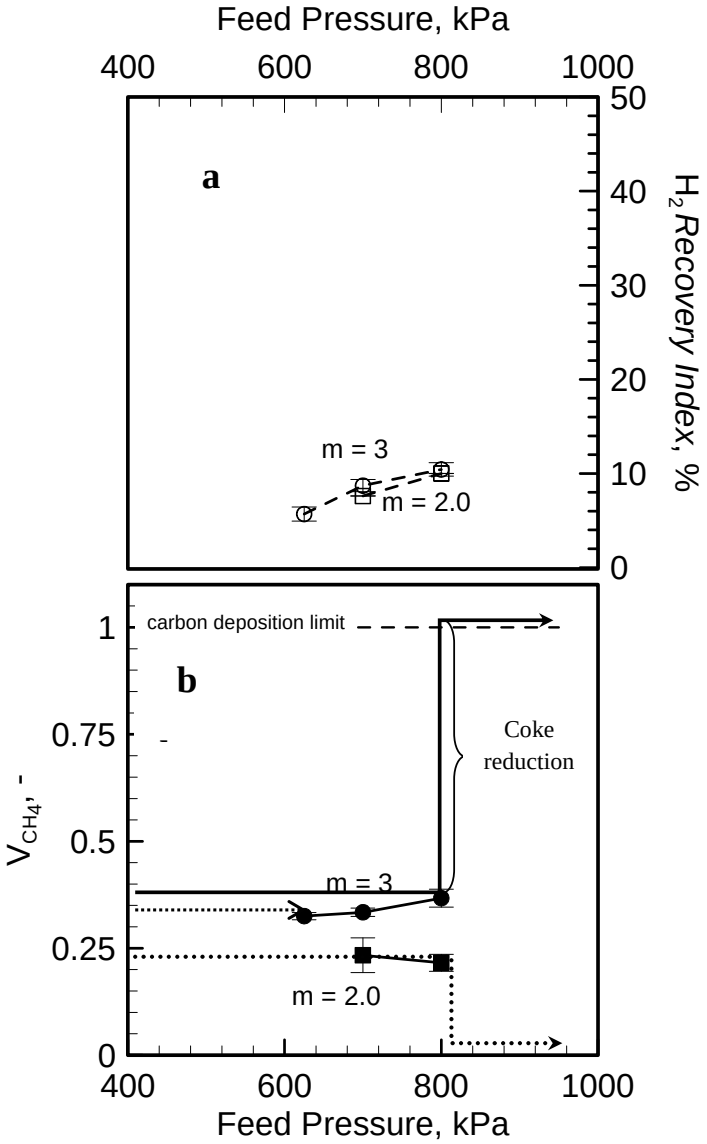

Fig. 48 – a) H_2 *Recovery Index* and b) V_{CH4} parameter as a function of the Feed Pressure for the *MR1*. Operating condition: GHSV = 1200 h^{-1}; T = 500°C. Design parmeters: A_m/V_{cat} = 0.42 cm^2 cm^{-3}; L_s/A_m = 11.6 cm^3 (*STP*) cm^{-2} min^{-1}.

As the reaction temperature increases, at fixed feed pressure, the coke formation is reduced in agreement to the Kleinert's considerations [22], figure 49. In the specified operating conditions,

a reagents molar ratio equal to 3 combined to 600°C is still enough to obstacle the coke formation inside of MR since, probably, the sintering rate is not high. The increasing feed pressure hinders the coke formation rate while hydrogen is extracted.

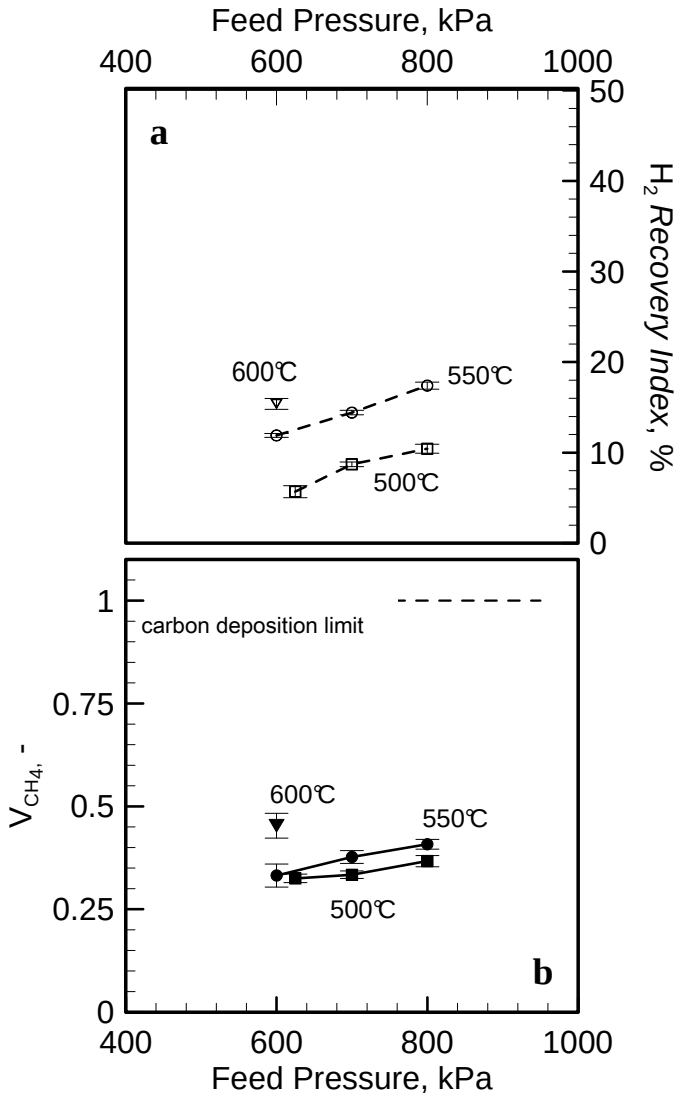

Fig. 49 – a) H_2 *Recovery Index* and b) V_{CH4} parameter as a function of the Feed Pressure for *MR1* at m = 3. Operating conditions: m = 3; GHSV = 1200 h^{-1}. Design parameters: A_m/V_{cat} = 0.42 cm^2 cm^{-3}; L_s/A_m = 11.6 cm^3 *(STP)* cm^{-2} min^{-1}.

As figure 50 shows, V_{CH4} increases as feed pressure increases. The occurring of this small increase of V_{CH4} values in correspondence of the increasing feed pressure carries out to a reduction of the coke but in comparison to the figure 48, at each molar ratio, V_{CH4} values are lower than the ones regarding *MR1*.

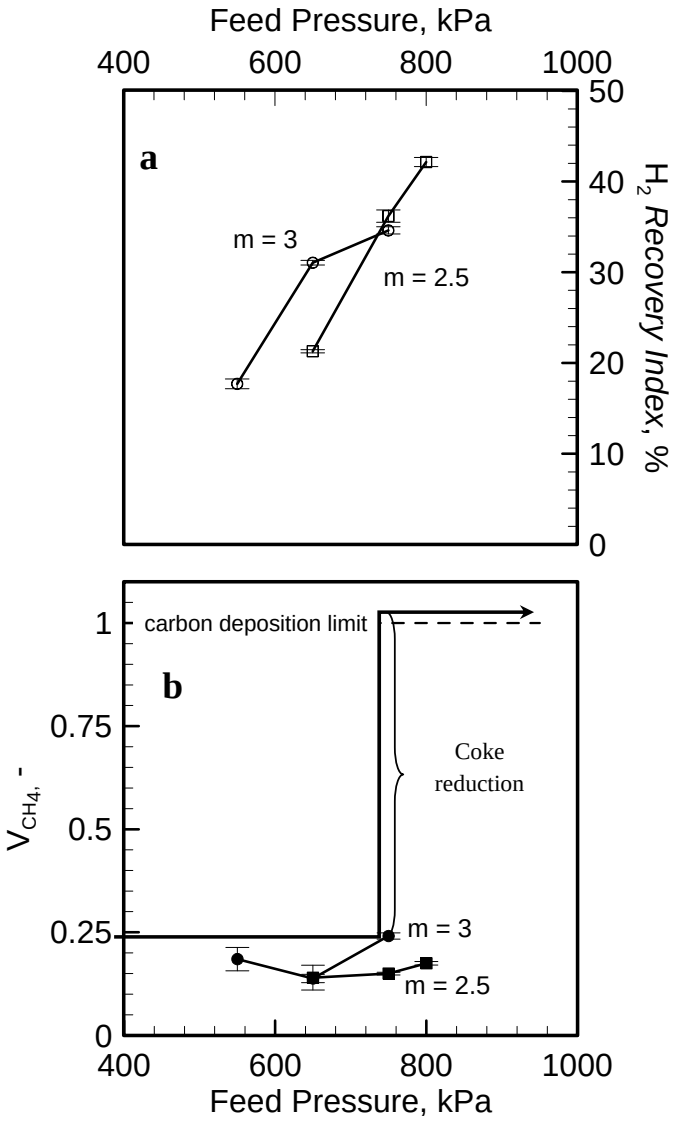

Fig. 50 - a) H_2 *Recovery Index* and b) V_{CH4} parameter as a function of the Feed Pressure for the *MR3* at two different reagents molar ratios. Operating conditions: GHSV = 4200 h^{-1}; T = 550°C; A_m/V_{cat} = 2.1 cm^2 cm^{-3}; L_s/A_m = 8.4 cm^3 *(STP)* cm^{-2} min^{-1}.

Membrane reactor *MR3* shows the best performance with respect to the previous MRs (*i.e.* a 68% methane conversion and 42.5% hydrogen recovery), but it is present higher carbon formation tendency ($V_{CH4}\rightarrow 0$), see figures 50. Obviously, both a high feed molar ratio and feed pressure reduce this tendency (*e.g.* the V_{CH4} value increases).

In figure 51 for each reagents molar ratio, an increase of methane conversion carries out to a furthermore increase of H_2 Overall Yield. This last is defined as the moles number of hydrogen recovered by the membrane per moles methane fed to the reformer according to Li's theoretical definition [127]. Overall yield is independent by the reagents molar ratio except at the lowest methane conversions. In this case, a high reagents molar ratio reduces the hydrogen overall yield (*e.g.* the highest dilution of hydrogen and reduction of its driving-force). A 29% increase of methane conversion (from 0.53 to 0.68), at a fixed reagents molar ratio, involves about an 80%

increase of Overall Yield. A 22% increase of methane conversion, instead, produces a 25% increase of V_{CH4} (*i.e.* lower coke formation tendency or $V_{CH4} \rightarrow 1$). At a low reagents molar ratio, V_{CH4} value is less influenced by the conversion.

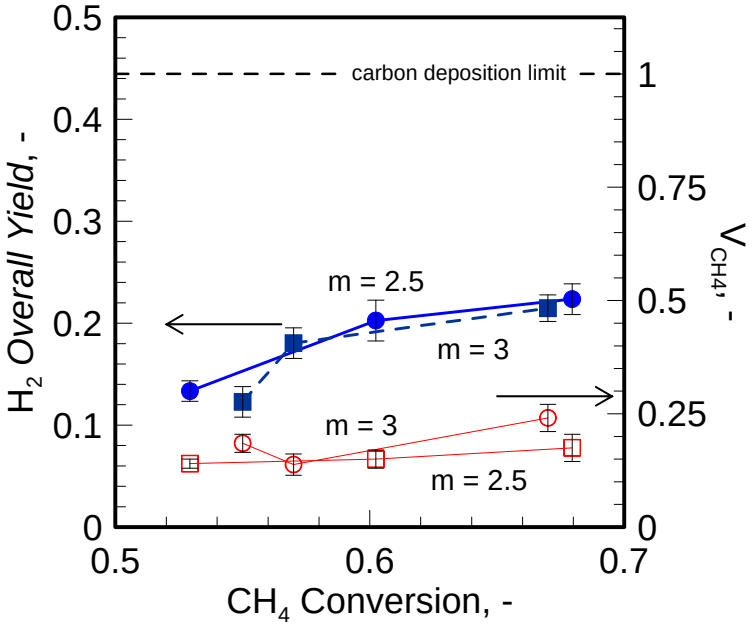

Fig. 51 – Coke formation and Overall Yield as a function of the methane conversion in *MR3*: Operating conditions: GHSV = 4200 h^{-1}; T = 550°C. Design parameters: (**non-distributed**) A_m/V_{cat}= 2.1 cm^2 cm^{-3}; L_s/A_m = 8.4 cm^3 cm^{-2} min^{-1}

The catalyst distribution allows dosing the catalyst in MR allowing also a progressive and almost complete methane conversion. In fact, a high amount will be used where the reagents are present in low amount since they are partially converted. This strongly will favour methane conversion. Moreover, it reduces the coke formation since the reagents will react progressively in catalyst bed and step-by-step they meet an increasing catalyst amount. The particular operating and design conditions limit both sintering and coke formation rate. Therefore, high pressures have favoured the reduction of the coke amount up to zero with respect to previous MRs. As a consequence, a lower reagent molar ratio (m = 2.5) has been possible, see figure 52.

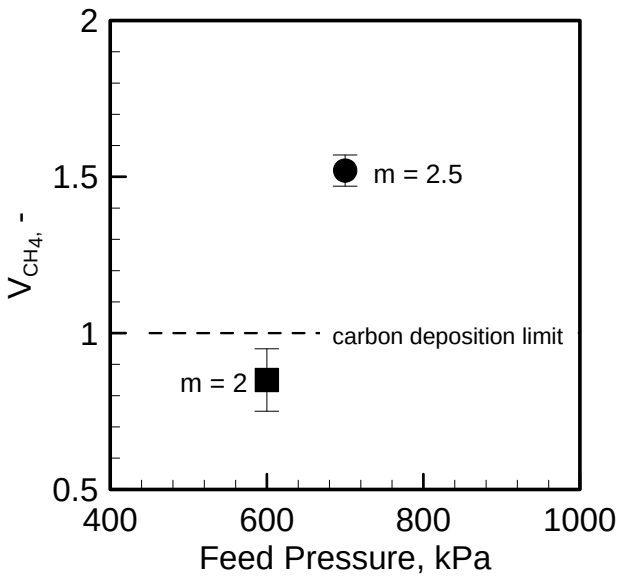

Fig. 52 - Coke formation as a function of the Feed Pressure in *MR4*. Operating conditions: T = 550°C. Design parameters: L_s/A_m = 2 cm^3 cm^{-2} min^{-1}; A_m/V_{cat} = 10 cm^2 cm^{-3}.

Membrane reactor (*MR3*) works in conditions such that carbon deposition (V_{CH4}<1) is increased on the catalyst active surface as table 11 shows. With respect to previous membrane reactors, *MR4* with a catalyst distributed along the membrane does not present coke formation.

Table 11 – Comparison between two different MRs in terms of carbon deposition tendency. Feed reagents molar ratio equal to 3.

Membrane Reactors	**A_m/V_{cat}, cm^2 cm^{-3}**	**L_s/A_m, cm^3(*STP*) cm^{-2} min^{-1}**	**V_{CH4}**
MR1	0.42	11.6	0.41
MR3	2.1	8.4	0.25
MR4_ dist. catalyst	10	2	1.5

In figure 53, the H_2 Overall Yield and V_{CH4} parameter as a function of methane conversion is showed for *distributed* catalyst condition in comparison with the one for *non-distributed* catalyst. In both cases, at every reagents molar ratio, as methane conversion increases both H_2 Overall Yield and V_{CH4} parameter increase. The catalyst distribution reduces the coke formation if MR works by methane conversions higher than 70% and a reagent molar ratio equal to 3. It means methane will be utilized only for MSR reaction. When the methane conversion is low, the coke formation increases at lower reagent molar ratios by the presence of a large methane amount in the catalyst bed. On the contrary, Overall Yield of hydrogen is lower respect to *non-distributed* catalyst condition since higher hydrogen production at the end of catalyst bed is not counterbalanced by the permeation rate. Hydrogen remains in the retentate stream. Only for

methane conversions higher than 90%, it will be possible to reach hydrogen Overall Yields higher than 25%, at reagents molar ratio equal to 2.5.

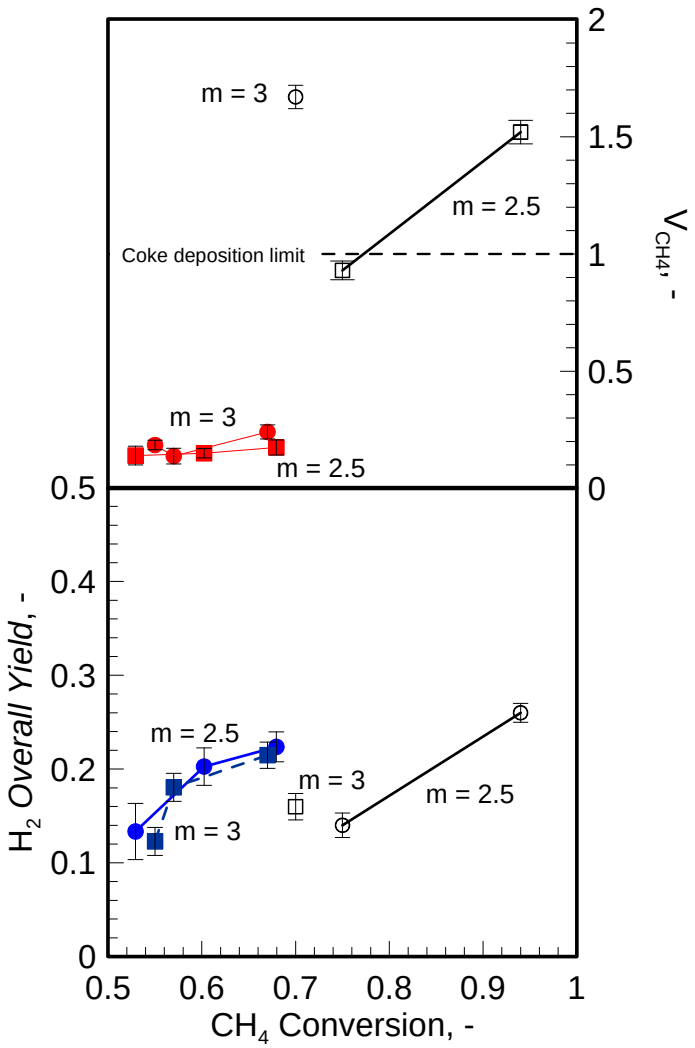

Fig. 53 – V_{CH4} value and H_2 *Overall Yield* as a function of CH_4 conversion. Operating conditions: T = 550°C; GHSV = 4200 h^{-1}. Design parameters: a) (*full symbols, non-distributed catalyst*) A_m/V_{cat} = 2.1 cm^2 cm^{-3}; L_s/A_m = 8.4 cm^3 cm^{-2} min^{-1}; b) (*empty symbols, distributed catalyst*) A_m/V_{cat} = 10 cm^2 cm^{-3}; L_s/A_m = 2 cm^3 cm^{-2} min^{-1}.

Both hydrogen and air have been alternatively used in the catalytic bed to validate the carbon deposition. Air, instead of oxygen, has been used to avoid further the sintering of the catalyst. The presence of CO_2 has been evidenced by Gas Chromatographic analysis. This means on catalyst surface coke was present. CO_2 amount was gradually decreasing in the time while air flowed. This evidenced that all coke was burning. The same check has been carried out by using hydrogen. In this case, by GC analysis the presence of methane has been evidenced. Of course, in the regeneration tests of the catalyst air has been chosen since it is cheaper with respect to hydrogen.

The presence of carbon deposition has been evidenced by SEM (Scanning Electron Microscopy) and EDX (Energy Dispersive X-Ray) analysis. As result by comparing the EDX analysis for the fresh and exhaust catalyst pellets, respectively, there is an experimental evidence of coke on catalyst particle (figure 54). Figures 55-57 show EDX analysis carried out in different zones of the catalyst surface and for different particles. A considerable peak corresponding to the carbonaceous specious is an evidence of the carbon presence on the pellets surface. Figure 58 shows an EDX analysis referred to an exhaust particle. The reduced peaks of Nickel evidence no catalyst. The presence of a peak of S_i (silica) indicates that it is present a part of support and this could give a confirmation of a plausible breakdown of the support. Figure 59 shows catalyst exhausted after an experimental tests cycle compared to the fresh catalyst before the reaction. This puts in evidence the break-down of the catalyst particle support as a consequence of the coke formation in ***whiskers*** form. Figures 60 and 61 show a SEM magnification of two exhausted catalyst particles having different size, respectively.

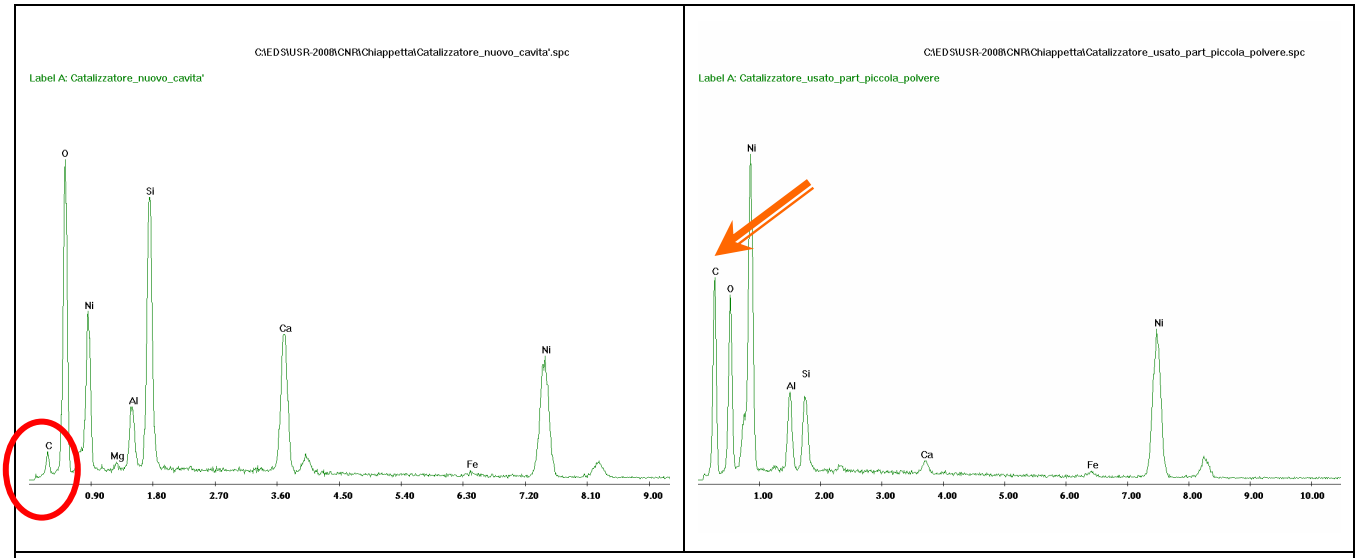

Fig. 54– An EDX analysis for a fresh and exhausted catalyst particle, respectively.

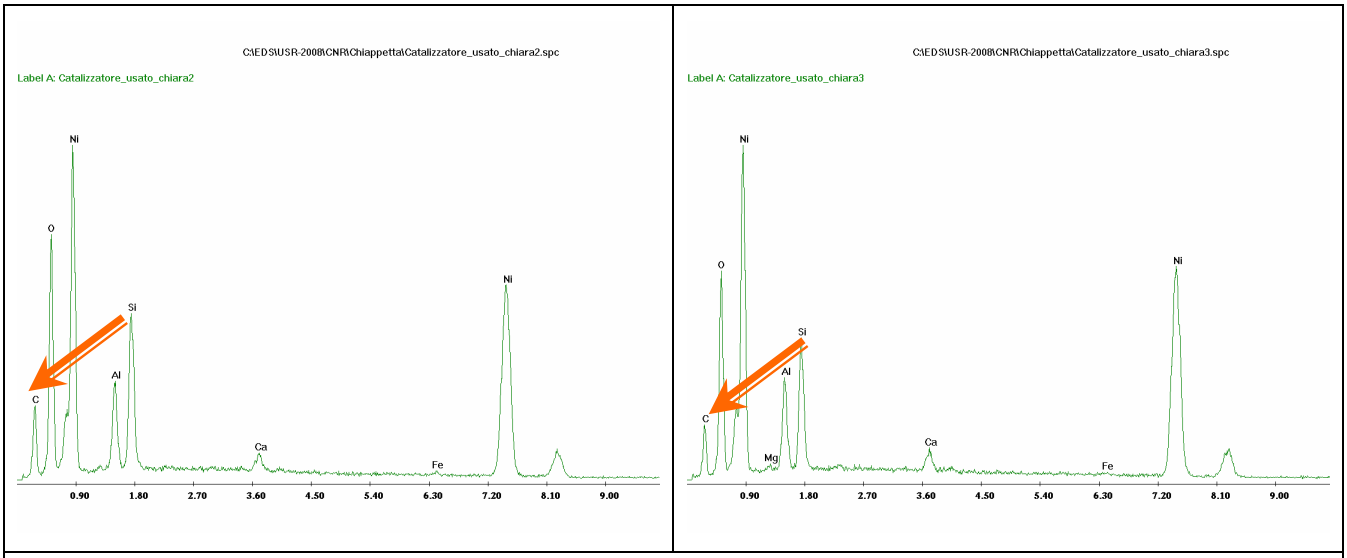

Fig. 55 – An EDX analysis for an exhausted catalyst particle.

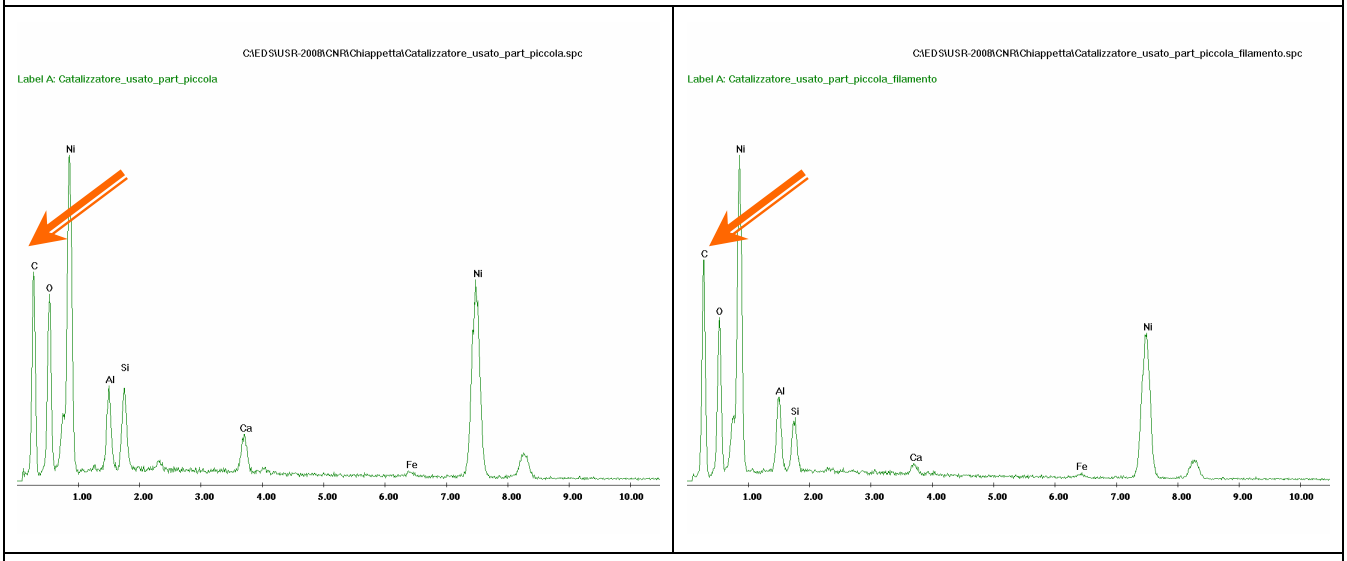

Fig. 56 – An EDX analysis for a exhausted catalyst particle having a smaller size.

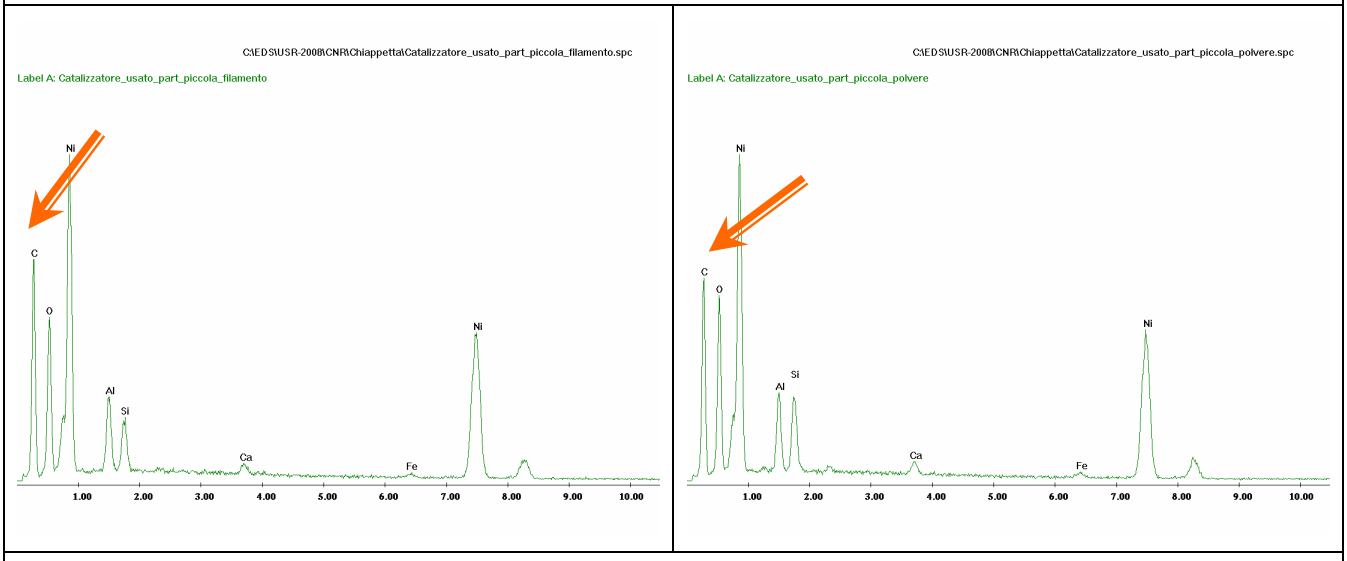

Fig. 57 – An EDX analysis for a exhausted catalyst particle having a smaller size.

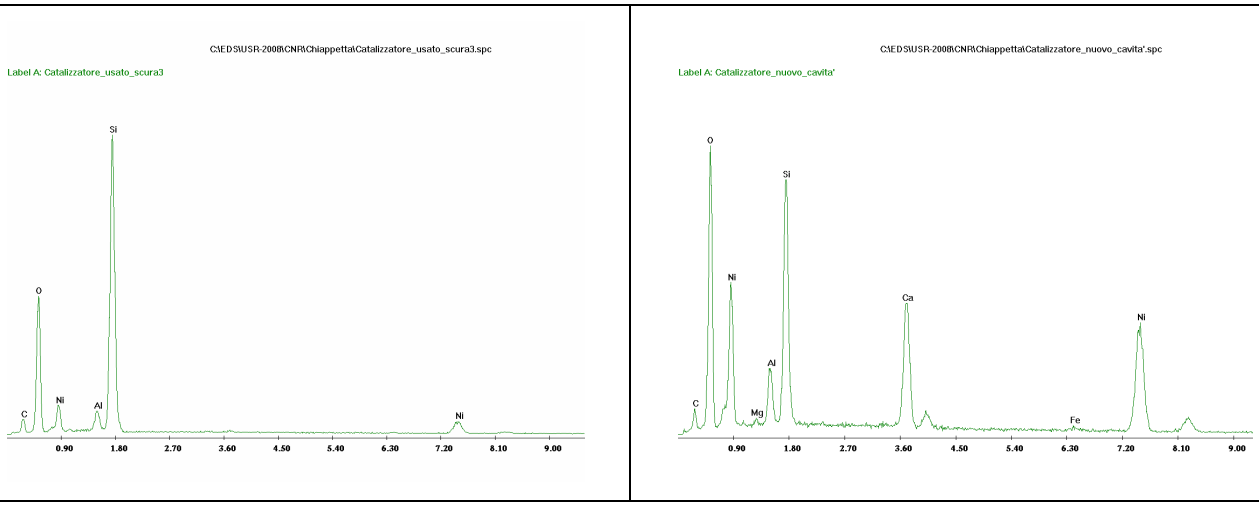

Fig. 58 – An EDX analysis on a piece of only support for both fresh and exhausted catalyst particle.

Fig. 59 – Catalyst exhausted after an experimental tests cycle and fresh catalyst, respectively.

Fig. 60 – Exhausted catalyst particle.

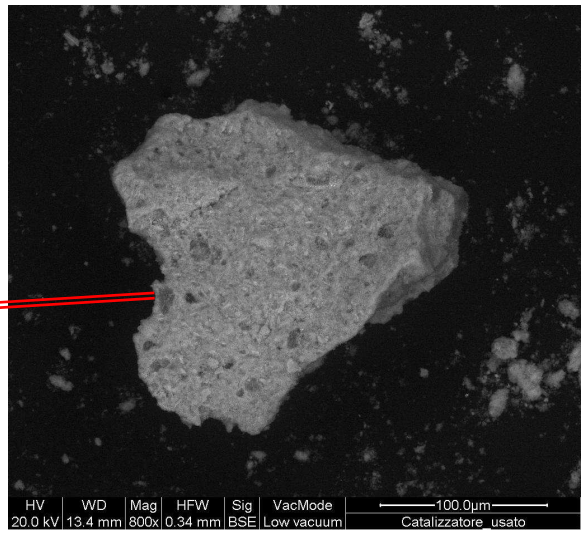

Fig. 61 – Magnification of catalyst particle.

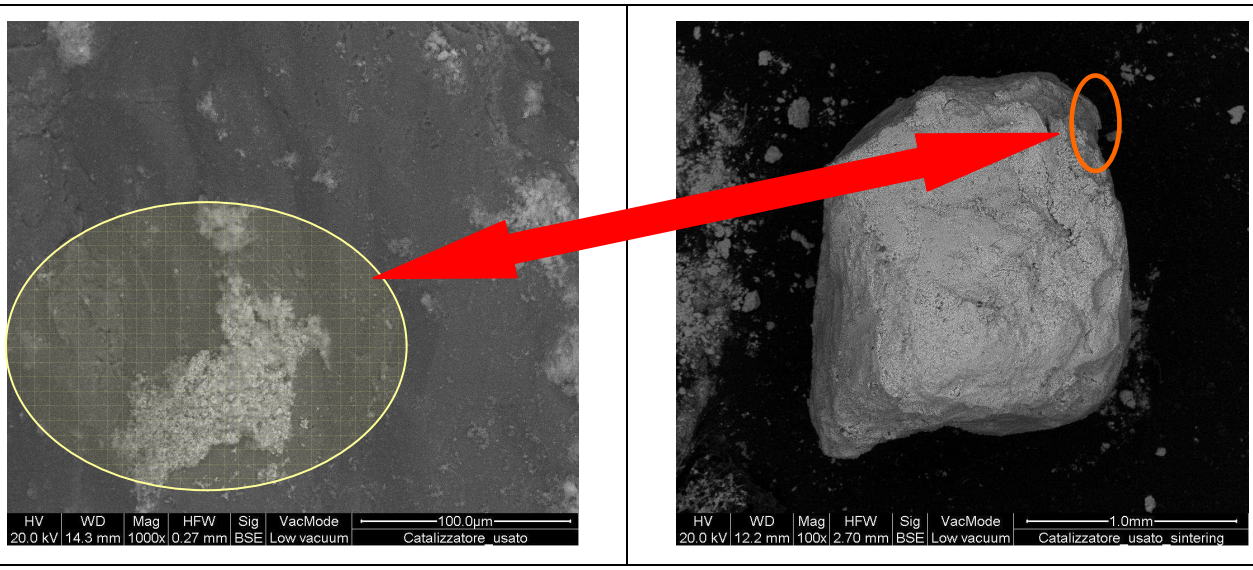

Fig. 62 – Ni-*Cluster* onto an exhausted catalyst particle.

Figures 62-63 show a cluster of Ni due to the possible mechanism of sintering by coalescence. In figure 63, the Ni particles migration in a concave zone of the pore suggests a process due to high initial sintering rates. The migration proceeds as long as there is the possibility that the cluster can grow in the portion of pore cavity in which it resides. At this step, the particle size is stabilized [134, 135].

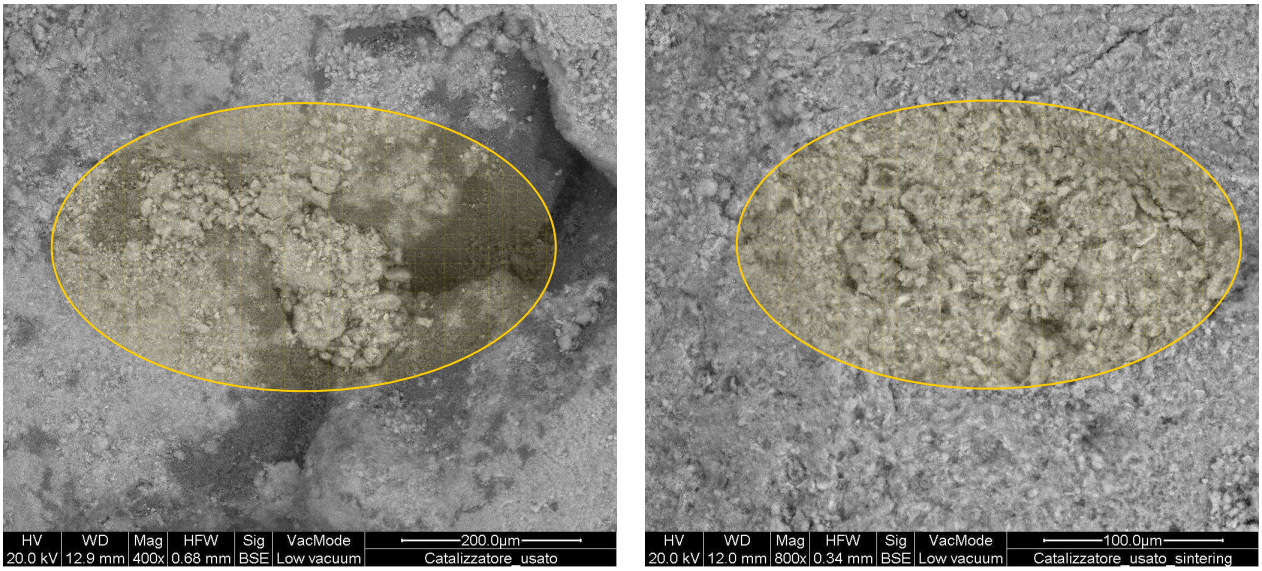

Fig. 63 – Ni-*Cluster* into a cavity of an exhausted catalyst particle.

5.1.1.7 Sensitivity analysis in a Pd-*based* MR with WGSR

In this case, besides the feed pressure effect on the MR performance also the study of the effect of a different sweep gas flow rate on permeate side has been tackled. This allows establishing the operative mode for a mitigation of the magnitude of the temperature *hot-spots* present during the exothermic WGS reaction and, contemporarily, to favour the hydrogen permeation. In addition, a catalyst distribution has been considered along the MR for the same target. A *SF* parameter (sweep factor) has been defined. It represents the ratio between sweep flow rate on permeate side and limiting reagent flow rate on the retentate side. In this case, the catalyst bed has been considered inside the membrane differently to the previous experimental case for MSR.

5.1.1.7a Influence of total feed pressure

As reported in literature, conventional reactors and hydrogen purification membranes at high pressures are used for WGS reaction due to their compatibility with the gasifiers working at severe conditions of pressure and temperature even if this reaction is, in particular, insensitive to pressure [136]. Consequently in this work the effect of the total feed pressure on the performance of a non isothermal MR, where the WGS takes place, has been investigated. Axial and radial temperature and concentration profiles have been analysed for three different pressure values (110 kPa, 500 kPa and 2000 kPa).

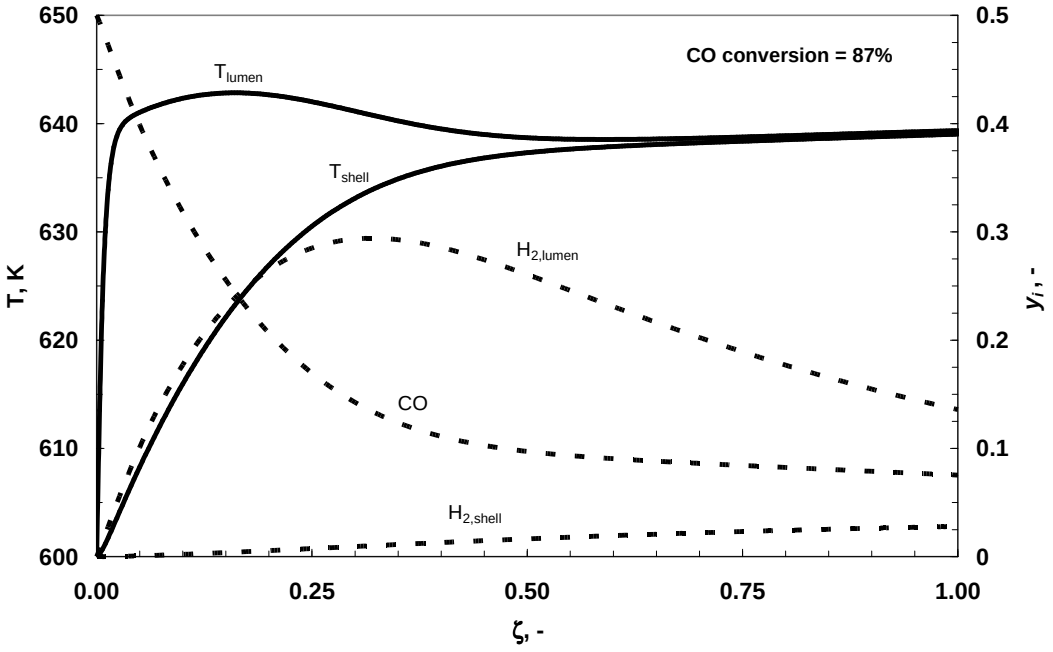

Fig. 64 - Temperature (T, solid lines) and concentration (y_i, *dotted lines*) profiles along the reactor at a feed pressure equal to 110 kPa. Operating conditions: $T_{feed} = T_{shell} = 600$ K; *SF* = 10.

In the first part of the reactor, at each feed pressure value, it is possible to observe a temperature increase in the lumen side due to the heat produced by reaction not balanced by the heat released to the shell side, see figures 64-66.

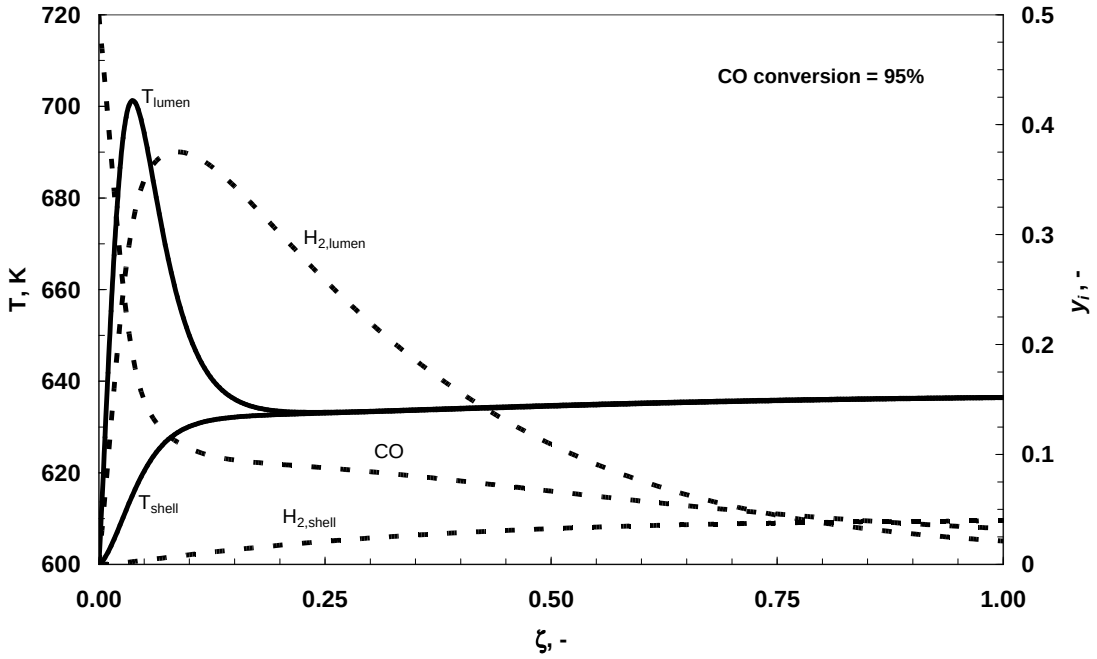

Fig. 65 - Temperature (T, solid lines) and concentration (y_i, *dotted lines*) profiles along the reactor at a feed pressure equal to 500 kPa. Operating conditions: $T_{feed} = T_{shell} = 600$ K; *SF* = 10.

This net heat load, available, increases as feed pressure rises. In particular at 500 kPa (figure 65), a significant temperature hot spot takes place close to the MR inlet. It results, as a consequence of the quick development of the heat of reaction, not balanced either by an efficient heat exchange towards the shell side (slow hydrogen permeation rate) or by a significant contribution of the endothermic reverse reaction.

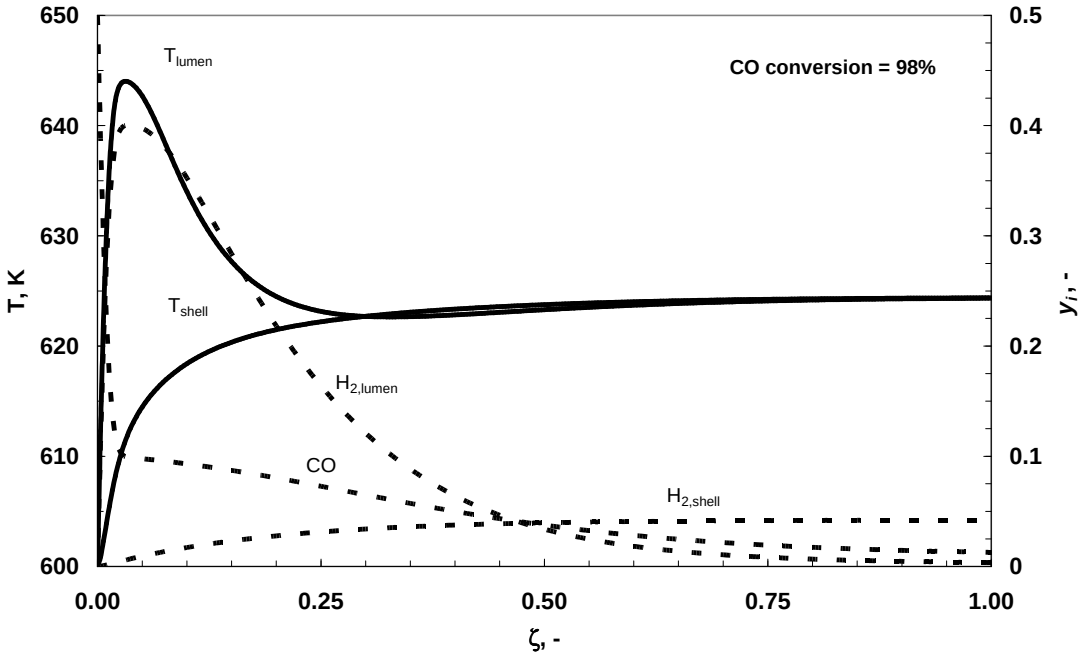

Fig. 66 - Temperature (T, solid lines) and concentration (y_i, *dotted lines*) profiles along the reactor at a feed pressure equal to 2000 kPa. Operating conditions: $T_{feed} = T_{shell} = 600$ K; *SF* = 10.

As to the simulations performed at higher lumen pressures (*e.g.* 2000 kPa), differently from the previous case, they show a considerable reduction of the temperature hot spot intensity. As a consequence of the quick consumption of the reagents, the reverse reaction rate becoming more important lowers sharply the net forward rate and takes away heat from the reaction ambient. Furthermore, the high hydrogen partial pressure favouring the permeation towards shell side reduces the heat load removing sensible heat. In summary, the lumen temperature results lower than the previous case. At each pressure value, the more significant temperature variations occur on the reactor axis and they tend to diminish shifting towards the reactor wall due to the cooling by the sweep gas, as showed in figures 66 and 67. The increase of the feed pressure produces a high conversion of the reagents, available in a large amount, in distances closer to the MR inlet. As a consequence, the conversion increases gradually in the whole catalytic bed achieving a final value of 87% at 110 kPa, whereas it fastly attains a plateau value for higher pressures (95% and 98% at 500 kPa and 2000 kPa, respectively). The presence of a peak for the hydrogen composition in the reaction zone depends on the balance between the hydrogen production and permeation rates. As the feed pressure increases, hydrogen generation rate increases as well; thus the peak occurs closer to the reactor inlet approaching a higher value (+ 37%) shifting from 110 kPa to 2000 kPa. As a consequence of an enhanced hydrogen driving force along the membrane reactor, the final hydrogen content on the retentate side is reduced of the 97% shifting from 110 kPa to 2000 kPa, while it increases on shell side of 50%, figures 64 and 66. Furthermore, the

position of the peak of hydrogen concentration and the temperature hot spot coincides as the feed pressure value is high (*i.e.* 2000 kPa); instead at lower feed pressures the two peaks are distinct and the maximun of temperature occurs before the hydrogen one depending on the different heat and mass transport rates. Typically, a decrease in the efficiency of hydrogen separation occurs in a MR for effect of a decrease of the hydrogen flux through the membrane. It is due to a lowering of the hydrogen concentration in the radial direction (*i.e.* hydrogen partial pressure) close to the membrane interface during the permeation, as showed by Itoh as two models based respectively on an ideal flow and radial diffusion are compared [137]. According to these observations, the temperature and hydrogen concentration profiles in the radial direction have been investigated at different feed pressure values and axial positions, see figures 67 and 68.

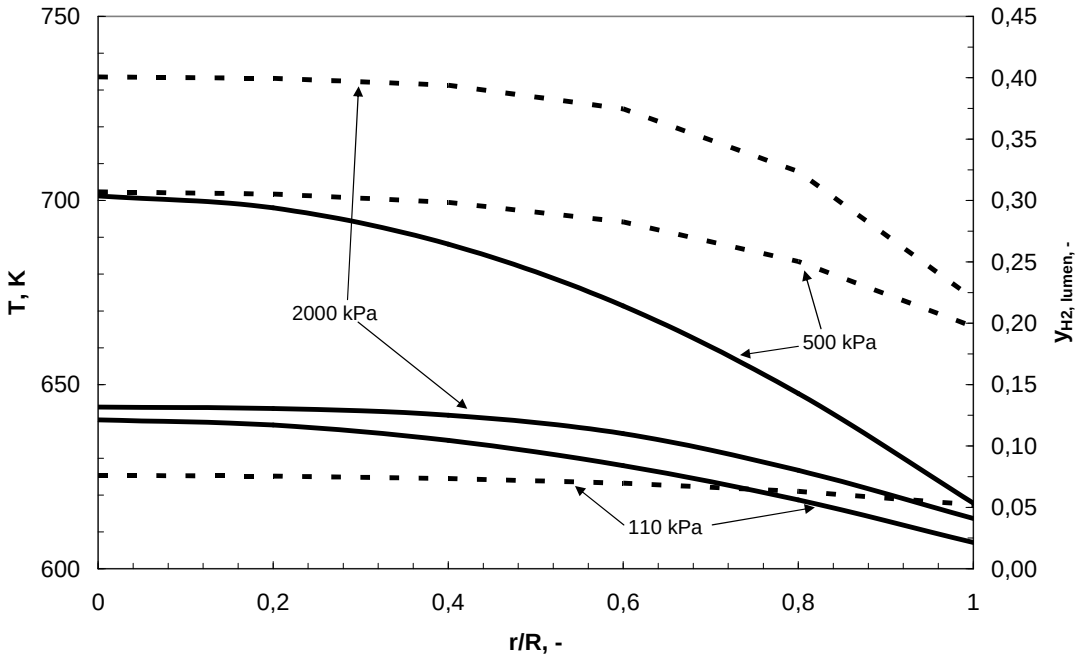

Fig. 67 - Lumen temperature (T, solid lines) and hydrogen composition ($y_{H2,lumen}$, *dotted lines*) vs. dimensionless radial position (at $\zeta = 0.04$, corresponding to the maximum temperature in the lumen side at 500 kPa) for three different feed pressure values. Operating conditions: $T_{feed} = T_{shell} = 600$ K; $SF = 10$.

The parabolic shape of the temperature and hydrogen composition curves at each pressure for ζ=0.04 (figure 67) suggests that most of the resistance to the mass and heat transfer is close to the wall of the membrane and only a small amount is localised in the central core of the reactor. For what concerns the hydrogen composition, the higher feed pressure (2000 > 500 >110 kPa) the higher hydrogen production; however, the slow permeation rate of this product combined to its high production rate at high feed pressures causes a radial concentration gradient that reduces, at 110 kPa, due to the slowest permeation and reaction rates. At 500 kPa, the radial temperature

gradients are more severe since the axial coordinate has been selected in correspondence of its maximum temperature. At 2000 kPa a flattening of the radial temperature profile in the central part, typical of a 1-D description, is produced because of the most of the conversion already takes place close to the inlet of the membrane reactor.

Figure 68 shows lumen temperature and hydrogen composition radial profiles at $\zeta = 0.2$ where the effect of temperature hot spot is distant. At 110 kPa, a parabolic profile of temperature is still evident, due to a reduced heat exchange across the membrane. At higher pressure values, a flat temperature profile takes place since heat exchange results more efficient.

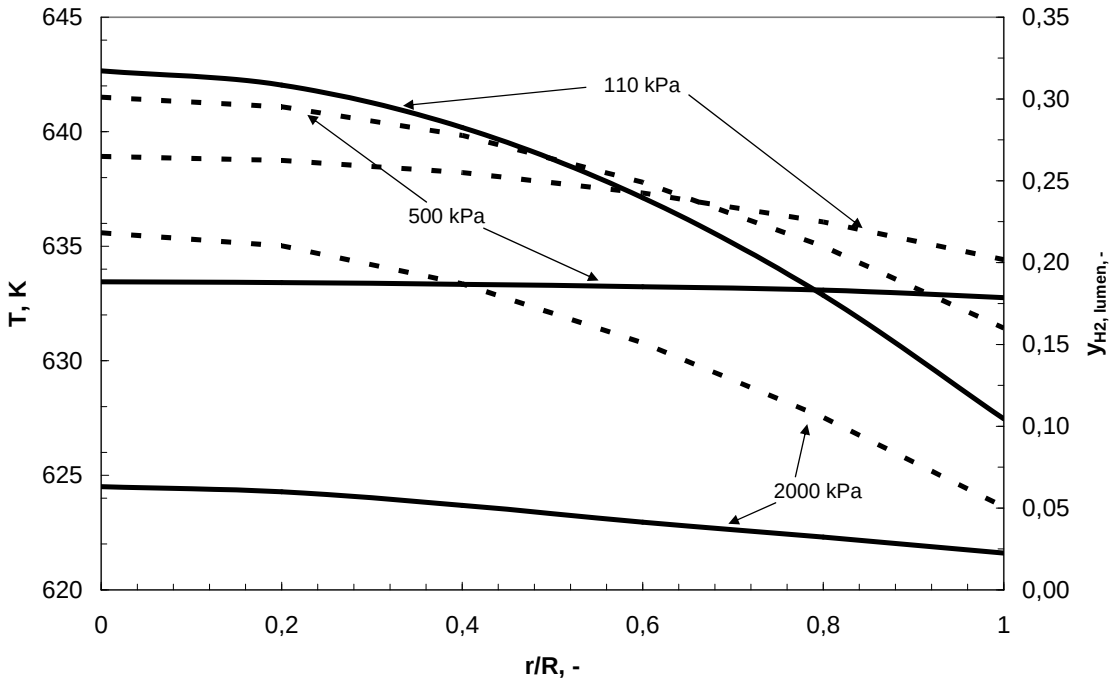

Fig. 68 - Lumen temperature (T, solid lines) and hydrogen composition ($y_{H2,\ lumen}$, *dotted lines*) vs. dimensionless radial position (at $\zeta = 0.2$) for three different feed pressure values. Operating conditions: $T_{feed} = T_{shell} = 600$ K; *SF* = 10.

As a high hydrogen production rate is combined to a moderate permeation rate, a parabolic hydrogen composition profile is still observed (see figure 68 at 500 kPa). At 2000 kPa, in spite of the highest hydrogen production rate in the reactor, hydrogen content in the lumen side is lower due to the more significant role of the driving force on the hydrogen permeation with respect to 110 kPa, as discussed in details for figures 64-66.

These results confirm that in a MR, for the WGS, the high pressure allows to combine both a higher recovery of hydrogen on shell side and a more efficient management of the heat transfer across the membrane.

5.1.1.7b Effect of sweep gas on MR performance

The sweep gas use in the membrane reactors is suggested since, enhancing the driving force, it increases the hydrogen permeating flow. In non-isothermal systems, it could favour also the heat exchange allowing a better control of the temperature in exothermic reactions. Therefore, the effect of sweep gas temperature and flow rate has been analysed in the following sections.

5.1.1.7b.1 Inlet temperature

The influence of the sweep gas inlet temperature is represented in the figures 69-72. If the inlet temperature on the shell side increases (from 500 K to 700 K) at the same feed pressure, the peak of lumen temperature for feed pressures lower than 2000 kPa rises as well as due to a lower heat load transferred across the membrane towards the shell side. At T_{shell} = 700 K, the heat transferred by the sweep gas stream adds to the heat generated by the reaction, determining a fast temperature increase in the first part of the reactor ($\zeta < 0.05$). This trend results more significant at low feed pressures (110 kPa, figure 69), where the rate of forward reaction is accelerated by the heat entering from the shell side and not opposed by the occurring of the endothermic reverse reaction and hydrogen permeation (*e.g.* removal of sensible heat). Thus, a temperature hot spot higher than that observed in figure 64, where $T_{shell} = T_{lumen}$ = 600 K, arises.

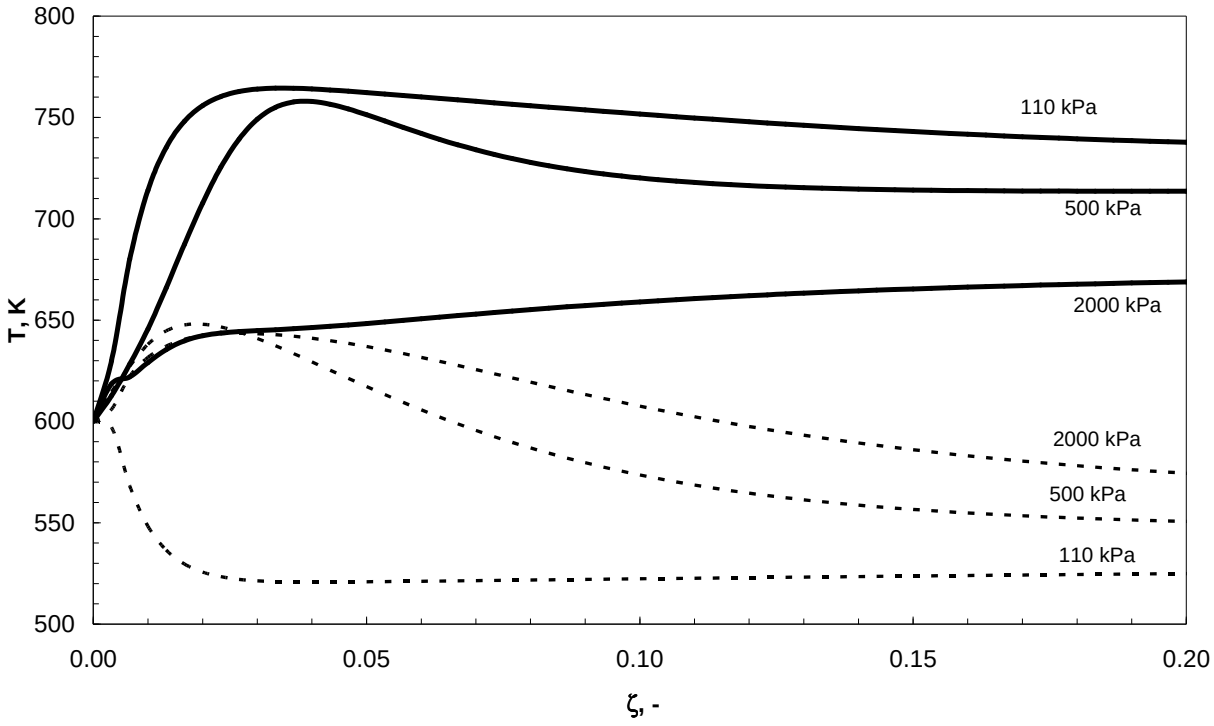

Fig. 69 - Lumen temperature vs. dimensionless axial length as a function of feed pressure for two different sweep gas inlet temperature values: (500 K, *dotted lines*) and (700 K, solid lines). Operating conditions: *SF* = 10.

On the contrary, as the temperature on shell side is lower than the lumen side one, because heat is continuously extracted by the sweep gas stream and the reaction and permeation rates are slowed down. This fact determines a lower hydrogen recovery on shell side (figure 72) combined with higher hydrogen content in the lumen side (figure 71).

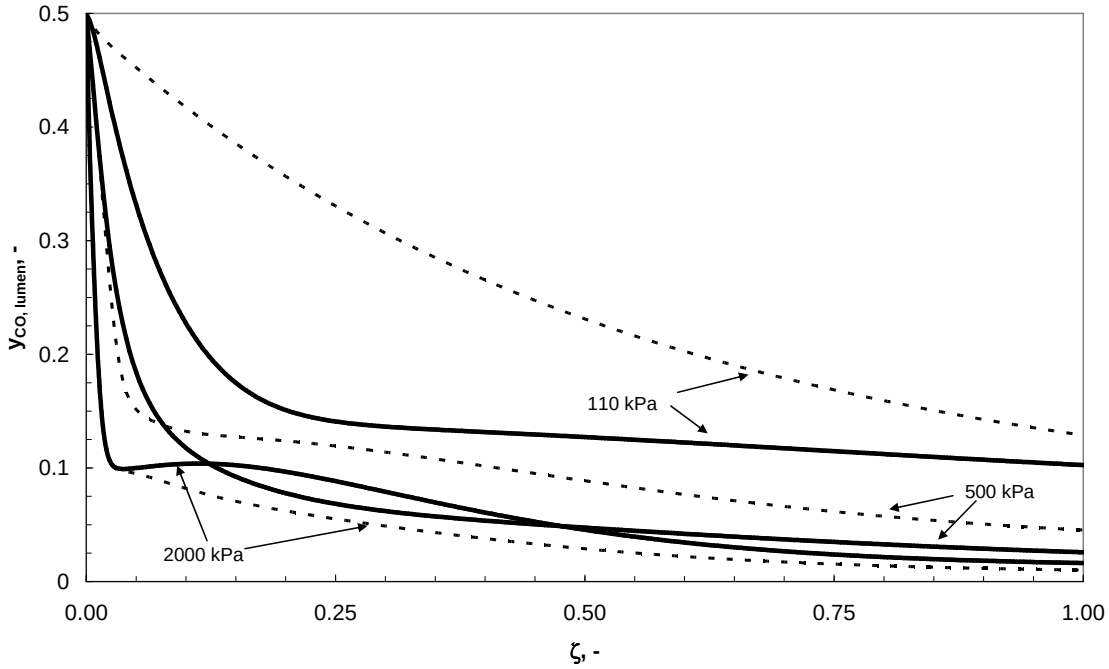

Fig. 70 - CO lumen composition vs. dimensionless axial length as a function of feed pressure for two different sweep gas inlet temperature values: (500 K, *dotted lines*) and (700 K, solid lines). Operating conditions: *SF* = 10.

On the other hand, as feed pressure is high (*i.e.* 2000 kPa), the effect of sweep gas temperature is not significant on the MR performance, because hydrogen recovery, CO conversion and hydrogen content respectively in lumen side are invariant with the investigated temperatures, see figures 70-72.

At 2000 kPa, as $T_{shell} > T_{lumen}$, the consumption of the reagents is still significantly higher than at low pressures (figure 70) and favours the reverse reaction that, for its endothermic character, takes away quickly a part of reaction heat. As the hydrogen permeation towards the shell side becomes considerable, the forward reaction again prevails causing a progressive increase of the lumen temperature along the reactor as showed also in figure 69. At feed pressure of 500 kPa, an intermediate behaviour with respect to the previous cases has been observed. As to the trend of hydrogen and CO composition profile, it is similar to that of 2000 kPa, whereas the temperature profile is closer to that of 110 kPa.

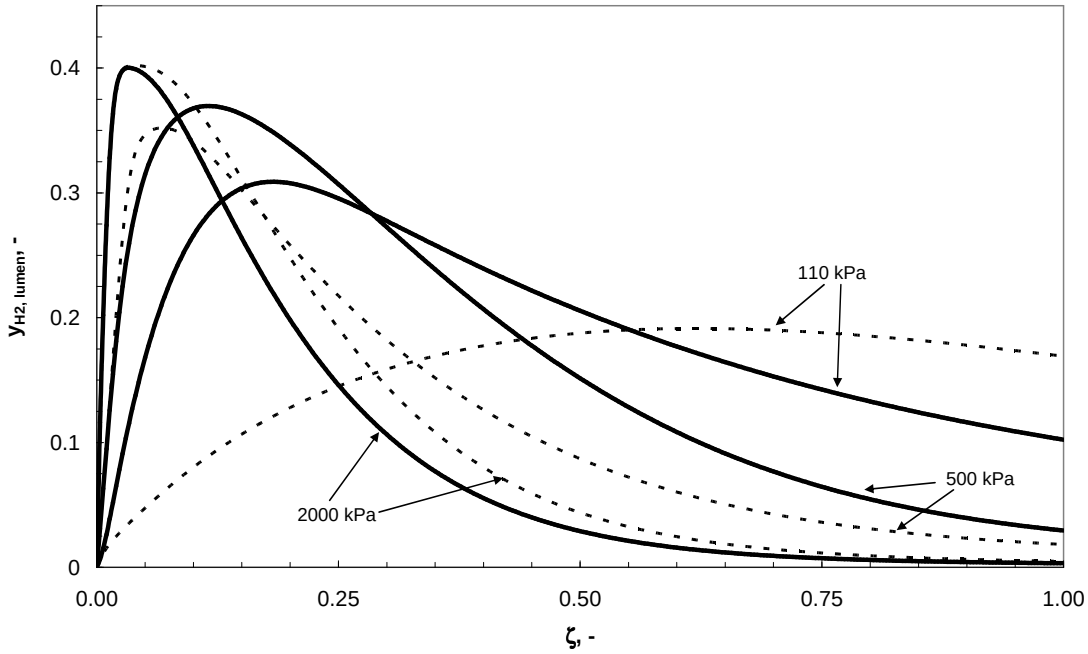

Fig. 71 - H_2 lumen composition vs. dimensionless axial length as a function of feed pressure for two different sweep gas inlet temperature values: (500 K, *dotted lines*) and (700 K, solid lines). Operating conditions: *SF* = 10.

The temperature of the sweep gas does not affect the hydrogen concentration on shell side as the feed pressure is equal to 2000 kPa. The same trend is confirmed at 500 kPa, although the hydrogen amount results lower.

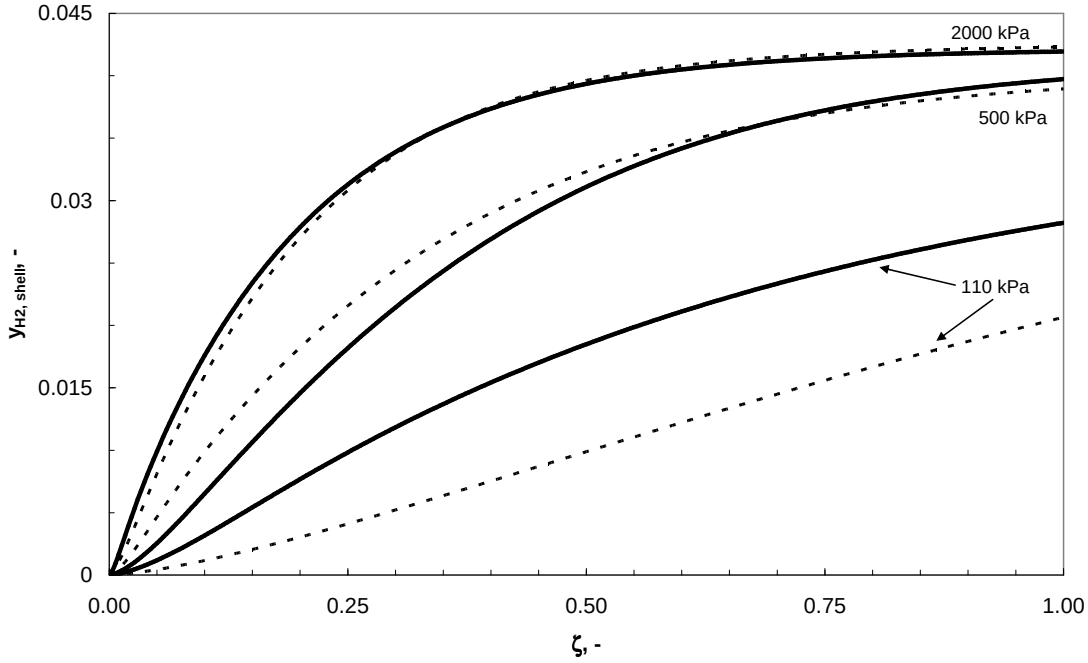

Fig. 72 - H_2 shell composition vs. dimensionless axial length as a function of feed pressure for two different sweep gas inlet temperature values: (500 K, *dotted lines*) and (700 K, solid lines). Operating conditions: *SF* = 10.

At a feed pressure of 110 kPa, the value of $y_{H2,\ shell}$ at the exit does not change at 600 K and 700 K, respectively, whereas if T_{shell} is equal to 500 K, $y_{H2,\ shell}$ results significantly lower (-27%) as shown in figure 72. In addition, the rate of increase of hydrogen concentration ($y_{H2,\ shell}$) on shell side depends on the T_{shell}.

These results put in evidence that at high feed pressures the influence of the sweep gas temperature on MR performance is not significant, while at a feed pressure equal to 110 kPa this variable becomes very important.

5.1.1.7b.2 Inlet flow rate effect on MR performance

Low sweep gas flow rates cause a significant increase of lumen temperature only at low feed pressure values (110 kPa). In fact, at this pressure value for ζ=0.5, as sweep gas flow rate decreases of an order of magnitude the increase of lumen temperature is equal to 200 K (+25%), as shown in figure 73.

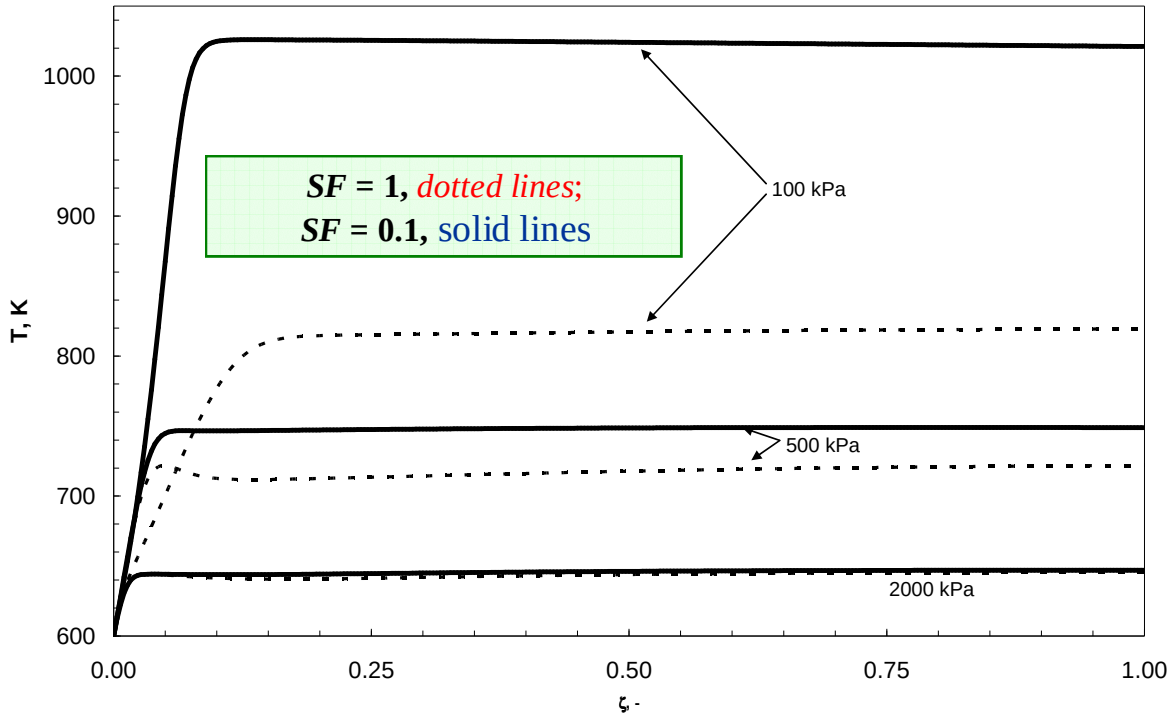

Fig. 73 - Lumen temperature vs. dimensionless axial length as a function of feed pressure for two different sweep gas flow rates: (0.00117 mol min^{-1}, *dotted lines*) and (0.000117 mol min^{-1}, solid lines). Operating conditions: $T_{shell} = T_{feed}$ = 600 K.

In this case the warming is due to a reduced cooling capability of the sweep gas stream; the heat of reaction, remaining inside the reactor, produces a generalised decrease of the global conversion value because of the endothermic reverse reaction is favoured. Thus, if the sweep gas flow rate becomes 100 times lower than reference value (*i.e. SF* = 0.1) the conversion changes

from 87% to 54% with a CO content enhanced of three times. The hydrogen content in the lumen side results almost doubled. As feed pressure increases, both the heat production and exchange rates rise determining a generalised decrease of the lumen temperature. Thus, at a sweep gas flow rate of 0.00117 mol min^{-1} (*i.e. SF* = 1), moving from 110 kPa to 2000 kPa a reduction of 170 K for the lumen temperature occurs, while at 0.000117 mol min^{-1} (*i.e. SF* = 0.1) a reduction of 370 K is obtained. At 500 kPa, if the sweep gas flow rate is ten times lower, the lumen temperature increases of 30 K (figure 73) while a percentage decay of ten is calculated for the conversion (86% → 76%).

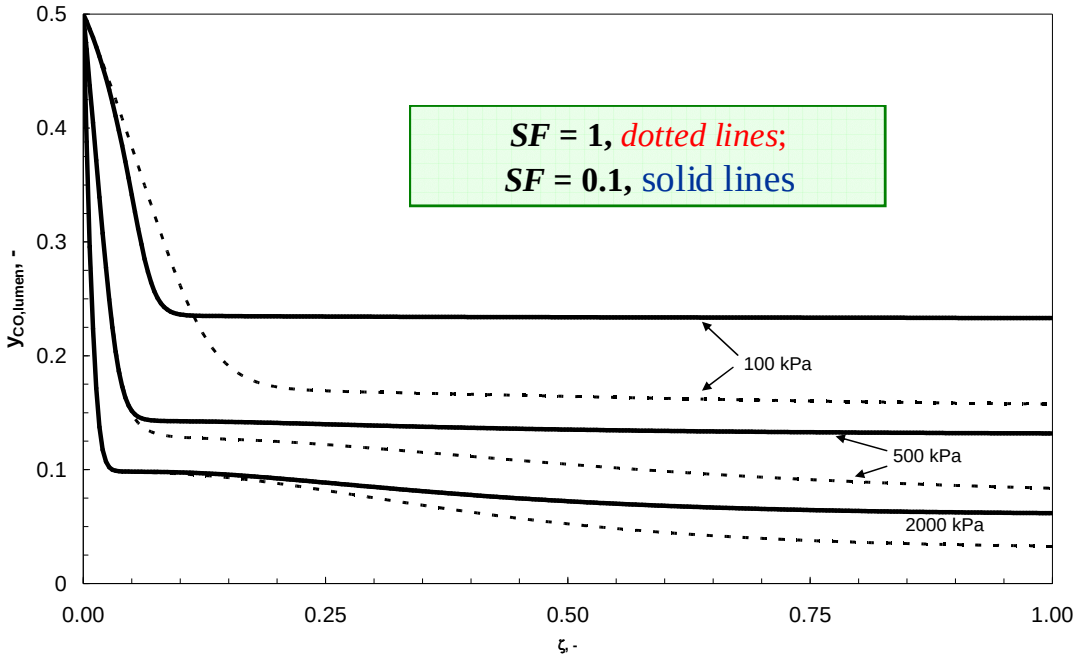

Fig. 74 – CO lumen composition vs. dimensionless axial length as a function of feed pressure for two different sweep gas flow rates: (0.00117 mol min^{-1}, *dotted lines*) and (0.000117 mol min^{-1}, solid lines). Operating conditions: $T_{shell} = T_{feed} = 600$ K.

For what concerns the composition at the exit of membrane reactor on lumen side, the CO content increases of two thirds (figure 74), while the H_2 one becomes about three times higher (figure 75).

At feed pressure equal to 2000 kPa the temperature profile is practically independent on sweep gas flow rate (figure 73). However, the conversion moves from 95% to 90% as the sweep gas flow rate decreases of 10 times, while the CO content doubles and H_2 concentration increases of about 300%.

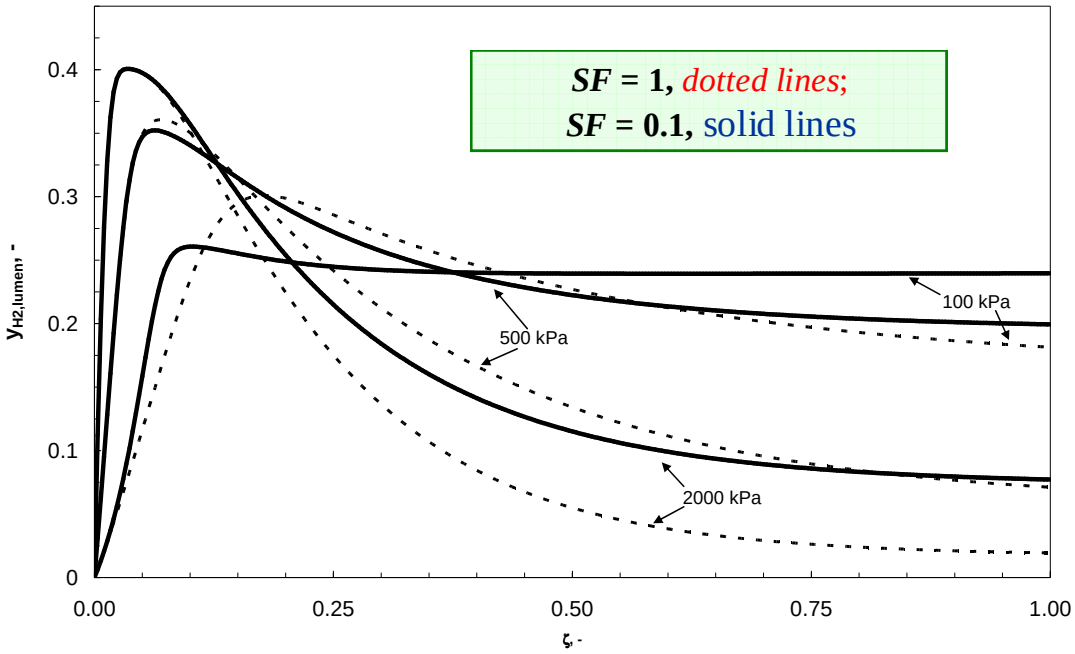

Fig. 75 - H_2 lumen composition vs. dimensionless axial length as a function of feed pressure for two different sweep gas flow rates: (0.00117 mol min^{-1}, *dotted lines*) and (0.000117 mol min^{-1}, solid lines). Operating conditions: $T_{shell} = T_{feed} = 600$ K.

On the basis of the results discussed above, at high feed pressure values (2000 kPa) the effect of sweep gas temperature and flow rate on the performance of the membrane reactor is less significant than at low feed pressure (110 kPa). However, at 2000 kPa is more convenient to operate with a sweep gas at lower temperature (*e.g.* 500 K) than lumen temperature in terms of hydrogen recovery and CO conversion; nevertheless a low sweep gas flow rate favours a higher H_2 purity level (*i.e.* the dilution of the valuable product is reduced) without risk of an anomalous increase of lumen temperature. At 500 kPa is still opportune to work at $T_{shell} < T_{feed}$ as to H_2 recovery and CO content in lumen side, while a low sweep gas flow rate is not advantageous as at 2000 kPa. On the contrary, at 110 kPa for a MR it is absolutely not recommended to operate at low sweep gas flow rate, while a sweep gas temperature at least equal to lumen temperature is suggested in order to achieve a high CO conversion and H_2 recovery on shell side, respectively.

5.1.1.7c Effect of the catalyst mass distribution

Another mode to control the intensity of temperature hot spot and use efficiently MR is to operate on the catalyst distribution. This solution could be an alternative to the use of side-streams and inert pellets to control the temperature profiles in addition to an external intermediate cooling applied successfully also to laboratory scale reaction systems by Hwang and Smith [138].

As previous discussed, close to the MR entry an excess of heat is generated by the high conversion value of the fresh reagents. In the rest of the unit, at high feed pressures, a reduced increase of the conversion has been observed. Therefore, the opportunity to dose the catalyst along the membrane reactor has been considered by setting a lower catalyst mass where the hot spot occurs and a higher catalyst amount in the zone where the increase of the conversion is negligible. As a consequence, two different catalyst distributions (linear and exponential) have been investigated in addition to the constant mode described previously. A qualitative picture of all catalyst distribution modes is reported in figure 76. The results, in terms of temperature and hydrogen concentration profiles, on both lumen and shell sides, have been compared with those discussed in the previous sections for a constant catalyst allotment.

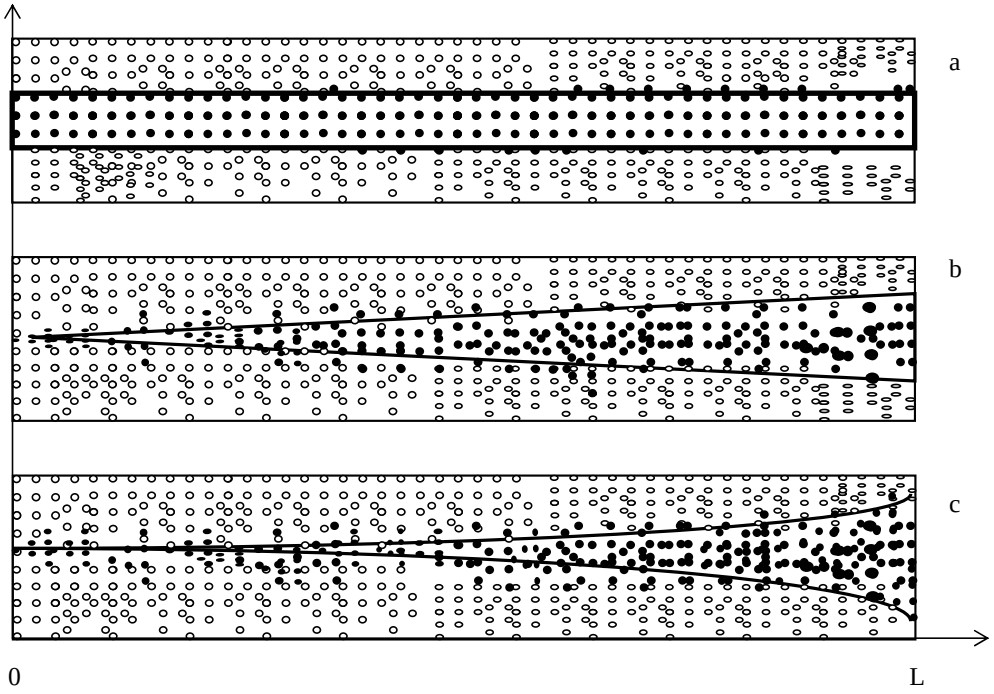

Fig. 76 - Catalyst distributions along the membrane reactor: (a) constant, (b) linear, (c) exponential. Black circles represent the catalyst pellets, while white circles represent inert particles.

The simulations, in figure 77, show how a catalyst mass that increases linearly along the MR produces a temperature *hot-spot* less significant with respect to an exponential distribution.

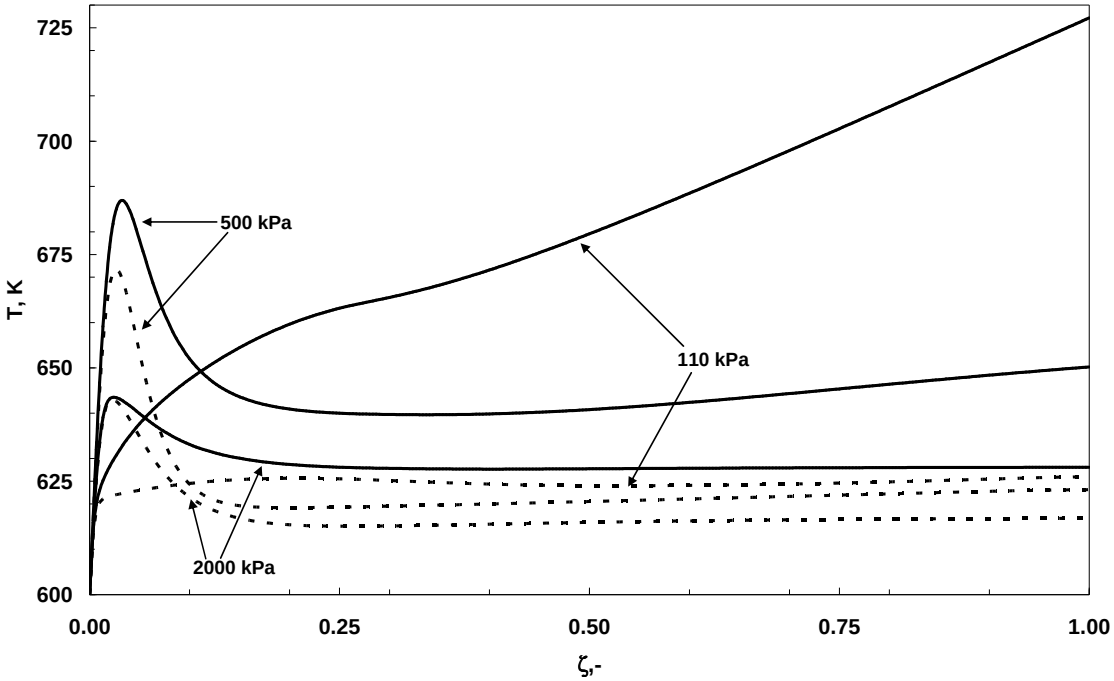

Fig. 77 - Lumen temperature vs. dimensionless axial length as a function of feed pressure for two different catalyst distributions: linear (*dotted lines*) and exponential (solid lines). Operating conditions: $T_{feed} = T_{shell} = 600$ K; *SF* = 10.

At 2000 kPa, the effect of the feed pressure on the temperature profile is preponderant with respect to the catalyst distribution. In fact, the hot spot intensity does not change while only the outlet temperature in the lumen side results slightly lower as a linear distribution is considered. On the contrary, at 500 kPa, an influence of the catalyst distribution is observed since the temperature hot spot is reduced: 700 K for constant, 687 K for exponential and 672 K for linear modes, respectively. As to the outlet temperatures, the lowest value (623 K) is still for the linear type, while the highest one (650 K) is for the exponential mode.

At 110 kPa, a linear distribution lowers further both the *hot-spot* intensity and outlet temperature (625 K) with respect to the value for the constant mode (643 K). An exponential distribution generates a progressive increment of the temperature in the whole catalytic bed. In this case, the combination of a large amount of the reagents still unconverted and catalyst in the second half of the reactor produces an uncontrolled warming of the unit with a consequent decrease of the conversion. The conversion value, at 110 kPa, changes from 87% to 59% moving from a linear to an exponential allocation. This behaviour confirms the fundamental role of the linear distribution at low feed pressure values.

For what concerns the hydrogen concentration, similar profiles are observed for all catalyst distributions independently on the feed pressure (figures 78 - 79).

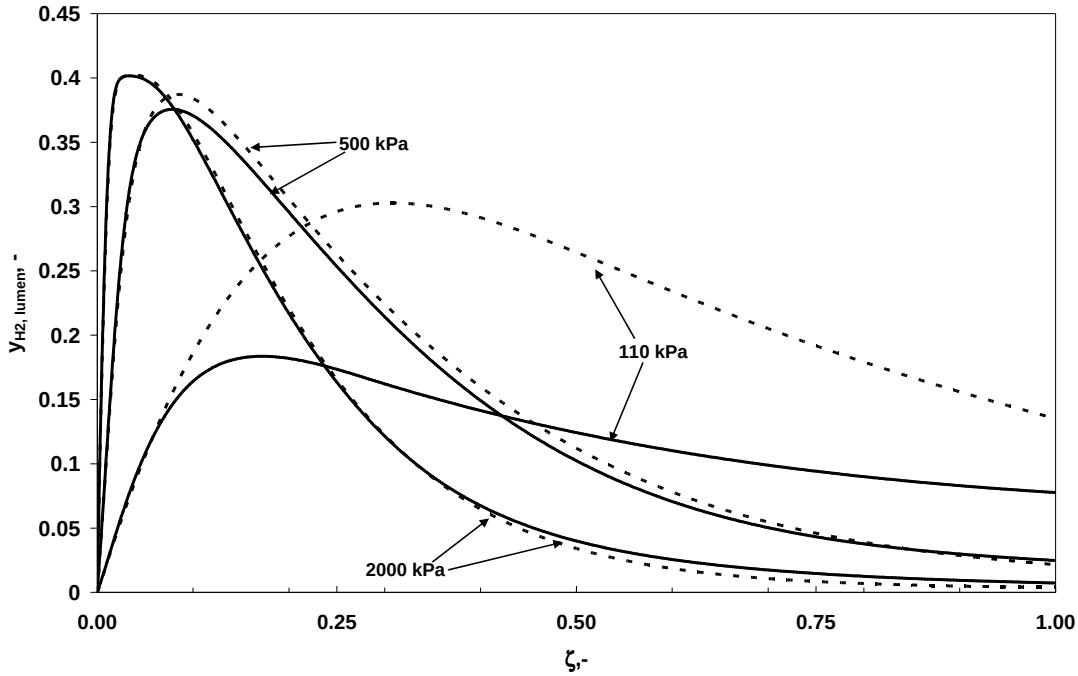

Fig. 78 - H_2 lumen composition vs. dimensionless axial length as a function of feed pressure for two different catalyst distributions: linear (*dotted lines*) and exponential (solid lines). Operating conditions: $T_{feed} = T_{shell} = 600$ K; *SF* = 10.

However, if at high pressures (2000 kPa) the advantage of a linear catalyst distribution is moderate, it becomes progressively more significant at 500 kPa and 110 kPa with respect to an exponential distribution.

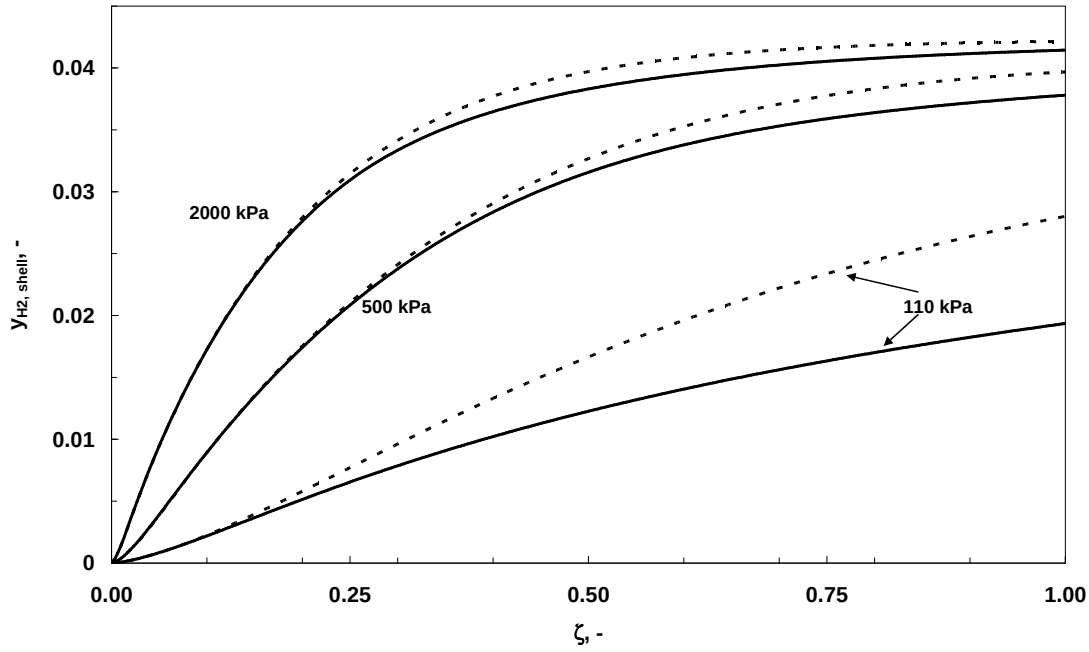

Fig. 79 – H_2 shell composition vs. dimensionless axial length as a function of feed pressure for two different catalyst distributions: linear (dotted lines) and exponential (solid lines). Operating conditions: $T_{feed} = T_{shell} = 600$ K; *SF* = 10.

In figure 80, theoretical CO conversion for both modes (*non-distributed* and distributed) is showed at 500 kPa that represents the best feed pressure condition in terms of MR performance.

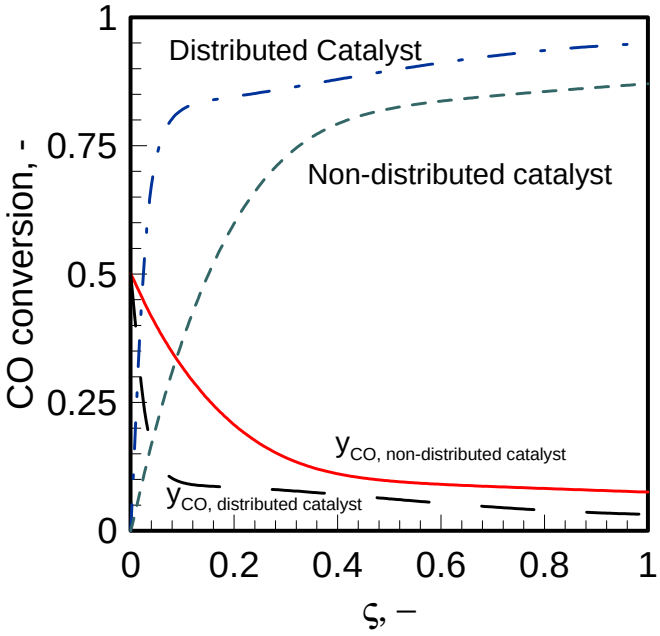

Fig. 80 – CO conversion and CO molar fraction in feed as a function of dimensionless reactor length at two different catalyst distribution modes at 500 kPa. Operating conditions: $T_{feed} = T_{shell} = 600$ K; *SF* = 10.

A linear distribution allows reaching a higher CO conversion than *non-distributed* catalyst bed (constant distribution mode).

Fig. 81 shows the hydrogen recovery as a function of dimensionless reactor length (ς) for different sweep gas flow rate and two feed pressure at the same sweep gas flow rate. In a *non-distributed* catalyst, the hydrogen recovery increases along the membrane but it results larger as the sweep gas flow rate on permeate side decreases. As previously said, a lesser amount of sweep gas on shell side produces an increasing temperature in the catalyst bed since the heat exchange is reduced. This higher temperature allows increasing mass exchange through the palladium-*based* membrane. At fixed sweep gas flow rate, as the feed pressure increases also the hydrogen recovery increases (see figure 81 at 2000 kPa).

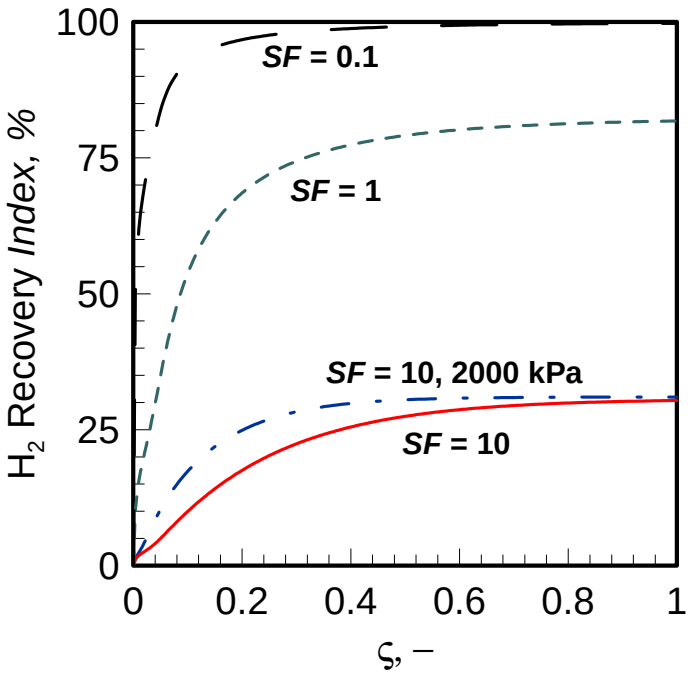

Fig. 81 – H_2 Recovery Index as a function of dimensionless reactor length at different sweep gas flow rates. Operating Condition: *non-distributed catalyst*; 500 kPa and $T_{feed} = T_{shell} = 600$ K.

This behaviour confirms the necessity to work without or at a lower sweep gas flow rate. In terms of hydrogen recovery both modes give more and less the same results. As already said for MSR, a distribution of catalyst does not always improve the recovery in the MR. Figure 82 shows how already previously mentioned; an increase of the feed pressure inside the MR having a catalyst distribution allows enhancing of hydrogen recovery through the membrane.

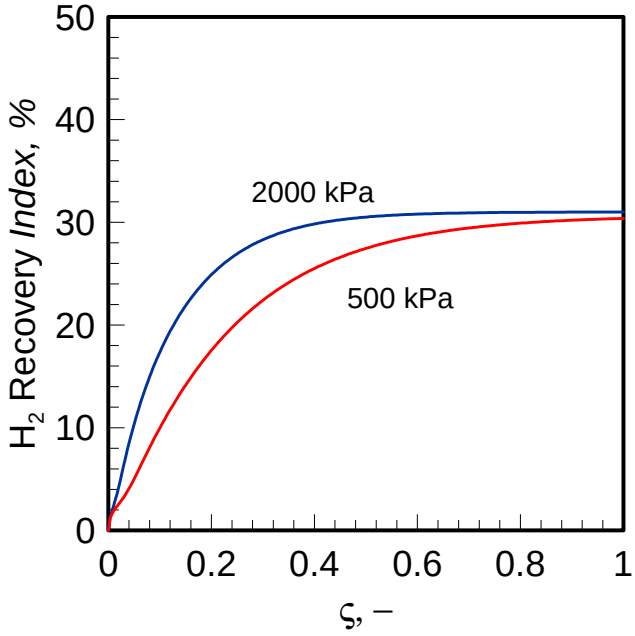

Fig. 82 – H_2 Recovery *Index* as a function of dimensionless reactor length (ς) at different feed pressure. Operating Condition: $F_{N2,\ shell} = 0.0117$ mol min^{-1} for a distributed catalyst mode.

This improvement is rather moderate, as already observed for methane steam reforming, since produced hydrogen is in presence, step-by-step along the reactor, of a reduced membrane surface.

Table 12 compares the theoretical results obtained by this model with the experimental results in literature. This shows a good agreement in terms of both CO conversion and H_2 recovery.

Table 12 – Theoretical results compared with the literature ones at T_{feed} =600 K; H_2O/CO = 1.

CO Conversion, -	**H_2 Recovery *Index*, %**	**L_s/A_m, $cm^3\ cm^{-2}\ min^{-1}$**	**A_m/V_{cat}, $cm^2\ cm^{-3}$**	**Operating mode**		**Reference**
0.94 (500 kPa)	**31**	**0.5**	**5**	**sweep**	**distributed**	*This model*
0.95 (100 kPa)	40	0.8	5	sweep	non-distributed	[139]
0.90 (600 kPa)	80	9	1	no-sweep	non-distributed	[140]
0.95 (400 kPa)	30	20	0.83	no-sweep	non-distributed	[141]

Conclusions

This thesis has shown an overview of the process integration and intensification engineering aspects by attractive MRs technology to improve both pure hydrogen recovery and production as well as exceed the mass transfer and thermodynamic limitations of the conventional reforming and shift reactors. Even if the ultra-pure hydrogen production on small scale by means of reforming or water gas shift reactions in conventional reactors is too expensive and complex due to the high number of equipments required in the MSR process, an undersized MRs can guarantee a straightforward and economic small scale hydrogen production. In fact, the integration of a membrane in a conventional reactor allows a reduction of the total number of equipments, simplification of the hydrogen separation steps downstream of reforming membrane reactor or reduces the number of shift reactors. The feed pressure represents an important design parameter that can be used to improve the mass exchange through the membrane. Notwithstanding the compression expenses are high, however, the use of a sweep gas stream on permeate side could add a supplementary cost for the hydrogen separation steps subsequent to the reactor in MSR process. High pressures allow working with both high hydrogen recoveries through the membrane and reduced membrane surfaces; consequently, reduced reactor volumes. The hydrogen permeability coupled to a small membrane area represents an important parameter to realize the most advantageous combination of the MSR and hydrogen permeation in MR.

In an MSR-*based* membrane reactor, a suitable combination of the high pressure driving force to the design parameters (A_m/V_{cat} and L_s/A_m) can lead to an optimal design and improvement of its performance without the use of a sweep gas stream on permeate side. However, the maximum H_2 recovery is a trade-off between reaction rate (hydrogen production), mass transport (hydrogen permeance) and the thermodynamic limit which has a reverse dependence from the feed pressure. The performance of four different MRs has been analyzed. An increase of the methane conversion equal to 50% was obtained by increasing the ratio A_m/V_{cat} from 0.42 to 2.1 $cm^2\ cm^{-3}$ whereas the L_s/A_m ratio was 11.6 cm^3(STP) $cm^{-2}\ min^{-1}$. A methane conversion about three-times as much as thermodynamic equilibrium limit (of a conventional reforming reactor) was obtained when the L_s/A_m ratio was reduced to 8.4 cm^3(STP) $cm^2\ min^{-1}$, in the smaller scale membrane reactor (*MR3*). In addition, a methane conversion (68%) about three-times exceeding the traditional reactor equilibrium conversion and a H_2 recovery of 43% have been reached operating at 800 kPa, with A_m/V_{cat} = 2.1 $cm^2\ cm^{-3}$ and L_s/A_m = 8.4 cm^3(STP) $cm^{-2}\ min^{-1}$ in the same membrane reactor (*MR3*). In the same catalyst volume, a higher methane load in feed with

respect to the membrane surface area produces a large amount of hydrogen that is not extracted quickly by palladium membrane due to its low permeation rate (low hydrogen recovery). Even if higher GHSV values are reached in *MR3*, a methane conversion 2.5-times higher than TREC is obtained. By doubling approximately (*e.g.* a 78% percentage increase) the value of L_s/A_m ratio, at 800 kPa, methane conversion decreases of a value equal to the 30% whereas hydrogen recovery, instead, decreases of a value equal to the 75%.

MR4 has a catalyst volume that with respect to previous MR is distributed along the axial direction. In this case an increase of the ratio A_m/V_{cat} at 10 cm^2 cm^{-3} has improved the mass exchange through the membrane compared to the catalyst amount necessary to uphold the reforming reaction. The effect of the L_s/A_m ratio has been analyzed to evaluate the catalyst production capacity with respect to the membrane extraction ability. At 700 kPa and L_s/A_m = 2 cm^3 cm^{-2} min^{-1}, chemical conversion in MR is four-times higher than thermodynamic equilibrium conversion of a TR and equal to 94%. The existence of a higher catalyst amount in a zone, at the end of membrane, where the reagents are partially converted assures a higher methane conversion at which the presence of the membrane contributes. Hydrogen recovery (46%) will be close to the value obtained in the previous MR tested (*MR3*). The permeation flow rate is low since hydrogen meets an insufficient membrane surface for the extraction. With respect to thermodynamic equilibrium conversion, MR presents, however, methane conversions three-times higher at each reagents molar ratio. By increasing the L_s/A_m ratio, the less significant hydrogen amount produced during the MSR is not able to permeate efficiently the membrane (*e.g* lower driving-force). When this lower hydrogen amount is combined to the low residence times both contribute to reduce considerably the hydrogen recovery (*e.g.* an about 80% reduction). The performance for *MR3* at m = 2.5 have been compared to the ones for *MR4*. At 700 kPa, by distributing a catalyst volume inside the MR, a 20% increase of hydrogen recovery and 42% increase of methane conversion are possible, respectively. Instead, in comparison to the TREC a four-time increase of methane conversion (*i.e.* 94%) is, as already said, obtained.

The selective and continue withdrawal of hydrogen through the palladium membrane can shift also the chemical equilibrium of the methane decomposition reaction towards a high carbon formation. Carbon deposition on the catalyst is a pervasive problem; in particular, for a smaller scale MR the stability is largely compromised. For a successful smaller-size MR with a *non-distributed* catalyst in methane steam reforming process, it is convenient to combine a reagents molar ratio higher than three to the high pressures in order to reduce the occurring carbon formation.

Alternatively, the catalyst distribution allows also a progressive and almost complete methane conversion since a high catalyst amount is used where the reagents are present in low concentration since they are partially converted. Moreover, it helps to reduce the coke formation since the reagents will react progressively in the catalyst bed and step-by-step they meet an increasing catalyst amount. This increases the spill-over of the water on the catalyst surface reducing the methane cracking. In addition, the increasing feed pressure can contribute to the reduction of the coke amount in *MR4* with respect to the previous MRs. As a consequence, a lower reagent molar ratio (m = 2.5) is possible.

According to the previous results, a theoretical analysis for the complete understanding of the behaviour of a MR, where an exothermic reaction (WGS) occurs, has been developed taking into account both mass and heat transport phenomena. By means of this approach it is possible to combine opportunely the operation and design parameters for achieving high conversion and hydrogen recovery values. An appropriate choice of the feed pressure, sweep gas flow rate and temperature has a beneficial effect on the driving force for hydrogen permeation, conversion and temperature profile, mitigating eventual dangerous hot spots or avoiding a membrane failure. For the same aim, the opportunity to tune the catalyst along the MR has been established. At high feed pressures, the influence of the sweep gas temperature and flow rate on the performance of the MR is less remarkable than at low feed pressure. At 2000 kPa it is more convenient to operate with a sweep gas at lower temperature (*e.g.* 500 K) than lumen temperature in terms of hydrogen recovery and CO conversion; a low sweep gas flow rate, nevertheless, favours a higher H_2 purity level, without risk of an anomalous increase of lumen temperature. On the other hand, at 110 kPa it is strongly suggested to use a large sweep gas flow rate at the same temperature of the feed stream in order to achieve a high CO conversion and H_2 recovery.

A catalyst mass linearly increasing along the MR is more efficient than an exponential and constant distribution to control the temperature hot spots. However, even if at high pressures (*e.g.* 2000 kPa) the advantage of a linear catalyst distribution is moderate, it becomes progressively more significant at 500 kPa and 110 kPa with respect to an exponential distribution. At 500 kPa, it is still opportune to work at $T_{shell} < T_{feed}$ referred to both H_2 recovery and CO content in lumen side, while a low sweep gas flow rate is not advantageous as at 2000 kPa. On the contrary, at 110 kPa for a MR an operation at low sweep gas flow rate is absolutely not recommended while a sweep gas temperature at least equal to feed temperature is suggested in order to achieve high CO conversion and H_2 recovery on shell side.

References

1. S.A. Bhat, J. Sadhukhan, *AIChE Journal* 2 (55) (2009) 408;
2. D.L. Trimm, *Catalysis Today* 37 (1997) 233;
3. G. Saracco, H.W.J.P. Neomagus, G.F. Versteeg, W.P.M. Van Swaaij, *Chem. Eng. Sci.* 54 (1999) 1997;
4. G. Iaquaniello, A. Mangiapane, P. Ciambelli, V. Palma, E. Palo, *Chem. Eng. Trans.* 8 (2005) 19;
5. Brochure, Hydrogen production – Steam methane Reforming (SMR), www.nyserda.org;
6. W. Yu, T. Ohmori, T. Yamamoto, A. Endo, M. Nakaiwa, T. Hayakawa, N. Itoh, *Int. J. Hydrogen Energy* 30 (2005) 1071;
7. M. Oertel, J. Schmitz, W. Weirich, D. Jendryssek-Neumann, R. Schulten, *Chem. Eng. Technol.* 10 (1987) 248;
8. J. Tong, Y. Matsumura, *Catalysis Today* 111 (2006) 147;
9. D. Lee, P. Hacarlioglu, S. T. Oyama, *Topics in Catalysis* 29 (1-2) (2004) 45;
10. Y.M. Lin, G.L. Lee, M.H. Rei, *Catalysis Today* 44 (1998) 343;
11. J. Oklany, K. Hou, R. Hughes, *Applied Catal. A: Gen* 170 (1998) 13;
12. E. Kikuchi, *Catalysis Today* 56 (2000) 97;
13. K. Aasberg-Petersen, C.S. Nielsen, S. Lægsgarard Jørgensen, *Catalysis Today* 46 (1998) 193;
14. G. Marigliano, G. Barbieri, E. Drioli, *Chem. Eng. Proc.* 42 (2003) 231 – 236
15. C. Song, *Catalysis Today* 77 (2002) 17;
16. J.N. Armor, *J. of Membrane Science*, 147 (1998) 217;
17. D.K. Liguras, K. Goundani, X.E. Verykios, *J. Power Sources* 130 (2004) 30;
18. K. Kochloefl, Steam reforming, in: G. Ertl, H. Knozinger, J. Weitkamp (Eds.), Handbook of Heterogenous Catalysis, vol. 1, VCH, Weinheim, 1997, p. 1819, cited in [53];
19. F.A. Lewis, *Int. J. Hydrogen Energy* 20 (1995) 587;
20. J. Tong, Y. Matsumura, *Applied Catal. A: General* 286 (2005) 226;
21. J. Shu, BPA Grandjean, S. Kaliaguine, *Applied Catal. A: General* 119 (1994) 305;
22. A. Kleinert, G. Grubert, X. Pan, C. Hamel, A. Seidel-Morgenstern, J. Caro, *Catalysis Today* 104 (2005) 267;
23. R. Bredesen., J. Sogge, *UN Seminar on the Ecological Applications of Innovative Membrane Technology in the Chemical Industry*, Cetraro, Calabria, Italy, May 1-4, 1996;
24. J. Shu, B. Grandjean, S. Kaliaguine, *Can. J. Chem. Eng.* 69 (5) (1991) 1036;
25. Y. Chen, H. Xu, Y. Wang, G. Xiong, *Catalysis Today* 118 (2006) 136;
26. R.S Willms, R. Wilhelm, S. Konishi, *Fusion Engineering and Design*, 28 (1995) 397;
27. F. Gallucci, L. Paturzo, A. Famà, A. Basile, *Ind. Eng. Chem. Res* 43 (2004) 928;
28. Y. Lin, S. Liu, C. Chuang, Y. Chu, *Catal. Today*, 82 (2003) 127;
29. K. Hou, M. Fowles, R. Hughes, *Chem. Eng. Sci.* 54 (1999) 3783;
30. J. Szegner, K.L. Yeung, A. Varma, *AIChE Journal* 43(8) (1997) 2059;
31. K.L. Yeung, R. Aravind, R.J.X. Zawada, J. Szengner, G. Cao, A. Varma, *Chem. Eng. Sci.* 49(24A) (1994) 4823;
32. S. Melis, A. Varma, C.J. Pereira, *Chem. Eng. Sci.* 52 (2) (1997) 165;
33. Buchanan J. S., Sundaresan S., *Chem. Eng. Com.* 52(1-3) (1987) 33;
34. Climate change 1995, *The science of climate change*, report of the intergovernmental panel on climate change, UNEP and WMO, Cambridge University press, 1996;
35. J.R. Petit, J. Jozel, *Nature* 399 (1999) 429 ;
36. T.P. Whorf, Mauna Loa Observatory, Haway, Institution of oceanography (SIO), University of California la Jolla, California, United States, 1999;

37. F. Gracceva, C. Manna, D. Palma, *Rapporto energia e ambiente 2007, analisi e scenari, ENEA Ente per le nuove Tecnologie, Energia e Ambiente*, ISBN 88-8286-165-1, 2008;
38. *The Hydrogen Economy: Opportunities, Costs, Barriers, and R&D Needs*, Committee on Alternatives and Strategies for Future Hydrogen Production and Use, National Academy of Engineering, National Academies Press available electronically in http://www.nap.edu/books, 2004;
39. J. M. Ogden, T. G. Kreutz and M. Steinbugler, *Fuels for Fuel Cell Vehicles: Vehicle Design and Infrastructure Issues*, SAE Technical Paper Series, 982500, 1998. http://www.princeton.edu/~energy/publications/pdf/1998/Fuels_FCvehiclesVdesign.pdf
40. M. Wietschel, U. Hasenauer, A. de Groot, *Energy Policy* 34 (2006) 1284;
41. R.A. Muller, *Technology for Presidents*, Technology Review Online, 2003;
42. W. Yu, T. Ohmori, T. Yamamoto, E. Endo, M. Nakaiwa, N. Itoh, *Chem. Eng. Sci.* 62 (2007) 5627;
43. Enciclopedia degli idrocarburi, VOLUME II / RAFFINAZIONE E PETROLCHIMICA
44. C.E.G. Padro, V. Putsche, *Survey of the Economics of Hydrogen Technologies*, NREL/TP-570-27079, 1999 available electronically in http://www.afdc.doe.gov/pdfs/27079.pdf;
45. http://www.hydrogen.energy.gov/h2a_analysis.html;
46. *The Hydrogen Economy: Opportunities, Costs, Barriers, and R&D Needs*, Committee on Alternatives and Strategies for Future Hydrogen Production and Use, National Academy of Engineering, National Academies Press, available electronically in http://www.nap.edu/books;
47. http://www.hydrogen.energy.gov;
48. W. Amos, *Costs of Storing and Transporting Hydrogen*, NERL/TP-570-25106, 1998, http://www.eere.energy.gov;
49. N.W. Ockwig, T.M. Nenoff, *Chem. Rev.* 107 (2007) 4078;
50. http://www.ecn.nl/docs/library/report/2008/e08043.pdf;
51. J. O'M Bockris, J.C. Weiss, *About the real economics of massive hydrogen production at 2010 AD*, in Hydrogen Energy VII, edited by T.N. Veziroglu and A. N. Protsenko, pp. 101-151. New York. Pergamon Press,1988;
52. Pamela L. Spath, Margaret K. Mann, *Life Cycle Assessment of Hydrogen Production via Natural Gas Steam Reforming*, 2001, report National Renewable Energy Laboratory/TP-570-27637;
53. J. Ogden, Lecture (Oct 2004), available electronically at http://www.its.ucdavis.edu;
54. S. Sircar, T. C. Golden, *Sep. Sci. Technol*. 35 (2000) 667;
55. J. Stocker, M. Whysall, G.Q. Miller, *30 years of PSA technology for hydrogen purification 2005*; UOP LLC: Des Plaines, IL, 1998;
56. R. Bredesen, K. Jordal, O. Bollard, *Chem. Eng Proc*. 43 (2004) 1129;
57. S. Adhikari, S. Fernando, *Ind. Eng. Chem. Res.* 45 (2006) 875;
58. J. Shu, B.P.A. Grandjean, S. Kaliaguine, *Catalysis Today* 25 (1995) 327;
59. G. Barbieri, A. Brunetti, G. Tricoli, E. Drioli, *J. of Power Sources* 182 (2008) 160;
60. A.N. Matzakos, S.L. Wellington, T. Mikus, J.M.Ward, U.S. Patent 6,821,501 B2, Nov. 23, 2004;
61. A.N. Matzakos, S.L. Wellington, *Novel Membrane Steam Reforming (MSR) Reactor for Pure Hydrogen Production*, Proc. Spring AIChE Meeting 2004;
62. H. Gunardson, *Industrial Gases in Petrochemical Processing*, Marcel Dekker, Inc.: 1998
63. J. Comas, M.L. Dieuzeide, G. Baronetti, M. Laborde, N. Amadeo, *Chem. Eng. J.* 118 (2006) 11;
64. G. Kolios, B. Glöckeler, A. Gritsch, A. Morillo, G. Eigenberger, *Fuel Cells* 5(1) (2005) 52

65. I. Yasuda, Y. Shirasaki, T. Tsuneki, T. Asakura, A. Kataoka, H. Shinkai, R. Yamaguchi, Proc. 6th international conference on catalysis in membrane reactors, (2004) 91 - 94
66. http://www.tokyo-gas.co.jp/pefc_e/dev-fc_13.html
67. A. Kleinert, G. Grubert, X. Pan, C. Hamel, A. Seidel-Morgenstern, J. Caro, *Catalysis Today*, 104 (2005) 267;
68. S.S. Bharadwaj, L.D. Schmidt, *Fuel Processing Technology*, 42 (1995) 109;
69. T.P. Tiemersma, D.L Hoang, S.H. Chan, *Applied Catalysis: A*, 268 (1–2) (2004) 207;
70. J.R. Lattner, M.P. Harold, *Int. J. Hydrogen Energy* 29 (4) (2004) 393 – 417
71. K. Damen, M. van Troost, A. Faaij, W. Turkenburg, *Prog. Energy Combust. Sci*. 32 (2006) 215.
72. .S. Bharadwaj, L.D. Schmidt, *Fuel Processing Technology* 42 (1995) 109;
73. I. Dybkjaer, *Fuel Processing Technology* 42 (1995) 85;
74. C. Pistonesi, A. Juan, B. Irigoyen, N. Amadeo, *Applied Surface Science* 253 (2007) 4427;
75. Y.H. Chen, C.C Yu, Y.C Liu, C.H Lee, *J. of Power Sources* 160 (2006) 1275;
76. R.M. Navarro, M.A. Peña, J.L.G. Fierro, *Chem Rev.* (2007) 1;
77. G.D.A. Duane, B. Myers, Brian D. James, John S. Lettow, C.E. Sandy Thomas, Reed C. Kuhn, *Cost and Performance Comparison of Stationary Hydrogen Fueling Appliances, DOE report*, Directed Technologies Inc., 2002.
78. Rostrup-Nielsen, J. R. In Catalysis Science and Technology; Anderson, J. R., Boudart, M., Eds.; Springer Verlag: Berlin, Germany, 1984; Chapter 1, cited in [76];
79. J. Wei, E. J. Iglesia, *Catal.* 224 (2004) 370;
80. Y. Matsumura, T. Nakamori, *Appl. Catal. A: General*, 258 (2004) 107;
81. J. Kim, B. Choi, J. Yi, *J. Chem. Eng. Jpn.* 32 (1999) 760;
82. M.C.J. Bradfort, M.A. Vannice, *Appl. Catal. A: General* 142 (1996) 97;
83. K. Hou, R. Hughes, *Chem. Eng. J.* 82 (2001) 311;
84. W.H.J. Stork, Molecules, catalysts and reactors in hydroprocessing of oil fractions, in: G.F. Froment, B. Delmon, P. Grange (Eds.), Hydrotreatment and Hydrocracking of Oil Fractions, Elsevier, Amsterdam, 1997, pp. 41–67.
85. http://herkules.oulu.fi/isbn9514269543/
86. C.H. Bartholomew, *Applied Catalysis A: General* 212 (2001) 17;
87. D.L. Trimm, Z.I. Onsan, *Catal. Rev. Sci. Eng.*, 43 (2001) 31;
88. J.R. Rostrup-Nielsen, *Catalysis Today* 118 (1993) 305;
89. J.R. Rostrup-Nielsen, I. Alstrup, *Catalysis Today* 53 (1999) 311;
90. J.R. Rostrup-Nielsen, *Stud. Surf. Sci. Catal.* 68 (1991) 85;
91. U. Balachandran, T.H. Lee, L. Chen, S.J. Song, J.J. Picciolo, S. E. Dorris, *Fuel* 85 (2006) 150;
92. I.B. Elkina, J.H. Meldon, *Desalination* 147 (2002) 445;
93. S.N. Paglieri, J.D. Way, *Sep. Purif. Method* 31 (2002) 1;
94. B.D. Morreale, M.V. Ciocco, R.M. Enick, B.I. Morsi, B.H. Howard, A.V. Cugini, K.S. Rothenberger, *J. Mem. Sci.* 212 (2003) 87;
95. F. Guazzone, E.E. Engwall, Y.H. Ma, *Catalysis Today* 118 (2006) 24;
96. P.P. Mardilovich, Y. She, Y.H. Ma, M.H. Rei, *AIChE J.*, 44 (1998) 310;
97. R.E. Buxbaum, P.C. Hsu, *US Patent Application*, 5 (149) (1992) 420;
98. G. Xomeritakis, Y.S. Lin, *AIChE J.*, 44 (1998) 174;
99. S. Tosti, L. Bettinali, V. Violante, *Int. J. of Hydrogen Eng.*, 25 (2000) 319;
100. J. Zhang, D. Liu, M. He, H. Xu, W. Li, *J. of Mem. Sci.* 274 (2006) 83;
101. D. Wang, J. Tong, H. Xub, Y. Matsumura, *Catalysis Today* 93–95 (2004) 689;
102. P. Quicker, V. Höllein, R. Dittmeyer, *Catalysis Today* 56 (2000) 21;
103. R. Dittmeyer, V. Höllein, K. Daub, *J. of Molec. Catalysis A: Chemical*, 173 (2001) 135;
104. T. Tsuru, K. Yamaguchi, T. Yoshioka, M. Asaeda, *AIChE J.*, 50 (2004) 2794;
105. G. Barbieri, G. Marigliano, G. Perri, E. Drioli, *Ind Eng Chem Res*. 40 (2001) 2017;

106. A. Bottino, A. Comite, G. Capannelli, R. Di Felice, P. Pinacci, *Catalysis Today* 118 (2006) 214;
107. E. Johannessen, K. Jordal, *Energy Conversion and Management*, 46 (2005) 1059;
108. R. Bredesen., J. Sogge, *UN Seminar on the Ecological Applications of Innovative Membrane Technology in the Chemical Industry*, Cetraro, Calabria, Italy, May 1–4, 1996;
109. S.T. Oyama, P. Hacarlioglu, *J. of Mem. Sci.* 337 (2009) 188;
110. P. Hacarlioglu, Y. Gu, S.T. Oyama, *J. of Natural Gas Chemistry* 15(2) (2006) 73;
111. Y. Chen, Y. Wang, H. Xu, G. Xiong, *Appl. Catal. B: Environ.* 80 (2008) 283;
112. Y. Matsumura , J. Tong, *Top Catal.* 51 (2008) 123;
113. T. Tsuru, T. Morita, H. Shintani, T. Yoshioka, M. Asaeda, *J. of Mem. Sci.* 316 (2008) 53;
114. Wagner, G.F. Froment, *Hydrocarbon Processing* 7 (1992) 69, cited in [29]
115. E. Gobina, K. Hou, R. Hughes, Chem. Eng. Sci. 50 (14) (1995) 2311;
116. S. Tosti, A. Basile, G. Chiappetta, C. Rizzello, V. Violante, *Chem. Eng. J.* 93 (2003) 23;
117. D.S. Newsome, P. Kellog, *Catal. Rev.-Sci. Eng.* 21(2) (1980) 275;
118. A. Criscuoli, A. Basile, E. Drioli, *Catalysis Today* 56 (2000) 53;
119. A. Basile, G. Chiappetta, S. Tosti, V. Violante, *Sep. Purif. Technol*., 25 (2001) 549;
120. H. Amandusson, L.G. Ekedahl, H. Dannetun, *J. of Mem. Sci.* 193 (2001) 35;
121. A. Li, W. Liang, R. Hughes, *J. of Mem. Sci.* 165 (2000) 135;
122. F.C. Gielens, R.J.J. Knibbeler, P.F.J. Duysinx, H.D. Tong, M.A.G. Vorstman, J.T.F. Keurentjes, *J. of Mem. Sci.* 279 (2006) 176;
123. F. Scura, G. Barbieri, G. De Luca, E. Drioli, *Inter. J. Hydrogen Energy* 33 (2008) 4183;
124. REB Research & Consulting. www.rebresearch.com
125. S.A. Koffler, J.B. Hudson, G.S. Ansell, *Trans. AIME* 245 (1969) 1735;
126. S. Tosti, L. Bettinali, V. Violante, *Inter. J. Hydrogen Energy*, 25 (2000) 319;
127. A. Li, C. J.Lim, J.R. Grace, *Chem. Eng. J.* 138 (2008) 452;
128. S. Uemiya, N. Sato, H. Ando, T. Matsuda, E. Kikuchi, *Appl. Catal.* 67 (1991) 223;
129. S.L. Jørgensen, P.E. H. Nielsen, P. Lehrmann, *Catalysis. Today* 25 (1995) 303
130. J.R. Grace, S. Elnashaie, C.J. Lim, *Int. J. Chem. React. Eng.* 3 (2005);
131. G. Chiappetta, G. Clarizia, E. Drioli, *Chem. Eng. J.* 136 (2008) 373;
132. *S. Uemiya, Top Catalysis* 29 (2004) 79*;*
133. G.F. Froment, *J. Mol. Catal. A: Chem.* 163 *(2000) 147;*
134. K.O. Christiansen, D Chen, R. Lødeng, A. Holmen, *Appl. Catal. A: Gen.* 314 (2006) 9;
135. C.H. Bartholomew, *Appl. Catal.* 107 (1993) 1, cited in [134]
136. M.V. Mundschau, X. Xie, C.R. Evenson, A.F. Sammells, Proc. 22nd Annual International Pittsburgh Coal Conference, (2005)
137. N. Itoh, W.C. Xu, K. Haraya, *Industrial & Engineering Chemistry Research*, 33(22) (1994) 197
138. S. Hwang, R. Smith, *Chem. Eng. Sci.* 59 (2004) 4229;
139. A. Basile, G. Chiappetta, S. Tosti, V. Violante, *Sep. & Purif. Tech.* 25 (2001) 549;
140. A. Brunetti, G.Barbieri, E.Drioli, *Chem. Eng. Sci.* 64 (2009) 3448;
141. A. Brunetti, G. Barbieri, E. Drioli, K.H. Lee, B. Sea, D.W. Lee, *Chem. Eng. and Proc.* 46 (2007) 119;
142. R.L. Kliski, O. Desponds, *Appl. Catal. Gen.* 101 (1993) 317;
143. D.R. Seok, S.T. Hwang, in: M. Misono, Y. Moro-oka, S. Kimura (Eds.), *Future Opportunities in Catalytic and Separation Technology*, Elsevier, Amsterdam, 1990, pp. 248–267.
144. E. Kikuchi, S. Uemiya, N. Sato, H. Inoue, H. Ando, T. Matsuda, *Chem. Lett.* (1989) 489;
145. S. Uemiya, N. Sato, H. Ando, E. Kikuchi, *Ind. Eng. Chem. Res.* 30 (1991) 585;
146. H. Yoshida, H. Takeshita, S. Konishi, H. Ohno, T. Kurasawa, H. Watanabe, *Nuclear Tech. Fusion* 5 (1984) 178;

147. G. Chiappetta, G. Clarizia, E. Drioli, *Desalination* 193 (2006) 267;
148. G. Chiappetta, G. Clarizia, E. Drioli, *Chem. Eng. J.* 124 (2006) 29;
149. A. Caravella, F.P. Di Maio, A. Di Renzo, *J. of Memb. Sci.* 321 (2008) 209;
150. A. Brunetti, A. Caravella, G. Barbieri, E. Drioli, *J. of Memb. Sci.* 306 (2007) 329;
151. T.P. Tiemersma, C.S. Patil, M. van Sint Annaland, J.A.M. Kuipers, *Chem. Eng. Sci* 61 (2006) 1602;
152. M. Sjardin, K.JJ. Damen, A.P.C. Faaij, *Energy* 31 (2006) 2523;
153. J. Xu, G. F. Froment, *AIChE J*. 35 (1989) 88.

Research activities

International Conferences

1. ICCMR9 - 9th International Conference on Catalysis in Membrane Reactors, 28th June – 2nd July 2009, Lyon, France;

2. ICHEAP-9 The Ninth International Conference on Chemical and Process Engineering, 10-13 May 2009, Rome, Italy;

3. ECCE6-European Congress of Chemical Engineering-6, 16-21 September 2007, Copenhagen, Sweden.

National Congress

1. Convegno Congiunto SCI Calabria - Sicilia, 1-2 December 2008, Rende (CS), Italy

Schools

1. Incontri Collegiali della Scuola di Dottorato "*Pitagora*" in Scienze Ingegneristiche, Università della Calabria, 2009.

List of publications

Journals

1. G. Chiappetta, G. Barbieri, E. Drioli, *Pd/Ag - based Membrane Reactors on small scale: assessment on the high pressure importance and design parameters*, Chemical Engineering and Processing: Process Intensification, *submitted*;
2. Chiappetta G., Barbieri G., Drioli E., *Effect of the pressure increasing and design parameters on Pd/Ag-based membrane reactor performance*, Chemical Engineering Transactions ISBN 978-88-95608-01-3 ISSN 1974-9791, DOI: 10.3303/CET0917278, 17 (2009) 81-82;
3. G. Chiappetta, G. Clarizia, E. Drioli, *Theoretical analysis of the effect of catalyst mass distribution and operation parameters on the performance of a Pd-based membrane reactor for water gas shift reaction*, Chemical Engineering Journal 136 (2008) 373–382.

Proceedings in International Conferences

1. **G. Chiappetta**, G. Barbieri, E. Drioli, *Membrane Reactors on small scale for the methane steam reforming reaction: assessment on the high pressure importance*, Proc. in 9th International Conference on Catalysis in Membrane Reactors, Lyon, June 28th – July 2nd 2009
2. G. Chiappetta, G. Barbieri, E. Drioli, *Effect of the pressure increasing and design parameters on pd/ag-based membrane reactor performance*, Proc. in ICHEAP-9 The

Ninth International Conference on Chemical and Process Engineering, 10-13 May 2009, Rome, Italy

3. G. Chiappetta, G. Clarizia, E. Drioli, *Trade-off between hydrogen production and temperature hot* spots *in the design of a membrane reactor***,** Proc. ECCE6-European Congress of Chemical Engineering-6, Copenhagen 16-21 September 2007, Sweden.

Proceedings in National Congresses

1. G. Chiappetta, G. Barbieri, E. Drioli, *Processo di reforming in Reattori a Membrana per la produzione d'idrogeno: effetto della pressione e dei parametri di progetto sulle prestazioni*, proc in Convegno Congiunto SCI Calabria- Sicilia, 1-2 December 2008, Rende (CS), Italy.

List of Symbols

A_m	Membrane surface area, cm^2
a_k	constant , -
Å	Angstrom unit, -
c_{H2}	H_2 concentration in metallic bulk, kmol m^{-3} or mol m^{-3}
c_i	concentration i-specie, kmol m^{-3}
c_{tot}	total concentration in feed, kmol m^{-3}
Cp_{H2}	H_2 heat capacity, kJ kg^{-1} K^{-1}
Cp_{mix}	heat capacity of gas mixture, kJ kg^{-1} K^{-1}
$D_{i,r}$	radial effective diffusivity, m^2 s^{-1}
$\mathbf{D_{H2}}$	H_2 diffusion coefficient, m^2 s^{-1}
d_p	average particle diameter, m
EDX	Energy dispersive X-ray
F_{CH4}	Methane molar flow rate, mol min^{-1}
F_{H2}	Hydrogen molar flow rate, mol min^{-1}
gge	Gasoline Gram Equivalent
GHG	Greenhouse gas, -
GHSV	Gas Hourly Space Velocity, h^{-1}
GJ	Giga Joule
h_w	Wall-heat transfer coefficient, kJ m^{-2} s^{-1} K^{-1}
J_{H2}	fickian H_2 flux, mol m^{-2} s^{-1}, cm^3(*STP*) cm^{-2} min^{-1} or kg m^{-2} s^{-1}
k_c	kinetic constant, atm^{-1} s^{-1}

K_τ	Threshold constant, bar
K_s	H_2 solubility constant, mol cm^{-3} $Pa^{-0.5}$
K_{eq}	equilibrium constant, -
L_s	limiting reagent flow rate (Methane Load) in feed, cm^3 min^{-1}
L_{tubo}	reformer tubes length
L	axial length of the catalyst bed, m
LHV	lower heating value
m	(H_2O /CH_4 or H/C) reagents molar ratio in feed, -
n	exponent in Sieverts' law
P_e	H_2 permeability, kmol m^{-1} s^{-1} $Pa^{-0,5}$ or mol m^{-1} s^{-1} $Pa^{-0.5}$
P	Total Pressure, kPa
P_{H2}	H_2 partial pressure, kPa
P_{CH4}	Methane partial pressure on retentate side, kPa
PSA	pressure swing adsorption
ppmv	part per million volumetric unit, -
Q^{sweep}	sweep flow rate, mol min^{-1}
R_{gas}	universal constant of the gas, J mol^{-1} K^{-1} or cal mol^{-1} K^{-1}
r	radial coordinate, m
R	Radius of the membrane tube, m
$\Re_i$	reaction rate kmol m^{-3} s^{-1}
SEM	Scanning electron microscopy
SF	Sweep Factor, -
T	temperature, K
T_w	Wall temperature, K
TREC	Equilibrium Conversion of a Traditional Reactor, -
u_s	superficial velocity referred to whole section of lumen side, m s^{-1}
USD	United States Dollar
V_{cat}	Catalyst volume, cm^3
V_{CH4}	Carbon deposition limit, -
v_{dep}	Carbon deposition kinetic rate
v_{rem}	Carbon removal kinetic rate
V_r	Reactor volume, m^3
$v_z = u_s/\varepsilon$	interstitial fluid velocity in the axial direction, m s^{-1}
X_{CH4}	methane conversion, -

X_e	Equilibrium Conversion of a Traditional Reactor, -
y	molar fraction, -
z	axial coordinate, m
δ	membrane thickness, μm
ζ,	dimensionless axial coordinate, -
ΔH^o_{298}	*Standard* molar heat of reaction, kJ mol^{-1}
ΔH	reaction enthalpy, kJ·$kmol^{-1}$
ΔRI_{H2}	H_2 Recovery *Index* deviation, -
ΔX_{CH4}	Methane conversion deviation, -
ε	bed voidage fraction, -
λ_{er}	effective radial thermal conductivity, kJ m^{-1} s^{-1} K^{-1}
ρ_g	mixture density, kg m^{-3}

Subscript

cat	catalyst
CH4	methane
dep	deposition
feed	feed side
g, gas	gaseous
H2	hydrogen
i	i-specie (CH_4, H_2O, CO, CO_2, H_2)
lumen	retentate side
m	membrane
mix	mixture
P	Permeate side
perm	permeate
R	Retentate side
ret	retentate
rem	removal
s	solubility
shell	permeate side
w	wall
τ	threshold

0	inlet
B	catalytic bed
mix	mixture